

Alma Mater Studiorum – Università di Bologna

DOTTORATO DI RICERCA IN

Ingegneria Chimica, dell'Ambiente e della Sicurezza

Ciclo XXVI

Settore concorsuale: AREA 09/D2

Settore scientifico disciplinare: ING/IND-24

**POLYMERIC MEMBRANES FOR CO₂
SEPARATION: EFFECT OF AGING, HUMIDITY
AND FACILITATED TRANSPORT**

Presentata da: Luca Ansaloni

**Coordinatore Scuola di Dottorato
Prof.ssa Serena Bandini**

**Relatore
Ing. Marco Giacinti Baschetti**

**Correlatori:
Prof. Giulio Cesare Sarti**

Ing. Matteo Minelli

Esame finale anno 2014

Dedicated to Maria

Table of Contents

<i>Introduction</i>	<i>1</i>
<i>1. Membranes for CO₂ separation</i>	<i>5</i>
1.1 Aging.....	14
1.2 Effect of water vapor.....	16
1.3 Facilitated transport membranes.....	18
<i>2. Mathematics of transport process</i>	<i>22</i>
2.1 Diffusion in a plane sheet.....	22
2.1.1 Permeation analysis.....	22
2.1.2 Sorption analysis.....	25
2.2 Diffusion with chemical reaction.....	26
<i>3. Experimental</i>	<i>28</i>
3.1 Sample preparation protocols.....	28
3.1.1 Matrimid [®] 5218 Polyimide.....	28
3.1.2 Facilitated transport membranes.....	29
3.1.2.1 Materials.....	30
3.1.2.2 MWNTs amino-functionalization.....	31
3.1.2.3 Membrane preparation procedure.....	32
3.2 Permeation.....	35

3.2.1	<i>Dry gas permeation</i>	36
3.2.2	<i>Humid gas permeation</i>	38
3.2.3	<i>Mixed gas permeation</i>	40
3.3	<i>Sorption</i>	42
3.4	<i>IR Spectroscopy</i>	44
3.5	<i>Density</i>	45
4.	Results	47
4.1	<i>Aging and thermal treatment effect in Matrimid</i>	47
4.1.1	<i>Thermal treatment</i>	49
4.1.2	<i>Aging</i>	58
4.2	<i>Water vapor effect on gas permeability in Matrimid</i>	62
4.2.1	<i>Water Vapor Sorption</i>	63
4.2.2	<i>Gas permeability under humid conditions</i>	67
4.2.2.1	<i>Activation Energy</i>	76
4.3	<i>Facilitated transport membranes</i>	77
4.3.1	<i>MWNTs characterization</i>	79
4.3.2	<i>Membrane performance at 15 atm</i>	80
4.3.3	<i>Membrane performance at 28 atm</i>	84
4.3.4	<i>Effect of the inorganic loading</i>	87
4.3.5	<i>Effect of sweep side RH</i>	89
4.3.6	<i>Effect of temperature</i>	90
4.3.7	<i>Effect of membrane thickness</i>	94
5.	Modeling	97
5.1	<i>Free Volume Theory</i>	97
5.2	<i>NELF Model</i>	100
5.3	<i>Theoretical consideration on thermal treatment and aging results</i>	103
5.4	<i>Modeling humid gas permeability</i>	105
5.4.1	<i>Free volume based empirical model</i>	106
5.4.2	<i>Integrated NELF & Free Volume Theory approach</i>	114
5.5	<i>Analysis of the facilitated transport: thickness influence</i>	123
	Conclusions	127
	Appendix	133
A.1.	<i>Thermal treatment and Aging in Matrimid</i>	133

<i>A.2. Humid permeation in Matrimid</i>	134
<i>A.3. Facilitated transport membranes</i>	135
<i>Bibliography</i>	136
<i>List of Publications</i>	149
<i>Acknowledgments</i>	151

Introduction

In the past century, due to a fast worldwide development of industrial production, an intensive exploitation of Earth resources took place, especially in terms of raw materials consumption and environmental pollution. Starting from the 21st century, the climate changes, the rise of new developing countries, the elongation of life expectation and the increase of world population stressed out that the old growth concept was not pursuable anymore, and it was unquestionably necessary to adopt a new model of development with a strong focus on sustainability [1]. Hence, one of the biggest challenges currently facing the world is the elaboration of a shared strategy to support a sustainable industrial growth [2].

In process engineering field, a fundamental importance is attributed to the so called "Process Intensification" strategy, whose purpose is the improvement of the manufacturing and processing steps towards final products through the minimization of the equipment volume, the energy consumption, the waste production and the environmental impact [3,4].

Membrane-based technology falls excellently within Process Intensification strategies, since membrane units have a smaller ecological footprint compared to traditional plants of corresponding capacity and have the potential to replace partially or completely most of them [5]. Membrane engineering provided already interesting solutions, currently applied at industrial scale, such as reverse osmosis membranes for water desalination, microfiltration and ultrafiltration modules for pharmaceutical industries and barrier materials for food packaging [6].

The appeal of gas separation membranes at the industrial level is constantly growing, thanks to their competitiveness compared to traditional separation processes [7–9]. Even though membrane technology potentialities were known long before 1980, only in the past three decades their attractiveness started to growth at the industrial level, becoming a \$150 million/year market at the beginning of the year 2000 with an expected 5 folds increase by 2020 [10]. The principal applications in this field are related to the separation of incondensable species. Besides nitrogen removal from

air, the CO₂ purification represents the largest area of membrane development: natural gas sweetening [9], post-combustion products purifications [7], refinement of gaseous fuels from biological production [11] and hydrogen recovery from water gas shift reactors [12], are only some of the possible applications exploiting membrane-based technologies for CO₂ separation.

Recently, the focus of research has concentrated on the development of new high performing materials able to make the technology suitable for a wide range of applications and to increase the economic convenience of the separation process. Among the novel materials for CO₂ separation, polyimides represent one of the most promising one, thanks to their high selectivity coupled with good thermal and mechanical stability [9]. Other interesting classes of polymers are represented by PIMs (polymer with intrinsic microporosity), which are dense selective layer with molecular sieving features able to guarantee high trans membrane flux [13] and thermally rearranged (TR) polymers, obtained through a thermally induced rearrangement of polymeric chains [14] able to achieve high CO₂ permeability and good separation performance. Furthermore, the transport properties of polymers can be tuned also by embedding nanofillers within the polymer matrix (so called Mixed Matrix Membranes, MMMs), which are usually able to achieve an appreciable transport rate enhancement with negligible effect on separation factor. Remarkable results have been obtained by using fillers with particular CO₂ affinity, such as metal organic framework (MOFs) [15], zeolites [16] or cyclodextrin [17]. In the end, also groups with a specific CO₂ reactivity could be included within the polymeric matrix, achieving excellent separation performances both in terms of permeability and selectivity [18,19].

However, although the performance achieved under "ideal conditions" in the lab scale (i.e. low pressure, pure gas permeation experiments) are excellent, issues frequently arise for the scaling-up of the process in real industrial conditions, such as plasticization, aging and competitive sorption [20,21], which can be related to the presence of binary or ternary gas mixtures. In addition, also the presence of impurities and contaminants may create troubles for membrane separation technology [22,23]. Therefore, the investigation of material transport properties in

the presence of minor compounds (e.g. water, hydrogen sulphide, small hydrocarbons), and on a long time scale have to be carried out for a reliable and complete material description. A lack of an adequate knowledge of these phenomena can indeed jeopardize the future scale-up of this technology.

In the present thesis work, two different types of membranes will be considered and studied as suitable materials for CO₂ separation: a commercial polyimide, namely Matrimid[®] 5218, whose separation mechanism is based on solution diffusion theory, and a polyamines (PAm) based mixed matrix membranes containing multi-walled nanotubes, which exploit the facilitated transport mechanism to separate CO₂ from the other compounds present in the feed gas composition.

The influence of thermal treatment, physical aging and presence of water vapor on the gas transport properties of the polyimide material will be investigated. In particular, Matrimid self standing samples will undergo a different thermal treatment and the transport properties will be examined by means of permeability measurements in a pure gas permeation apparatus, using CO₂ and CH₄ as gaseous penetrants. Afterwards, the performance stability of samples with different thermal histories will be monitored for a period of 6 months, in order to investigate the effect of the aging phenomenon on the polymeric matrix.

The treatment protocol able to give the best performance in terms of separation and stability, will then be employed to study the effect of water vapor on gas permeation, by means of a humid permeometer apparatus. Four gaseous species, with different features, will be used to characterize the material transport properties in wide activity range (0 - 0.75) and under different thermal conditions. At the same time, pure water vapor sorption experiments will be carried out, allowing a direct correlation between the measured permeability and the water concentration within the membrane matrix. Based on the observed results, a novel modeling approach will be proposed to enlighten the transport mechanisms involved for the considered conditions.

On the other side, facilitated transport membranes will be synthesized and their transport properties will be studied for high pressure separation application, in particular for natural gas sweetening. Different polyamines will be used in the membrane synthesis together with a PVA-base network acting as barrier substrate.

Moreover, multi walled carbon nanotubes (MWNTs) will be embedded in the matrix, in order to avoid mechanical stability issues, frequently suffered by these membranes under high pressure conditions. The transport properties will be characterized up to 28 atm and the influence of several parameters (inorganic loading, water content in the gaseous stream, operative temperature and selective layer thickness) will be investigated in order to find the optimal conditions able to maximize the separation performances.

1. Membranes for CO₂ separation

In view of global warming and climate changes related to the greenhouse effects, CO₂ capture and storage is nowadays of fundamental importance, and membranes offer a valid solution for a wide variety of mitigation actions. The CO₂ removal can be performed mainly in two different steps of the productive process. In pre-combustion separation, the acid compounds are removed from the gaseous stream, such as from the conversion products of fossil fuel into CO₂ and H₂ (e.g. steam reforming followed by water-gas shift reaction), natural gas extraction and biological energy production. The treatment helps also to increase the fuel heating value and it is necessary to meet the specifications to avoid pipelines corrosions [4,24]. Furthermore, post-combustion separation is fundamental to avoid large releases of greenhouse gases in the atmosphere, as the flue gas is mainly composed by CO₂ and N₂, coming from the air used on the combustion stage [25].

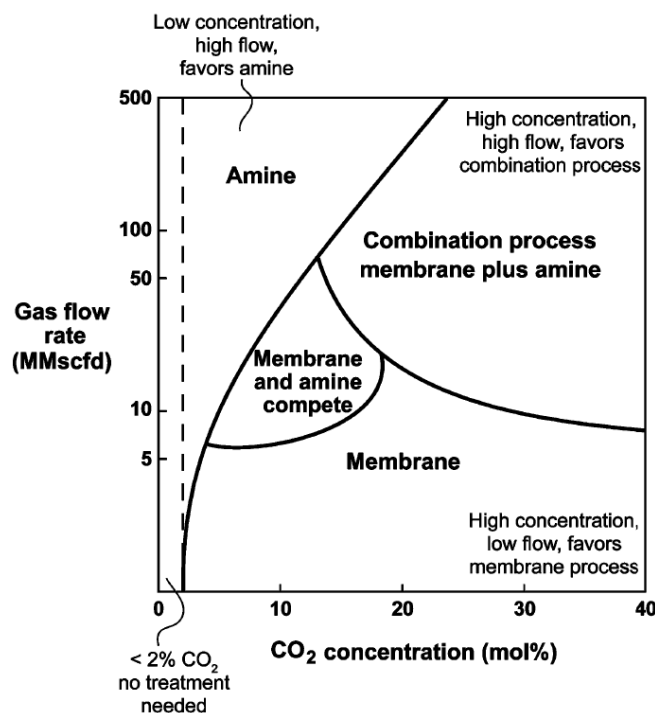


Figure 1.1 - Comparison between membrane and amine absorption processes for CO₂ removal as a function of the CO₂ concentration and the gas flow rate (from Ref. [9]).

Even though solvent absorption (amine or carbonate compounds) is still the main separation technology applied for purification of gaseous stream coming from large productive plants, membranes modules competes strongly with them in a wide range of operative conditions and are commonly preferred to satisfy logistic constrains, e.g. offshore installations, or when reduced size are required. As showed in Figure 1.1, membranes are preferable in case of high CO_2 concentration, able to ensure a sufficient driving force, and for rather low flow rate, in order to limit the surface area required to meet the separation goal, hence maintaining the economical convenience of the process.

Membrane-based gas separation is a chemical potential driven transport process and is usually performed through dense selective layers, which can separate different gaseous species, thanks to their structural or thermodynamic properties. In Figure 1.2, a schematic representation of the transport across a selective layer is reported.

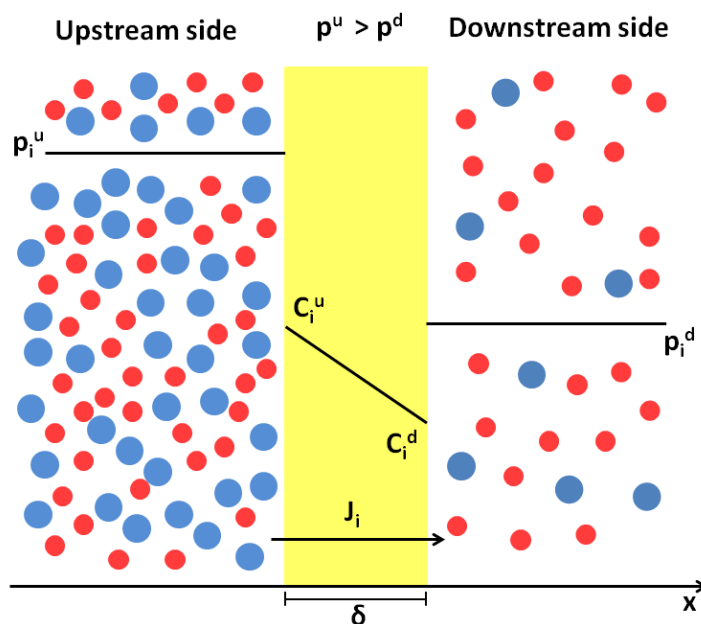


Figure 1.2 - Permeation process scheme in a selective layer (re-adapted from [26])

Among the intrinsic parameters, experimentally determined and useful for material characterization, gas permeability is the fundamental one. Theoretically, it is

described as the amount of gas permeating across the polymeric layer per unit time and unit area scaled on the pressure drop and the membrane thickness:

$$P_i = \frac{J_i \cdot \delta}{p_i^u - p_i^d} \quad (1.1)$$

where J_i is the gas flux per unit area of the i species, δ is the membrane thickness and p_i^u , p_i^d are the partial pressure of component i on the upstream and downstream side of the membrane respectively.

Permeability can be expressed by several units, but the most common one is the Barrer, defined as:

$$1 \text{ Barrer} = 10^{-10} \frac{\text{cm}^3(\text{STP}) \cdot \text{cm}}{\text{cm}^2 \cdot \text{cmHg} \cdot \text{s}} = 3.364 \cdot 10^{-16} \frac{\text{mol}}{\text{m} \cdot \text{s} \cdot \text{Pa}} \quad (1.2)$$

Another important parameter is the permeance, frequently used as reference to fix separation targets for real applications or to compare membranes with other separation technologies. It is defined as the ratio between the permeability and the selective layer thickness and usually measured in *GPU* (gas permeation unit):

$$1 \text{ GPU} = 10^{-6} \frac{\text{cm}^3(\text{STP})}{\text{cm}^2 \cdot \text{cmHg} \cdot \text{s}} = 3.3 \cdot 10^{-1} \frac{\text{mol}}{\text{m}^2 \cdot \text{s} \cdot \text{Pa}} \quad (1.3)$$

Conceptually, several theoretical formalisms have been proposed to describe the diffusion of small molecules across a dense polymeric layer, and likely the most accurate one is the Free Volume Theory (FVT) [27], whose exhaustive walk-through will be given in Chapter 5. Theoretically, molecules motion through the membrane can be described as a jumping mechanism and depends on the free volume (V_f) of the polymer as well as on the available energy, necessary to overcome the polymer-polymer interaction forces. Hence, the permeation of low molecular weight penetrants can be viewed as a temperature activated process, involving local motions of chains segments, schematically reported in Figure 1.3, which temporarily permits the opening of narrow constriction separating volume elements.

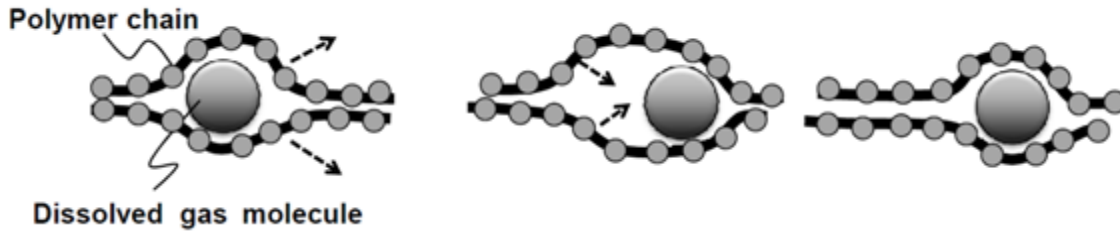


Figure 1.3- Schematic representation of small molecules motion across a membrane

Based on the previous consideration, the permeability coefficient tends to increase along with the fractional free volume ($FFV = V_f / \hat{V}$, \hat{V} is the polymer specific volume), and their relationship is expressed by means of an exponential equation:

$$P_i = A_i \cdot \exp\left(-\frac{B_i}{FFV}\right) \quad (1.4)$$

where A_i and B_i are constant parameters characteristic for the polymer-penetrant pair.

In this view, the operative temperature plays a key role in the permeation process, affecting the membrane performance. The behavior is usually represented through the Arrhenius equation [28]:

$$P_i = P_{i,0} \cdot \exp\left(-\frac{E_{P,i}}{RT}\right) \quad (1.5)$$

where $E_{P,i}$ is the activation energy of permeation, $P_{i,0}$ is a pre-exponential factor, R is the ideal gas constant and T is the absolute temperature.

Increasing the degree of detail in the description, the transport of molecules across a dense selective layer can be represented by the well-known solution diffusion mechanism [5]. Conceptually, the gas molecules permeation may be described in three steps: at first, the penetrant is absorbed in the upstream gas-membrane interface, then it diffuses across the polymer layer and finally it is desorbed on the downstream side. Considering the sorption and desorption step at the equilibrium and expressing the diffusion coefficient with Fick's law, the penetrant flux can be written as:

$$J_i = D_i \cdot S_i \cdot \frac{\Delta p_i}{\delta} \quad (1.6)$$

where Δp_i is the partial pressure difference of component i across the membrane, D_i is the diffusion coefficient and S_i is the solubility coefficient, expressed as $\Delta C_i / \Delta p_i$, where ΔC_i is the concentration jump between the two gas-membrane interfaces (see Chapter 2 for the exhaustive description). The permeability can thus be expressed as:

$$P_i = D_i \cdot S_i \quad (1.7)$$

Solubility expresses the thermodynamic partitioning coefficient, which depends mainly on temperature and penetrant condensability, whereas diffusivity is related to the kinetic properties of the polymer-penetrant system, function of temperature, size and shape of the molecules and volume available for penetrant diffusion in the polymeric matrix. The temperature influence on both coefficients can be expressed with a similar exponential equation, already reported for permeability (Eq. 1.5):

$$D_i = D_{i,0} \cdot \exp\left(-\frac{E_{D,i}}{RT}\right) \quad (1.8)$$

$$S_i = S_{i,0} \cdot \exp\left(-\frac{\Delta H_{S,i}}{RT}\right) \quad (1.9)$$

where $E_{D,i}$ is the activation energy of the diffusion process, $\Delta H_{S,i}$ is the heat of sorption and $D_{i,0}$ and $S_{i,0}$ are T independent pre-exponential factors. In this view, Equation 1.5 may be decoupled into two contributions and $E_{P,i}$ can thus be expressed as the sum of the enthalpy of solution ($\Delta H_{S,i}$) and the energy required for gas molecule to jump from an available site to another ($E_{D,i}$).

The other important parameter is the separation factor, which determines at which extent the separation is performed. In particular, considering two gaseous species, i and j , the membrane selectivity is defined through the following equation [5]:

$$\alpha_{i,j} = \frac{y_i^d / y_j^d}{y_i^u / y_j^u} \quad (1.10)$$

where y is the molar fraction of species i and j for the downstream (d) and the upstream (u) side of the membrane. Usually, this parameter depends on the particular process and the molar fraction must be experimentally detected. Nevertheless, if the downstream pressure approaches zero, the selectivity can be considered a characteristics of the ternary system represented by the polymeric matrix and the dissolved penetrants. In this fashion the previous equation can be written as [29]:

$$\alpha_{i,j} = \frac{y_i^d / y_j^d}{y_i^u / y_j^u} = \frac{1}{y_i^u / y_j^u} \frac{P_i}{P_j} \frac{p_i^u - p_i^d}{p_j^u - p_j^d} \approx \frac{P_i}{P_j} \quad (1.11)$$

where P_i and P_j are the permeability of the two gaseous species, as calculated from mixed gas permeation experiments. If pure gas permeability is considered respect to the mixed one, the so called "ideal" selectivity can be defined:

$$\alpha_{i,j}^{id} = \frac{P_{i,pure}}{P_{j,pure}} \quad (1.12)$$

This parameter gives only a rough estimation of the real selectivity, since the simultaneous presence of different penetrants can lead to unpredictable effects on the permeation process, such as competitive sorption or penetrant-induced swelling of the membrane matrix, due to the mutual interactions between the gaseous species and the single gas with the polymer structure.

Based on solution diffusion theory, also the selectivity can be decoupled in two different contributions:

$$\alpha_{i,j} = \frac{P_i}{P_j} = \frac{D_i}{D_j} \frac{S_i}{S_j} = \alpha_D \cdot \alpha_S \quad (1.13)$$

where α_D is the diffusivity contribution to the selectivity, being thus related to kinetic parameters, whereas α_S expresses the solubility influence on the separation factor, hence related to thermodynamic features.

Through the comparison of permeability and selectivity values for different glassy and rubbery polymer, whose separation properties are based on the solution diffusion mechanism, Robeson in 1991 [30] obtained one of the most helpful tool to judge the

membrane performance, the well-known Robeson Plot. In Figure 1.4 the plot is reported for CO_2/CH_4 separation and the black dotted lines correspond to the Robeson upper bounds, the state-of-the-art for the particular separation in membrane science at the time of the publications (1991 and 2008). Shifting the membrane results towards the upper limit corresponds to an improvement of the separation performance. Similarly, a linear relation has been obtained also for other gas pairs (CO_2/N_2 , H_2/CO_2 , O_2/N_2 and others [31]) when the selectivity was plotted together with the permeability of the more permeable penetrant. The shape of the found correlations points out the presence of a trade-off: an increase of P_i usually corresponds to the decrease of $\alpha_{i,j}$ and vice versa, so that the more permeable polymers usually show the lower selectivity values. Moving towards the upper right corner of the plot represents thus the biggest challenge for solution diffusion based membranes.

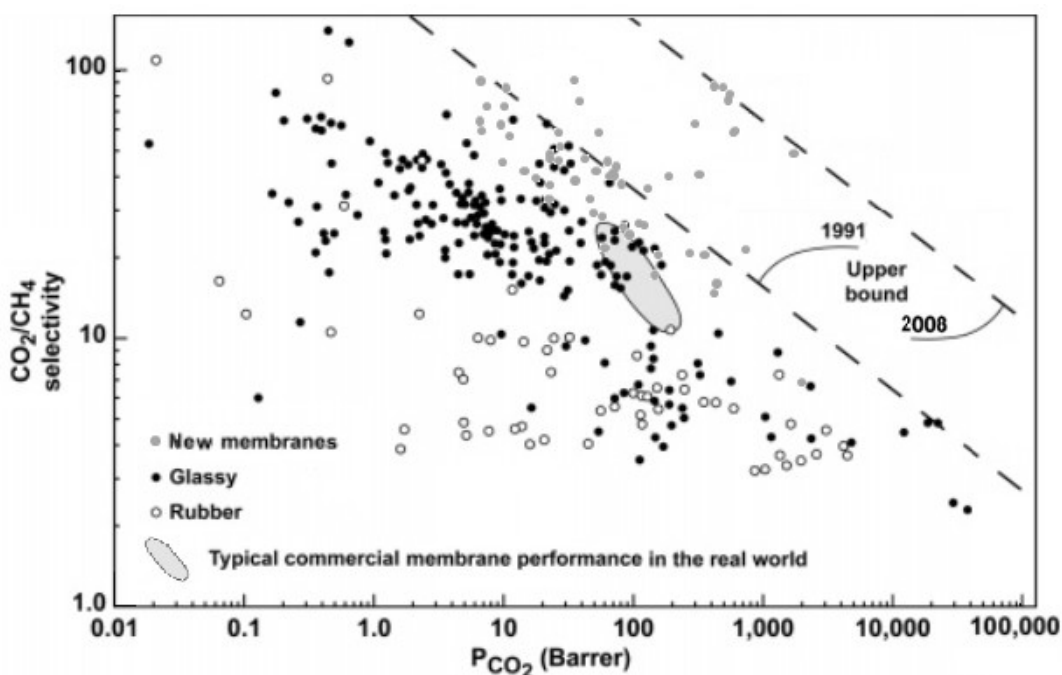


Figure 1.4 - Robeson Plot for CO_2/CH_4 separation [9]

Through the analysis of literature data obtained for different gas-polymer systems, a correlation has been found between the polymer transport properties and the kinetic

and thermodynamic characteristics of the penetrant. In particular, it has been observed that the diffusion coefficient scales accurately with the penetrant kinetic diameter, whereas the solubility correlates properly with the gas condensability, related to its critical temperature. Table 1.1 summarizes the values of these properties for the gaseous species investigated in the present thesis. Combining this information with the concept described by Equation 1.13, it is easy to understand that CO₂/H₂ separation is rather difficult to achieve for membranes. Indeed, thanks to the small kinetic diameter H₂ diffuses faster than CO₂, resulting in a $\alpha_D < 1$, but at the same time, due to the higher critical temperature, i.e. condensability, CO₂ is absorbed preferentially in the membrane matrix, giving $\alpha_S > 1$. The overall selectivity is given by the relative amount of each term, however the competitive behavior of the two parameters disadvantages the achievement of good separation performance. On the other side, membranes can accomplish very good results for CO₂/CH₄ or CO₂/N₂ separation, since the solubility-selectivity and the diffusivity-selectivity result simultaneously higher than 1, thanks to the smaller kinetic diameter and the higher condensability of CO₂ compared with the other gases.

	He	H ₂ O	H ₂	CO ₂	N ₂	CH ₄
d_k (Å) [30,32]	2.60	2.65	2.89	3.30	3.65	3.80
	He	H ₂	N ₂	CH ₄	CO ₂	H ₂ O
T _c (K) [33]	5.2	33	126	191	304	647

Table 1.1 - Kinetic Diameters and critical temperatures of the investigated gaseous species

Several polymeric materials have been developed spanning over a wide spectrum of macromolecules chemistry and resulting in very different morphology, such as the amorphous, semi-crystalline and crosslinked structures. However, these last two lattice configurations are not very interesting as membrane materials, since they usually present very low permeability values for all penetrants. Conversely, amorphous polymers present interesting features for gas separation applications.

Depending on their thermodynamic state at room temperature (whether their glass transition temperature, T_g , is below or above the atmospheric value) they can be classified as glassy or rubbery polymers respectively. Rubbers are equilibrium phases comparable, from the thermodynamic point of view, to liquids and they are characterized by high values of the diffusion coefficients for all the gaseous species, due to the molecular chain mobility and the high free volume. Hence, their selectivity is principally governed by the thermodynamic factor α_S , i.e. by the gas solubility. On the other side, glassy polymers are frozen in non equilibrium structures and, due to the kinetic hindrance of chains relaxation, they present a rigid polymeric lattice, so that diffusivity can vary significantly among the gaseous species. The selectivity can be influenced from both D and S , even though frequently α_D is usually the dominant factor.

Among all the materials recently developed, polyimides have been showed to be very promising for gas separation applications, since they are able to couple notable separation performance with good mechanical and thermal stability. Rather than the linear configuration, heterocyclic aromatic polyimides are the most interesting ones, since the imide group formed next to a benzene ring confers them a high thermal stability coupled with good physical and mechanical properties. Several polymerization protocols have been developed [34], but the most common one starts from the reaction of dianhydride and diamine monomers precursors (Fig. 1.5). By changing the reactive moieties a large variety of polymers can be obtained, normally named and classified basing on the dianhydride nature. The selectivity of these polymers is associated to their rigid molecular chains, generated from the strong intermolecular bonds between carbonyl group and the nitrogen atom, which impose major constraints to rotation and mobility of the chain elements. Furthermore, the very high thermal stability (T_g usually higher than 300°C) makes polyimides suitable for a wide variety of gas separation processes.

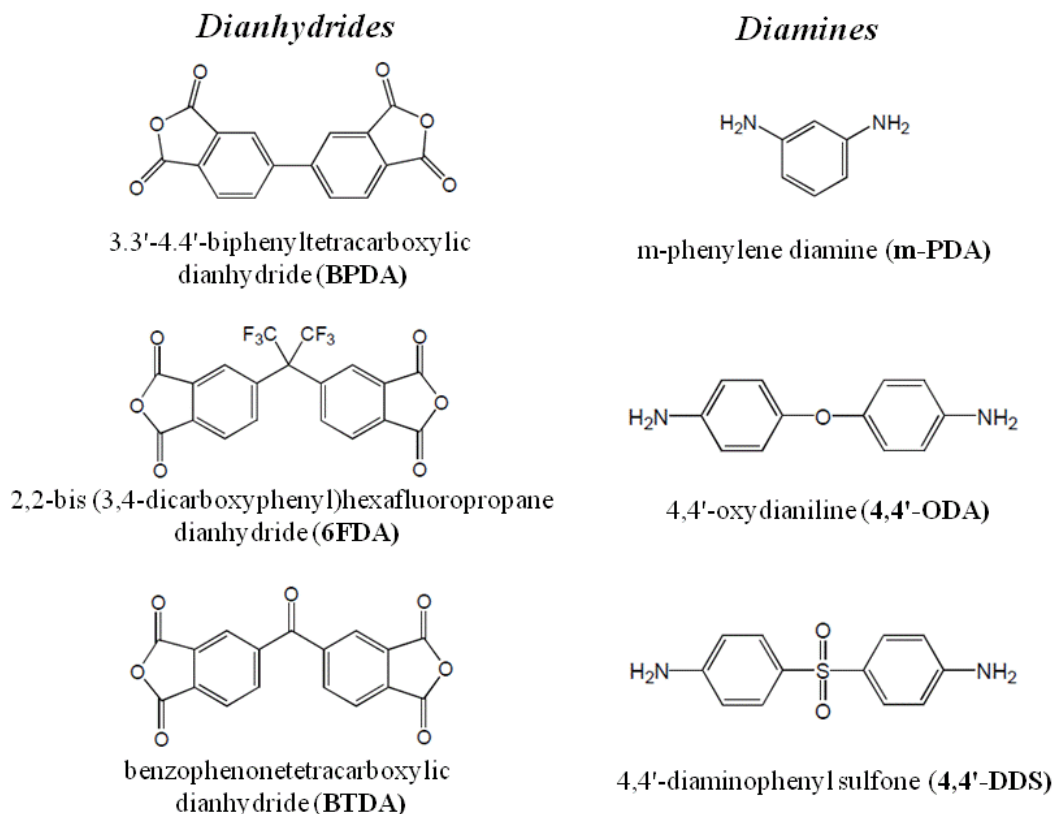


Figure 1.5 - Typical dianhydride and diamine moieties used in polyimides synthesis

1.1 Aging

As previously reported, glassy polymers present a structure far from the thermodynamic equilibrium condition and, in particular, they are characterized by an excess of the thermodynamic quantities (volume, enthalpy and entropy) compared to the equilibrium state [35,36]. The distance from equilibrium generates a driving force responsible of the spontaneous evolution of the polymer structure towards a state closer to the fully relaxed thermodynamic configuration. Frequently, physical aging is manifested through volume relaxations [37] of the specimen and, in general, both physical and mechanical properties are influenced by this phenomenon. Moreover, the aging process has been found to be temperature dependent: cooling down the sample, the molecular rearrangements causing the specimen densification slow down, since a lower energy amount is available for

chains relaxation. A model has been proposed by Struik [38] to describe the physical aging rate, expressed by means of the following equation:

$$\frac{d\hat{V}}{dt} = \frac{-(\hat{V} - \hat{V}_\infty)}{\tau(\hat{V}, T_g - T)} \quad (1.14)$$

where \hat{V} is the specific volume of the polymer at temperature T , \hat{V}_∞ is the specific volume at the equilibrium and τ is the characteristic aging time, function of \hat{V} and the distance of T from the glass transition temperature.

Coupling the Struik model with the Free Volume Theory, previously mentioned, produces a theoretical interpretation of physical aging and of its influence on the transport properties [39]. Indeed, the driving force responsible of the densification of the polymer structure generates a reduction of the amount of free volume available for penetrants to diffuse across the membrane over time [40,41]. In view of the mentioned relationship between permeability and free volume (Eq. 1.4), the aging process tends thus to reduce the transport rate across membrane, as frequently reported in literature [42,43]. In this concern, among the large amount of investigated polymeric materials, poly[1-(trimethylsilyl)-1-propyne] (PTMSP) presents the most representative results of this phenomenon. PTMSP is a glassy membrane with a considerably high free volume and consequently very good transport properties of small size penetrants. However, its use on real gas separation applications was hampered by a fast aging rate, involving a quick decline in the membrane performance [40].

Despite the negative effect on the membrane productivity, physical aging produces usually an increase of the separation factor [43,44]. The reduction of voids dimensions distribution affects more significantly the penetrant with the larger kinetic diameter, enhancing the membrane selectivity, in agreement with Robeson trade off [31]. In addition, the aging phenomenon has been demonstrated to be thickness-dependent: hence, to maximize the membrane permeance, thin selective layers (thickness $< 1 \mu\text{m}$) must be casted on porous supports, but thinner films undergo a fast aging rate, which can be up to an order of magnitude more rapid compared the thicker ones [39,45,46].

Similarly to physical aging, also thermal treatment produces a contraction of the lattice structure, which results in a decrease of the voids sizes and concentration in the polymer

matrix [36,47]. Hence, the thermal history of the polymer results to be of fundamental importance to define its transport characteristics, even though the principal effects are detected mainly in the region below T_g [38]. Accordingly, the time-temperature superposition principle can be used in order to describe the volume relaxation evolution [48] and the gas transport properties variations of a polymeric membrane [49] obtained from different thermal treatments. Moreover, other authors suggested that the variations of transport properties due to the previous history and the aging phenomenon cannot be described only through a simple free volume decrease, but they are related to a more complex rearrangement, affecting also the chains flexibility [50]. However, only few literature studies are currently devoted to the investigation of thermal treatment effect on glassy polymer permeation performance, hence more efforts have to be concentrated to achieve a full comprehension of this phenomenon.

1.2 Effect of water vapor

On the lab-scale, the principal efforts for novel membrane materials are often focused on maximizing the membrane performance and the measurement of permeability and selectivity are frequently performed on pure or mixed gases on a dry base. However, minor compounds frequently present in real application, such as water, low molecular weight hydrocarbons and hydrogen sulfide [51], can significantly affect the membrane performance and their effect must be taken into account for a reliable characterization of the separation process. Among the other compounds, water vapor can influence the membrane transport properties in various ways, depending on the hydrophobic or hydrophilic nature of the material and the affinity of H_2O molecule with the gaseous penetrant. Generally, hydrophilic materials undergo a relevant plasticization in presence of water vapor, causing an increase of their permeability and thus of their productivity; on the other side, in hydrophobic matrices the higher condensability of water favors its sorption to the detriment of the other gaseous species, generating a reduction of their transport rate.

Polyelectrolyte membranes (PEM), such as the perfluorosulphonated ionomers, due to the presence of ionic groups, present a very high water uptake (up to 20 wt% [52]) and a

relevant swelling upon sorption [53]. Such a strong impact of water on the membrane morphology influences significantly the transport properties and, in certain cases, it can also affect the transport mechanism, reversing the material selectivity [32]. Nafion and Aquivion appear to be on a dry base He selective, but as soon as the R.H. of the system is increased to 5% the CO₂ becomes the more permeable species. Many authors [32,54,55] suggested that under humid conditions water channels are formed across the membrane: on a dry base the diffusion is mainly controlling the permeation process, but in presence of water vapor the transport mechanism is controlled by the solubility of the gaseous penetrants in the H₂O liquid domains, formed in the membrane matrix. An even more drastic effect is obtained when the water vapor is present in the gas permeation through barrier materials. Microfibrillated cellulose (MFC) films displayed a water uptake close to 10 to 12 wt% [56] and as soon as the R.H. in the feed gas was increased to 20% the oxygen permeability of the film increased of 2 orders of magnitude and a further increment was observed approaching the saturation conditions.

On the other side, for polymers with a low water vapor uptake, the presence of water concentration in the gaseous stream corresponds to a decrease of the transport rate across the selective layer, due to competitive sorption. The higher critical temperature promotes H₂O in the competition with other penetrants for absorption in Langmuir voids. Polyimides are known to be hydrophobic or weakly hydrophilic materials [57]. The only exception is represented by the presence of sulfonated groups in the monomer structure, which enhance the water uptake [58,59]. The CO₂ and CH₄ permeability coefficients are reported to decrease in 6FDA and BTDA-based polyimides increasing the water activity of the feed stream up to 60% of the dry value, affecting barely the separation factor [60]. Similar results were obtained for a NTDA-based polyimide, where the CO₂ and N₂ transport rates underwent a 52% reduction compared to the dry values at a water activity close to 1 [61]. Pourafshari Chenar et al. [62] report comparable performance for a cardo-based polyimide hollow fiber membranes, where in presence of water both CO₂ and CH₄ permeabilities exhibit a decrease of 43% and 28% respectively. They investigated also a PPO based hollow fibers module, which, due to the high hydrophobicity of the material, showed a smaller decrease at increasing the water content in the separation process. Moreover, Reijerkerk et al. [63], studying the PEO-PPO-based block copolymer transport

properties under humid conditions, disclosed a marked decrease of gas (CO_2 and N_2) permeability at increasing the water concentration in the feed side, mainly related to the weekly hydrophilic behavior displayed by the water sorption isotherms for the investigated R.H. conditions.

Finally, also a behavior in between the two phenomena previously mentioned may be obtained with a simultaneous occurrence of competitive sorption and water-induced swelling. Bae et al. [64] disclosed the permeation properties of a poly(arylene-ether-sulfone)s membranes under humid conditions. They reported that both O_2 and H_2 permeability values decrease up to a 30% relative humidity and then start to increase along with the activity. The O_2 transport rate increases of 1 order of magnitude compared to dry conditions.

As described, water vapor can thus affect the transport properties of a polymer in various ways, which cannot be easily tailored in advance, unless a rough idea can be obtained from the material nature. Therefore, the characterization of membrane performance under humid condition is of fundamental importance for the reliable description of the material potentialities for gas separation applications.

1.3 Facilitated transport membranes

All the foregoing considerations concerned materials whose separation characteristics are based on a purely physical transport mechanism. A more efficient CO_2 separation can be achieved using membranes based on the facilitated transport mechanism [65,66], which exploits a chemical reaction between the CO_2 and basic compounds present within the membrane matrix. As reported in Figure 1.6, besides the solution diffusion transport, the CO_2 reacts with active sites present within the matrix, producing a chemical enhancement of the CO_2 flux across the membrane. The first facilitated transport membrane was proposed by General Electric in 1967, based on an cellulose acetate matrix swollen by an aqueous carbonate solution [67]. Nevertheless, in the past decade the study of these particular membrane for CO_2 separation has accelerated sharply.

The reactive species are called carriers and they can be classified based on their mobility: if the reactive moiety is linked to a low molecular weight molecules and is able to move

across the selective layer, they are referred as mobile carriers; on the other side, when the reagent group is directly bonded to a long chain structure and its mobility is rather limited in the membrane framework, they are identified as fixed carriers. In this fashion, the CO₂ transport is given by a double contribution, the ordinary transport based on the solution-diffusion mechanism and the carrier facilitated diffusion, due to the complex formation based on the reaction between CO₂ and carriers.

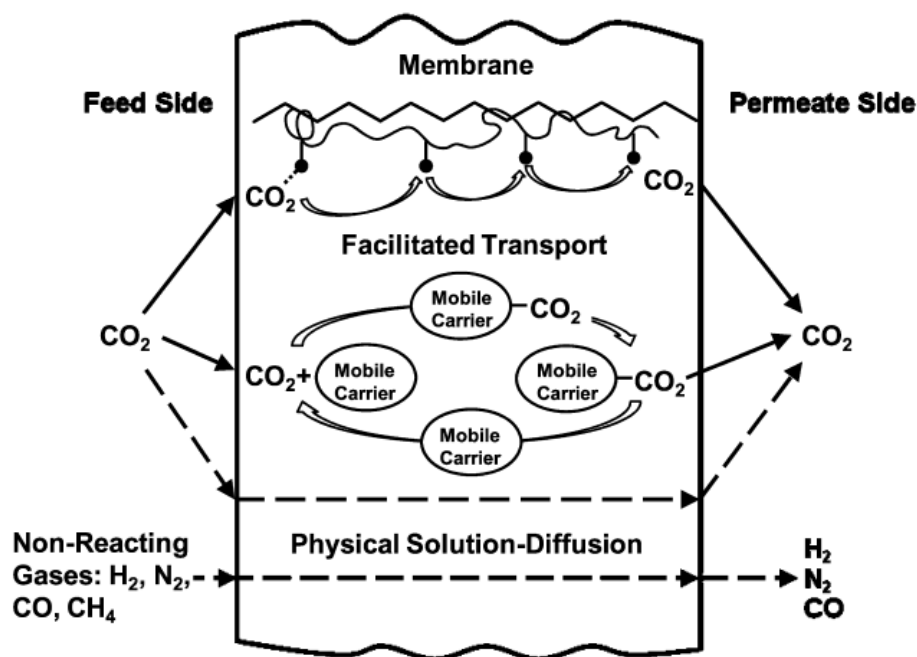


Figure 1.6 - Facilitated transport mechanism across a selective layer (from Reference [18])

When amines react with CO₂, the reaction scheme can be described by means of the zwitterion mechanism, where the carbamate ion is the activated complex responsible for the CO₂ transport. For unhindered amines, a two step reaction is involved:



At first, a zwitterion intermediate is formed, which can then be deprotonated by amines to form the carbamate ion. Considering the overall reaction of Equation 1.15 and 1.16, a single mole of CO₂ is reacting with two moles of amines [68].

However, when sterically hindered amines are involved in the reaction, the scheme is different. A sterically hindered amine is defined as either a primary amine in which the amino group is attached to a tertiary carbon or a secondary amine in which the amino group is attached to at least one secondary or tertiary carbon. Due to the attached alkyl group carbamate ion is not stable in water and reacts with H₂O to give the bicarbonate:



In the overall reaction (Eq. 1.15, 1.16 and 1.17) only one mole of amines reacts with the solute, improving the complex formation per unit of amines present in the membrane composition, hence the CO₂ transport [69]. Zhao et al. [69] demonstrated the importance of steric hindrance for solid membranes containing amines.

Moreover, KOH, when present in the membrane composition, can also act as mobile carrier, reacting with CO₂ to give potassium carbonate and bicarbonate (K₂CO₃ and KHCO₃) and the reaction for CO₂-carrier complex activation is given by the following equation [70]:



Water plays a key role for the transport mechanism, since it is involved in the reaction (Eq. 1.18) and it also enhances the ions and small molecules mobility, due to the water-induced swelling of the membrane matrix, whose highly hydrophilic nature is ensured by the large amount of amino groups present in the polymeric species.

In the past decade, several study highlighted that facilitated transport membranes are able to couple a large trans-membrane flux with high CO₂-selective feature [71,72] going beyond the previously mentioned solution diffusion trade-off. For 2 atm pressure conditions, Zhao & Ho [69] reported a CO₂ permeability slightly higher than 300 Barrer using only a fixed carrier (moderately hindered amines) together with a CO₂/H₂ selectivity close to 45 and a CO₂/N₂ selectivity of 340. Nevertheless, when part of the fixed carrier was replaced by smaller amine molecules [15] a significant enhancement of membrane performance was achieved (CO₂ permeability of 6500 Barrer and CO₂/H₂ selectivity of 340), highlighting the fundamental importance of the carrier mobility for the optimization of the facilitated transport. Similar results have been obtained by Zou et

al. [73], where both mobile and fixed carriers were present in the selective layer composition.

Unless the outstanding results obtained, stability remains the main issue of facilitated transport membranes, especially under high pressure conditions. Few authors [18,74] reported stable performance of these materials for a period of more than 400 h under low pressure conditions. However, high pressure conditions represent the biggest challenge for these particular membranes. Compaction of the selective layer could take place under such severe conditions [75], affecting drastically the separation performance and threatening the membrane integrity. At the same time carrier saturation phenomena [76] can also decrease the chemical contribution to the CO₂ transport, influencing necessarily the membrane efficiency. Bai & Ho [77] reported stable results for crosslinked PVA-based facilitated transport membranes at a feed pressure close to 30 bar, with a CO₂ permeability of 300 Barrer and a CO₂/H₂ selectivity of 18. Xing & Ho [78] showed very promising results for silica-modified PVA-POS membranes containing amines carriers at a feed pressure of 15 atm. However, no long term stability tests have been performed at the present time.

Facilitated transport membranes represent thus a very attractive outlook for membrane technology, mainly because of their ability to overcome the physical limits imposed to the other materials, which based their separation property on physical mechanism.

2. Mathematics of transport process

2.1 Diffusion in a plane sheet

2.1.1 Permeation analysis

Figure 1.2 represents the scheme of the diffusion process of gas molecules across a plane sheet, in absence of chemical interactions between the involved compounds. From the mathematical point of view, the system can be described by means of Fick's second law, for the particular boundary conditions (i.e. constant concentrations but different values at the two gas-membrane interfaces). In case of one-dimensional diffusion process, the problem can be addressed as follow:

$$\frac{\partial C_i}{\partial t} = D_i \cdot \frac{\partial^2 C_i}{\partial x^2} \quad (2.1)$$

$$\begin{cases} C(0, t) = C_i^u \\ C(\delta, t) = C_i^d \end{cases} \quad (2.2)$$

The complete solution has been proposed by Crank [79] and assuming the initial solute concentration $C_{i,0}$ within the membrane matrix negligible, the final expression is:

$$C_i(x, t) = C_i^u + (C_i^d - C_i^u) \frac{x}{\delta} + \frac{2}{\pi} \sum_{n=1}^{\infty} \frac{C_i^d \cos n\pi - C_i^u}{n} \sin \frac{n\pi x}{\delta} \exp\left(-\frac{D_i n^2 \pi^2 t}{\delta}\right) \quad (2.3)$$

where C_i^u and C_i^d are the penetrant concentrations at the gas-membrane interface in the upstream and downstream side respectively, t represents the time variable and δ is the selective layer thickness.

When the system reached the steady state ($t \rightarrow \infty$), the exponential term of the proposed solution vanishes and only the linear dependence is left to describe the concentration profile as a function the space variable. Hence, for the steady state conditions Equation 2.3 turns into:

$$\frac{C_i - C_i^u}{C_i^d - C_i^u} = \frac{x}{\delta} \quad (2.4)$$

which represents the linear concentration profile showed in the Figure 1.2.

The permeability definition given in Chapter 1 (Eq. 1.1) is obtained from the integration of Fick's first law for one-dimensional diffusion of the gas molecules [79], assuming the same conditions previously described. The solute flux is thus described as a product of the diffusion coefficient and the concentration gradient calculated on the thickness direction (Fig. 1.2):

$$J_i = -D_i \cdot \frac{\partial C_i}{\partial x} \quad (2.5)$$

Assuming a system with homogenous properties, D_i can be considered independent from the space variable, while the derivative term to estimate the concentration, C_i , can be calculated from Equation 2.5, thus obtaining:

$$J_i = D_i \cdot \frac{C_i^u - C_i^d}{\delta} = D_i \cdot \frac{\Delta C_i}{\delta} \quad (2.6)$$

where ΔC_i is the expression of the driving force of permeation. When the diffusion coefficient is not constant over the membrane thickness, a similar conclusion can be obtained considering an average value, $D_{i,average}$. Assuming no external mass transfer resistance and equilibrium conditions at both gas-membrane interfaces (so that $C_i^{eq} = C_i$ both for the upstream and downstream side), the solute concentration can be expressed as a function of the penetrant partial pressure, p_i , in the bulk phase by means of a thermodynamic partitioning coefficient, namely the solubility coefficient, S_i :

$$C_i^{eq} = S_i \cdot p_i \quad (2.7)$$

Equation 2.6 can be thus used to describe the penetrant concentration at both gas-membrane interfaces, even if commonly the solubility coefficient is different for the two boundary conditions. In case that an average solubility coefficient, $S_{i,average}$, is assumed, it is possible to calculate the driving force as:

$$C_i^{eq,u} - C_i^{eq,d} = S_{i,average} \cdot (p_i^u - p_i^d) \quad (2.8)$$

When the sorption isotherm is linear with the solute partial pressure, corresponding to a constant solubility coefficient, S_i , or if the downstream pressure is negligible compared to the upstream one and assuming a constant diffusivity with the thickness, Equation 2.6 leads back to Equation 1.8, which defines the solution diffusion mechanism.

Furthermore, the rate at which the solute is permeating at the downstream side gas-membrane interface is given by

$$J_i|_{x=\delta} = -D_i \left(\frac{\partial C_i}{\partial x} \right)_{x=\delta} \quad (2.9)$$

Substituting C_i from Eq. 2.3 and integrating the calculated flux respect to time, Equation 2.9 returns the total amount of gas permeated through the downstream surface, Q_t , at time t:

$$Q_i(t) = (C_i^d - C_i^u) \frac{t}{\delta} + \frac{2\delta}{\pi^2} \sum_{n=1}^{\infty} \frac{C_i^d \cos n\pi - C_i^u}{n^2} \left[1 - \exp\left(-\frac{D_i n^2 \pi^2 t}{\delta}\right) \right] \quad (2.10)$$

Considering a negligible concentration on the downstream side of the membrane and in the time limit approaching infinite values, Equation 2.10 turns into:

$$Q_i(t) = \frac{D_i \cdot C_i^u}{\delta} \left(t - \frac{\delta^2}{6D_i} \right) \quad (2.11)$$

The line described by Eq. 2.11 has an intercept at $Q_i(t) = 0$, defined as *time-lag*, θ_L :

$$\theta_L = \frac{\delta^2}{6D_i} \quad (2.12)$$

In Figure 2.1 a typical permeation curve is reported, showing the time lag extrapolation for the given steady state. The estimated values allows the diffusion coefficient calculation, hence the determination of the thermodynamic and kinetic contribution to the permeability coefficient.

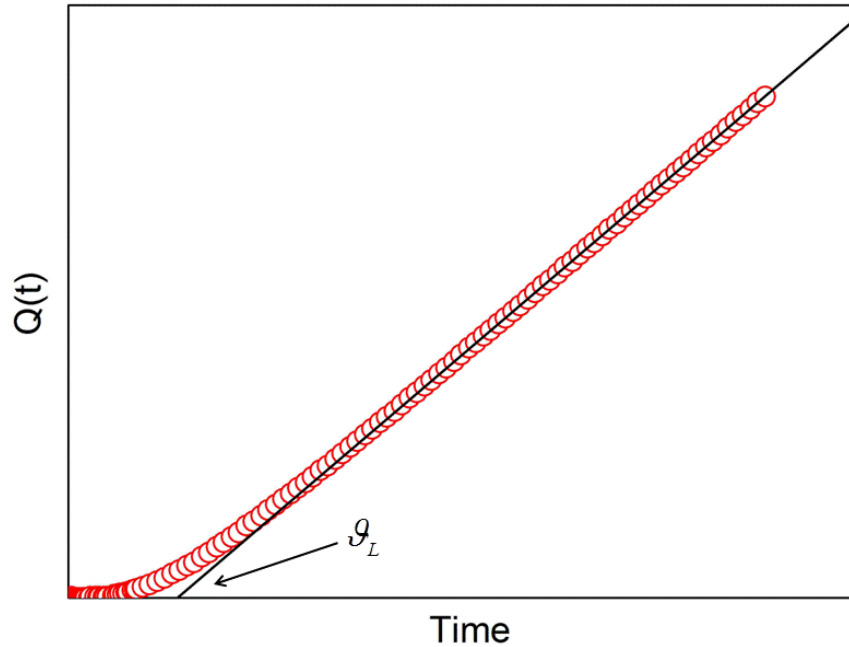


Figure 2.1 - Curve describing the permeated gas over time, showing the time-lag

2.1.2 Sorption analysis

When sorption measurements are performed the boundary conditions changes respect to the previous case, giving a different solution for the kinetics of diffusion of penetrant molecules in the specimen. Indeed, both slab's surfaces are exposed to the same pressure, hence the concentration value at the gas-membrane interface is kept constant, corresponding to C_i^E :

$$\begin{aligned} C_i(0,t) &= C_i^E \\ C_i(\delta,t) &= C_i^E \end{aligned} \quad t \geq 0 \quad (2.13)$$

Assuming that the initial solute concentration within the sample is equal to $C_{i,0}$, the solution of Fick's second law is proposed by Crank [79]:

$$\frac{C_i(x,t) - C_{i,0}}{C_i^E - C_{i,0}} = 1 - \frac{4}{\pi} \sum_{n=0}^{\infty} \frac{(-1)^n}{2n+1} \exp\left(-D_i \frac{(2n+1)^2 \pi^2 t}{4\delta^2}\right) \cos\left(\frac{(2n+1)\pi x}{2\delta}\right) \quad (2.14)$$

From the concentration profile by integration on the x axis, it is possible to calculate then the mass absorbed as a function of time, $M_i(t)$, that results to be:

$$\frac{M_i(t)}{M_{i,\infty}} = 1 - \sum_{n=0}^{\infty} \frac{8}{(2n+1)^2 \pi^2} \exp\left(-D_i \frac{(2n+1)^2 \pi^2 t}{4\delta^2}\right) \quad (2.15)$$

where $M_{i,\infty}$ is the final mass absorbed at the equilibrium condition.

The obtained relationship describes the diffusion kinetics in a sorption experiment and it is very helpful to determine the diffusion coefficient, starting from the experimental data, as it will be showed in the experimental part.

2.2 Diffusion with chemical reaction

When a reaction is involved in the kinetics of small molecules diffusion across a selective layer, the governing equations ruling the transport process must be updated, taking into account the reaction terms. Although the reaction scheme is usually rather complex, frequently a single overall reaction is considered to theoretically describe the process:



where A is the solute, B is the carrier and AB is the activated complex. Using this simplified approach, the solute A is absorbed at the upstream gas-membrane interface, reacts with the carrier giving the carrier-solute complex. As soon as the activated complex reaches the other membrane interface, it is de-complexed, the solute is desorbed on the downstream side and the carrier is immediately available for a new complexation. A scheme of the described transport is reported in Figure 2.1. Under these hypothesis and assuming a constant diffusion coefficient for all the chemical species involved, the one dimensional, steady state diffusion with reaction in an homogenous media [65] can be summarized as:

$$\frac{\partial C}{\partial t} = \frac{\partial^2 C_A}{\partial x^2} - k_f C_A C_B + k_r C_{AB} \quad (2.17)$$

$$\frac{\partial C}{\partial t} = \frac{\partial^2 C_B}{\partial x^2} - k_f C_A C_B + k_r C_{AB} \quad (2.18)$$

$$\frac{\partial C}{\partial t} = \frac{\partial^2 C_{AB}}{\partial x^2} + k_f C_A C_B - k_r C_{AB} \quad (2.19)$$

where C_A , C_B and C_{AB} are the solute, carrier and activated complex concentrations at the steady state, whereas k_f and k_r are the forward and reverse reaction constants respectively. The total carrier concentration C_T present in the membrane matrix is given by

$$C_T = C_B + C_{AB} \quad (2.20)$$

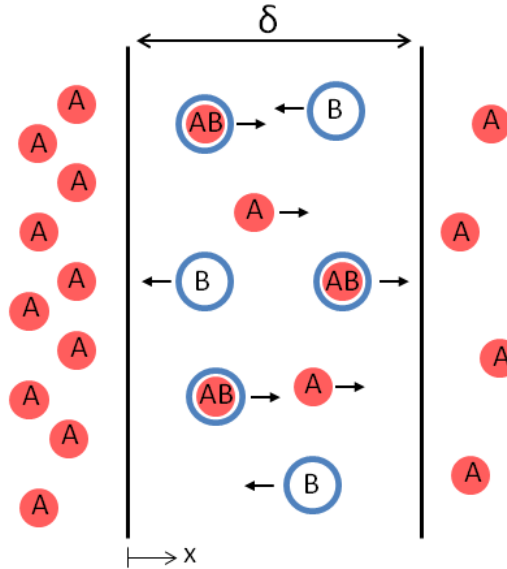


Figure 2.2 - Scheme of facilitated transport mechanism

In addition, assuming the hypothesis that the carrier compounds and the solute-carrier complexes are non volatile and are constrained to remain within the selective layer, the boundary conditions are:

$$\begin{cases} x = 0, C_A = C_{A0}, \frac{\partial C_{AB}}{\partial x} = \frac{\partial C_B}{\partial x} = 0 \\ x = \delta, C_A = C_{A\delta}, \frac{\partial C_{AB}}{\partial x} = \frac{\partial C_B}{\partial x} = 0 \end{cases} \quad (2.21)$$

However, despite the simplified approach (single overall reaction), a general solution cannot be obtained for the steady state of the system, due to the non linearity of the differential equations governing the transport process. Particular constraints must be applied to achieve a solution for the specific case, but they will be discussed at a later stage, in the modeling chapter.

3. Experimental

In the present chapter the samples preparation protocols and the experimental apparatus will be described. All the experimental work described in the present thesis has been developed in two different laboratories: the polyimide characterization has been performed in the laboratory of the Civil, Chemical, Environmental and Materials Engineering Department of the University of Bologna, whereas the synthesis and characterization of facilitated transport membranes was carried out at the William G. Lorie Department of Chemical and Biomolecular Engineering of the Ohio State University, during the period spent in Dr. W.S. Winston Ho research group.

3.1 Sample preparation protocols

3.1.1 Matrimid[®] 5218 Polyimide

The gas transport properties of a BTDA-DAPI polyimide (3,3',4,4'-benzophenone tetracarboxylic dianhydride and diaminophenylindane), whose commercial name is Matrimid 5218, supplied by Hunstman Advance Materials were deeply characterized. In Figure 3.1 the Matrimid structure formula is reported. The polymer, received in powder form, presents a T_g of about 320°C [80], an average molecular weight of 80000 g/mol [80] and a polydispersity index of 4.5 [81].

Self standing Matrimid films have been obtained through a solvent casting technique, starting from a 1 wt.% solution of polymer in high purity dichloromethane (DCM), provided by Sigma-Aldrich (anhydrous, purity $\geq 99.8\%$) [82]. A measured amount of solution was poured in a Petri dish, which was covered and left at room temperature for 24 hours in a clean hood in order to allow a slow solvent evaporation. The film was then detached from the Petri dish and the sample was dried in an oven under vacuum conditions for 24 hours, in order to ensure the complete removal of the solvent.

For the thermal treatment and aging characterization, four different temperatures, namely 50, 100, 150 and 200°C, were considered to investigate the effect of thermal history on

the membrane properties. Hereafter the samples dried at different temperatures will be indicated as Ma50, Ma100, Ma150 and Ma200, respectively. Moreover, the aging protocol consists in keeping the samples, before and after their characterization, into a controlled atmosphere chamber, purged with a N₂ stream to completely remove the water vapor, possibly present. The specimens were tested to investigate the CO₂ and CH₄ permeability immediately after the thermal treatment (48 h after casting) and then after 1000, 2000 and 3000 hours. For the thermal treatment and aging characterization, the specimens thickness was measured with a digital micrometer (Mitutoyo) with a precision of $\pm 1 \mu\text{m}$ and varies between 29-56 μm , with a standard deviation of 2-5 μm .

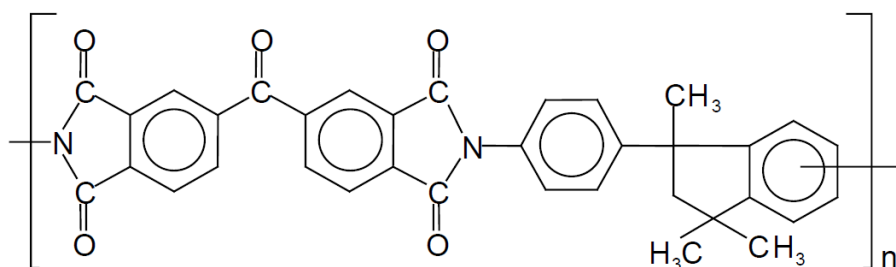


Figure 3.1 - Matrimid repeating unit

Considering the results obtained from aging study, the characterization of transport properties under humid conditions was performed on Matrimid samples, thermally treated at 200°C. For the permeation experiments, the thickness samples was measured by a digital micrometer (Mituyoto, precision of $\pm 1 \mu\text{m}$) and the values were about 25 μm with a standard deviation of 2 μm . For the density measurements, thicker samples were needed in order to decrease the experimental error related to the measurement. In this case specimen thickness was about 140 $\mu\text{m} \pm 2 \mu\text{m}$.

3.1.2 Facilitated transport membranes

In the present work, PVA-based facilitated transport membranes were studied in order to investigate their properties under high pressure conditions. Due to their outstanding mechanical property, amino-modified MWNTs have been added to the solid composition

as mechanical reinforcement, to prevent the compaction of the selective layer, reported to take place under high pressure conditions [19].

3.1.2.1 Materials

Polyvinylalcohol (PVA, Poval S-2217, 92% purity, MW 150,000, 87 – 89% hydrolyzed) was purchased from Kuraray America Inc. as a copolymer of vinyl alcohol and vinyl acetate, containing a minor amount of surfactant groups [83]. Potassium hydroxide (MW 56.11, KOH, $\geq 85\%$), glutaraldehyde aqueous solution (MW 100.12, 50 wt%), 2-aminoisobutyric acid (AIBA, 98%), 3-aminopropyltriethoxysilane (APTES, 99%) and ethylenediamine (EDA, $> 99.5\%$) were purchased from Sigma-Aldrich. Poly(allylamine hydrochloride) (PAA-HCl) with an average MW of 112,000 g/mol was purchased from Monomer-Polymer and Dajac Laboratories. Hydrochloric acid (36.5% – 38.0%, FW = 36.46), sulfuric acid (98%, FW = 98.08), nitric acid (2.6 M, FW = 63.01) and Acetone (99.7%, FW = 58.08) were bought from Fisher Scientific. AIBA and PAA-HCl were neutralized using KOH before usage by following the procedures reported in literature [69]. Lupamin[®] 9095, a commercial product from BASF, contains 7 wt% polyvinylamine (PVAm) and 14 wt% sodium formate in aqueous solution [84,85]. The PVAm in Lupamin[®] 9095 was purified using ethanol precipitation [86]. No further purification was carried out for all the other chemicals used in this work.

The MWNTs (Graphistrength[®] C100, 0.1 – 10 μm in length, 10 – 15 nm in diameter, and > 90 wt% purity) used in this work were gently provided by Arkema; nanoporous polysulfone composite supports (average pore size of 10 nm, thickness of 140 μm including non-woven fabric) was kindly provided by TriSep Corporation. Teflon supports (pore size ≥ 30 nm, thickness of 20 μm) were supplied by W.L. Gore & Associates. Feed gas cylinders of certified grades were purchased from Praxair Inc. The dry feed gas compositions used in this work are: 20% CO₂, 20.2% H₂, 59.8% CH₄ and 20% CO₂, 40% H₂, 40% N₂. Pre-purified argon was used as sweep gas.

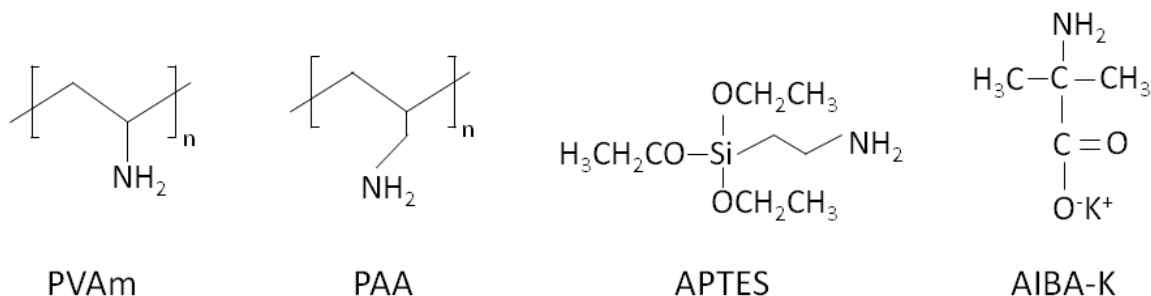


Figure 3.2 - Chemical structure of PVAm, PVA, APTES and AIBA-K

3.1.2.2 MWNTs amino-functionalization

The raw MWNTs were functionalized by bonding amino groups on the graphene walls and ending parts in order to increase their affinity with the hydrophilic membrane matrix.

The functionalization was carried out in two steps as showed in Figure 3.3.

At the beginning, 500 mg raw MWNTs were poured into a 120 ml acid-mixture (90 ml of H_2SO_4 and 30 ml of HNO_3 [87,88]) and the suspension was refluxed in a round-bottom flask at 120°C for 90 min. After the reaction, the suspension was cooled down to room temperature for 2 h. The residual acids were removed and the products were washed several times with reverse osmosis (RO) water in a vacuum filter using Teflon filtration membrane until the filtrate pH reached a constant value after consecutive washings. The resulting acid-treated MWNTs (AT-MWNTs) were dispersed in RO water using an ultrasonication bath (FS-30, Fisher Scientific) for at least 10 h until a limpid dispersion (~ 1 wt% AT-MWNTs) was achieved.

In the second step, the surface $-\text{COOH}$ and $-\text{OH}$ moieties on the prepared AT-MWNTs were further modified via condensation of small amine molecules to obtain the amino-functionalized MWNTs (AF-MWNTs) [89,90]. APTES was dissolved in acetone under stirring to prepare a 5 wt% solution. The APTES/acetone solution was then mixed with the prepared AT-MWNT dispersion at a weight ratio of 1:10 (APTES/AT-MWNT) and heated at 80°C for 30 min under vigorous stirring. Acetone was selected as the solvent for APTES instead of water to prevent fast polycondensation of $-\text{OH}$ groups in aqueous solution [91]. The aggregates formation would lead to the development of larger particles in the further functionalization steps. Finally, the reaction solution was ultrasonicated for 60 min, followed by centrifugation at 8000 rpm for 2 min to remove possible small

aggregates. The AF-MWNT concentration in the centrifuged dispersion was measured, normally within the range 0.6 – 1 wt%.

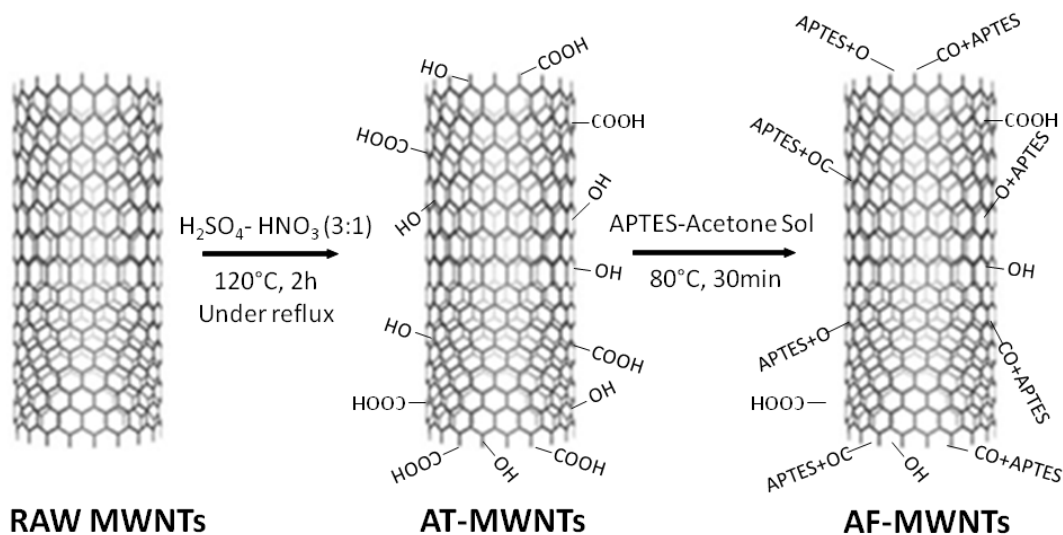


Figure 3.3 - MWNTs amino-functionalization

3.1.2.3 Membrane preparation procedure

Mixed matrix membranes were obtained by casting technique: the casting solution was prepared by homogeneously dispersing AF-MWNTs in crosslinked PVA/amines aqueous solution and then casted on a polysulfone composite support. After water evaporation, a thin mixed-matrix selective layer was formed on the support.

The polymeric matrix materials were synthesized by a two-step crosslinking reaction (Fig. 3.4). Initially, 3.3 g of PVA were completely dissolved in 18 g of water in a 250 ml flask and stirred for 24 h under mild stirring at room temperature overnight. One gram of APTES as well as a small amount (0.13 g) of HCl, needed to catalyze the reaction, was added to the aqueous PVA solution. The mixture was vigorously stirred at 80°C for 80 min. A sol-gel reaction took place via poly-condensation of the hydroxyl groups on PVA and silanol groups from APTES, generating a poly(vinylalcohol)-poly(siloxane) (PVA-POS) network [78]. PVA has been demonstrated to be very stable both in acid and alkaline environments [92].

The second step involves a based-catalyzed crosslinking reaction, using glutaraldehyde as crosslinking agent. Firstly, 2 g of KOH were added to increase the pH and then the aqueous PVA-POS solution was stirred for 15 min at 80°C. Afterwards, a stoichiometric

amount of glutaraldehyde was poured into the solution drop by drop under stirring to achieve a 100% crosslinking degree. The crosslinking reaction was carried out at 80°C for 2.5 h under vigorous stirring, able to prevent the occurrence of gel formation. As showed in Figure 3.4, the crosslinking takes place via condensation reaction and PVA is covalently linked due to intermolecular acetal linkages [18,78].

After stirring for 10 min, the mixture was ultrasonicated for 2 h to get the AF-MWNTs well dispersed in crosslinked PVA-POS solution. Based on the desired membrane composition, calculated amounts of polyamine solution, AIBA-K solution, KOH solution were sequentially added into the crosslinked PVA-POS/AF-MWNT mixed solution under vigorous stirring. AIBA-K (sterically hindered amine) and KOH acted as mobile CO₂ carriers. The long-chain polyamine (PAm) was used as fixed-site carrier and the performances of three polyamine structures (i.e., PAA, Lupamin[®]9095, and purified PVAm from Lupamin[®]9095) were evaluated. All the fixed carriers used in the present work belong to the unhindered amine family.

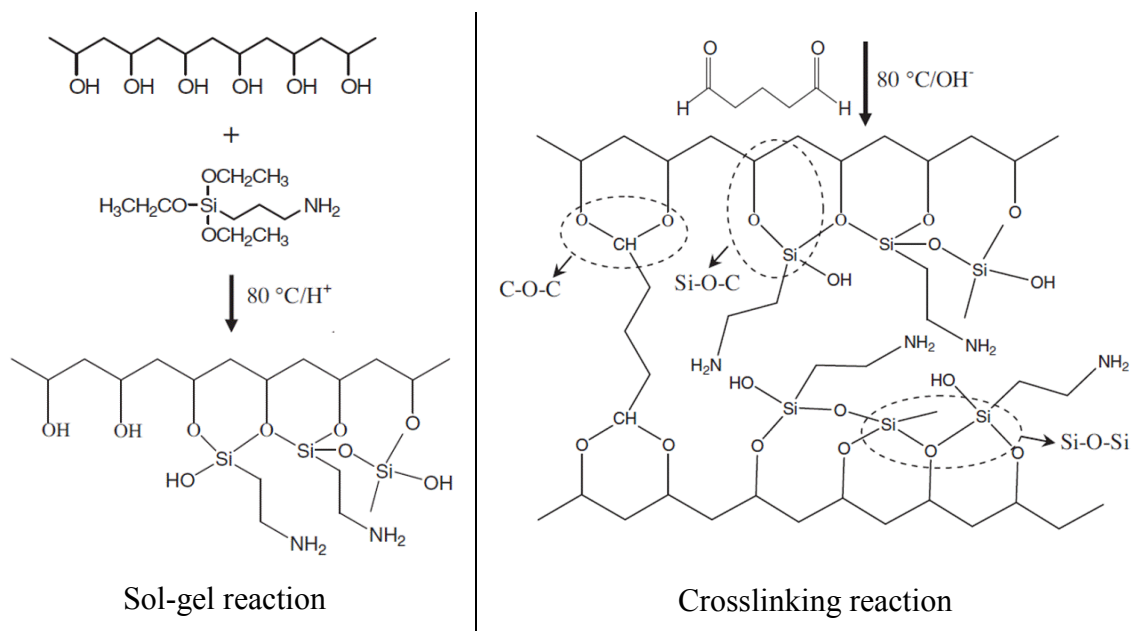


Figure 3.4 - Reaction scheme for the PVA-POS network [78]

The casting solution was prepared highly viscous in order to minimize the penetration into the pores of polysulfone support. In such a viscous solution, the residual

glutaraldehyde reacted actively with the long-chain polyamines to form high-molecule network, resulting in rapid gelling, even severe phase separation, in the casting solution. In this work, EDA was added into the casting solution (7 ~ 8 wt% of the total solid composition) to interrupt the reaction between glutaraldehyde and polyamine, making it possible to prepare a highly viscous, homogeneous casting solution without gelling [93]. In the end, the homogeneous casting solution was cast on a flat-sheet polysulfone composite support by means of a GARDCO adjustable micrometer film applicator (Paul N. Gardner Company) with a controlled gap setting. Water was then evaporated from the casted aqueous solution by convective air flow at 105°C for 20 min, followed by membrane curing in a muffle oven at 120°C for 6 h for the complete removal of water and complete the crosslinking reaction for PVA with glutaraldehyde. Due to its boiling point (108°C), EDA is believed to be completely removed during the curing process [93]. A sketch of the membrane preparation protocol is reported in Figure 3.5, whereas a complete list of the membranes composition is reported in Table 3.1.

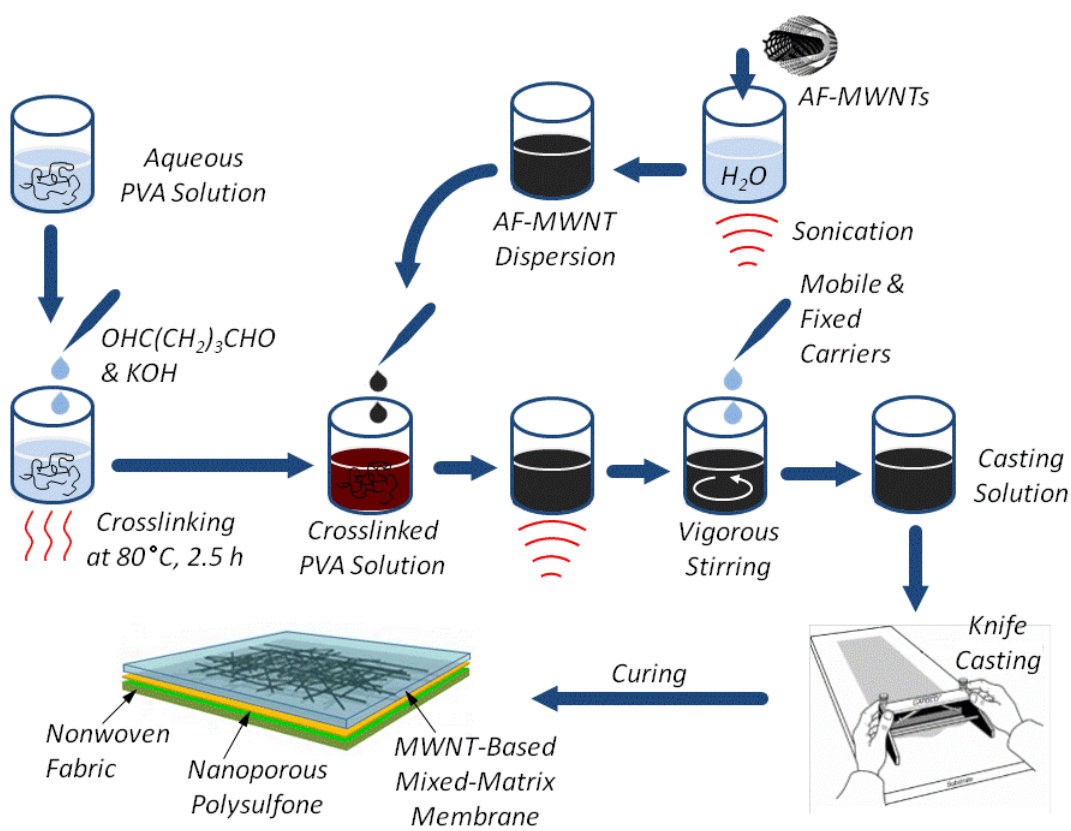


Figure 3.5 - Membrane preparation protocol (figure originally prepared by Dr. Yanan Zhao)

The total thickness of each solid membrane was measured by a Mitutoyo electronic indicator (Model 543-252B) with an accuracy of $\pm 0.5 \mu\text{m}$. The thickness of the selective layer was calculated by subtracting the polysulfone support thickness from the total thickness.

Sample	PAm	PVA (wt%)	AF-MWNTs (wt%)	KOH (wt%)	APTES (wt%)	PAm (wt%)	AIBA-K (wt%)	HM _w S (wt%)
S-01	A	20.2	2.1	19.0	5.4	22.3	31.0	32.9
S-02	A	20.5	2.2	16.8	5.2	23.6	31.7	33.5
S-03	A	22.8	1.9	19.3	0.2	28.2	27.6	32.3
S-04	B	20.9	2.2	17.6	5.3	24.4	29.7	37.0
S-05	B	23.6	2.4	14.8	4.9	29.3	25.0	42.9
S-06	C	25.2	2.5	19.4	5.2	20.9	26.8	51.3
S-07	C	24.1	2.4	17.7	5.0	24.0	26.7	53.2
S-08	C	23.3	2.3	17.1	6.1	25.8	25.4	55.2
S-09	C	24.0	2.4	16.3	6.1	26.4	24.8	56.5
S-10	C	23.7	2.4	16.5	6.0	26.1	25.4	55.8
S-11	C	23.6	2.3	16.7	6.3	26.2	25.0	56.0
S-12	C	24.2	0.0	17.1	6.4	25.5	26.8	56.1
S-13	C	22.9	6.9	15.6	5.8	25.2	23.6	53.9
S-14	C	23.6	2.3	10.6	6.3	46.4	10.8	76.2
S-15	C	23.6	2.3	21.4	6.3	46.4	0.0	76.2
S-16	C	23.6	2.3	26.8	6.3	41.0	0.0	70.8

Table 3.1 – Total solid compositions of MMMs synthesized in this work (polyamines, PAm: A = Lupamin[®], B = Purified PVAm, C = PAA).

3.2 Permeation

Several permeation experiments have been performed for the different materials presented in this work. In the paragraph, three permeation apparatuses, able to

characterize the membrane transport properties under different operative conditions, are described.

3.2.1 Dry gas permeation

The dry gas permeation apparatus allows to characterize the transport properties under dry conditions and in particular permeability and diffusivity of a particular penetrant can be measured. Hence, by means of the solution diffusion theory, also the solubility coefficient can be estimated.

The apparatus is based on a barometric technique in which diffusivity and permeability are evaluated by monitoring the pressure variations in a downstream volume V_d [94]. A layout of the apparatus is reported in Figure 3.6. The sample holder (Millipore high pressure filter holder, diameter 25 mm, filtration area $A = 2.2 \text{ cm}^2$) divides the system in two parts: the upstream high pressure side and the downstream low pressure side, whose volume is known from a previous calibration. The whole system is placed inside an incubator with a PID control system, which allowed a temperature management in a range from 25 up to 80°C with an accuracy of $\pm 0.1^\circ\text{C}$.

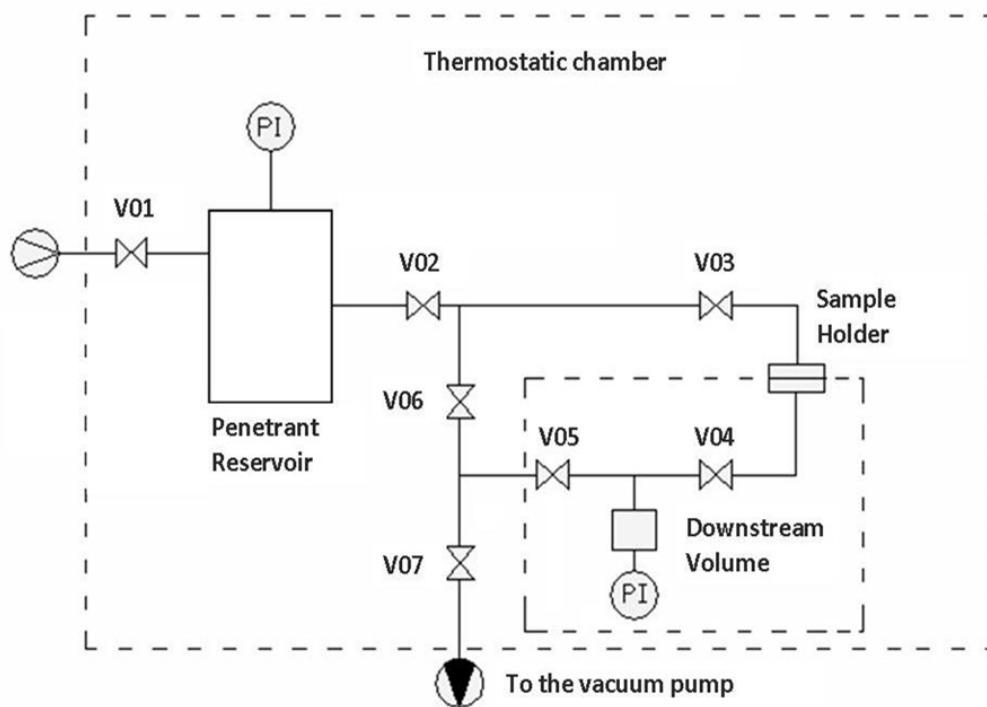


Figure 3.6 - Dry gas permeation apparatus [95]

After evacuating the sample completely and having performed a vacuum test to ensure the absence of leaks, the valves V05 and V06 (Fig. 3.6) are closed to isolate the samples from vacuum. Subsequently, valve V02 is opened, so that the upstream side of the membrane is exposed to the penetrant pressure, previously loaded in the reservoir, and the experiment begins. Simultaneously to the opening of valve V02, the acquisition software to monitor the downstream pressure variation is started, therefore the estimation of the characteristic time of diffusion is allowed. When steady state conditions are reached, the permeability is calculated from the permeability definition (Eq. 1.1), describing the molar trans-membrane flux by the variation of the downstream pressure through the ideal gas law:

$$P_i = \left(\frac{dp_i^d}{dt} \right)_{t \rightarrow \infty} \cdot \frac{V_d}{R \cdot T \cdot A} \cdot \frac{\delta}{(p_i^u - p_i^d)} \quad (3.1)$$

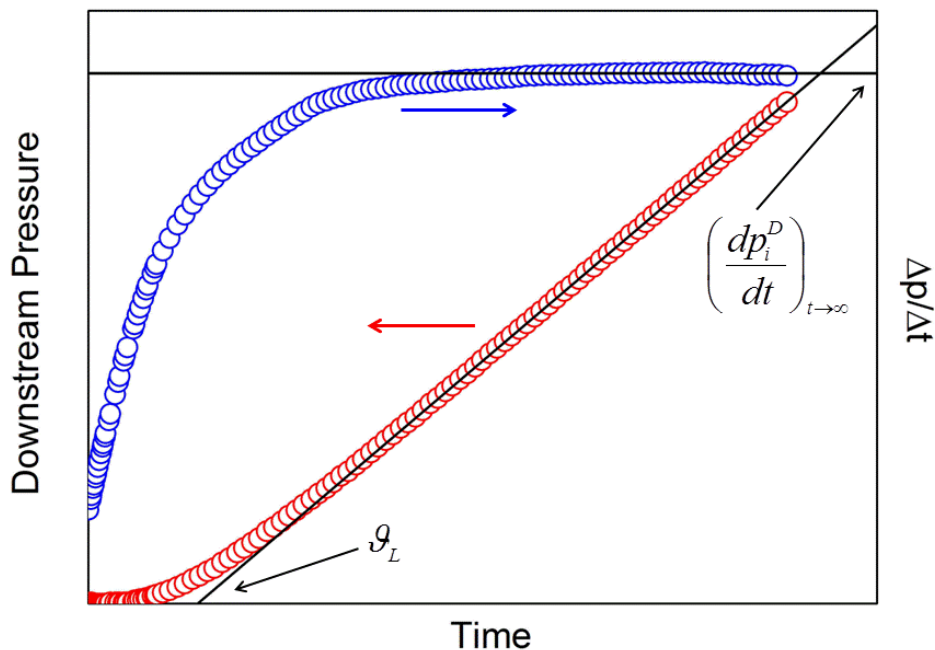


Figure 3.7 - Typical dry gas permeation experiment output

In Figure 3.7 a typical output from a pure permeation experiment is showed: the red dots indicate the variation of the downstream pressure over time as directly acquired from

manometer, whereas the blue dots represent derivative term calculated for a given pressure-time interval, chosen according to the process overall kinetics.

The present experimental set up allows also to analyze the kinetics of the transport process, to obtain the average diffusion coefficient through the so called time-lag method, theoretically described in paragraph 2.1.1. By means of Equation 2.12, the diffusion coefficient can be directly calculated from the measured data, estimating the ϑ_L from the best fitting line of the pressure variation with time (red curve), as showed in Figure 3.7.

3.2.2 Humid gas permeation

The humid gas permeation apparatus allows the evaluation of the gas permeability in a polymeric matrix in presence of a vapor in the permeation process. Similarly to the system described in the previous paragraph, the permeability measurement is based on a barometric technique and in particular on the evaluation of the pressure variation in the downstream side of the membrane. Water is the more common vapor used to perform this test, due to its frequent presence in the feed stream for many separation processes [51]. A scheme of the apparatus is reported in Figure 3.8 and a brief description of the test protocol will be discussed below.

After the sample is evacuated to ensure the complete solvent removal, the membrane is firstly conditioned with water, equilibrating the specimen at the water activity considered for the experiments. During the time needed by the membrane to reach the equilibrium conditions, a humid stream is created at the same water activity, by splitting the incondensable penetrant coming from the gas cylinder in two streams. One branch is saturated by bubbling into a reservoir filled with liquid water, and is subsequently mixed with the other dry branch. High precision flow controllers (dry branch FC01, wet branch FC02, Fig. 3.8), purchased from Bronkhorst (Model El Flow), allow to adjust the R.H. at the desired value, measured by an humidity sensor (Vaisala, HMT 330 Series). To prevent any effect on the membrane, the humid stream is created by flowing on the bypass circuit and released in the atmosphere (bypass valve V01, Fig. 3.8).

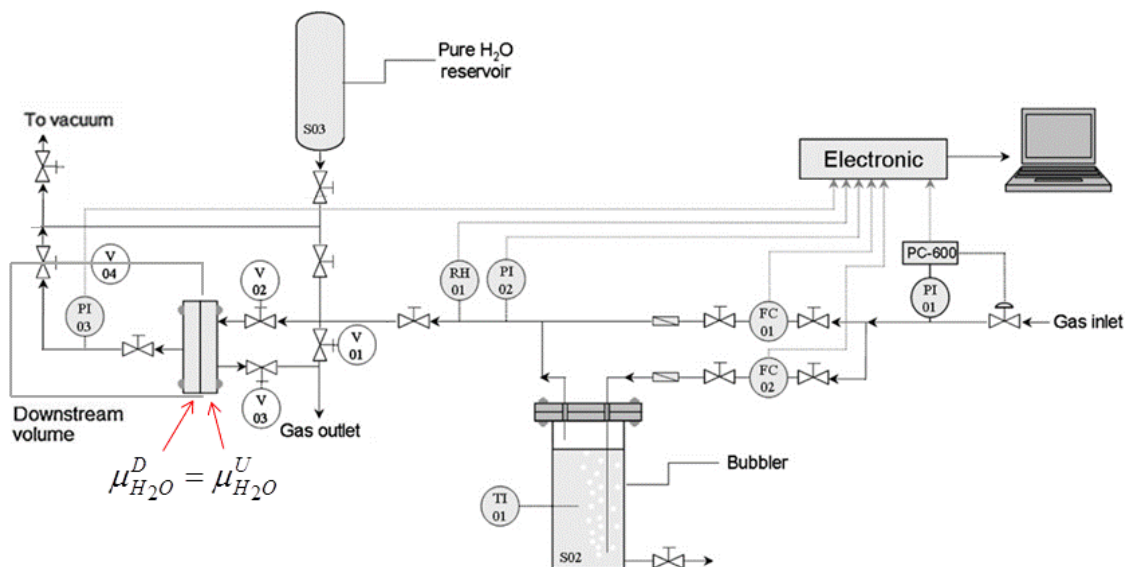


Figure 3.8 - Scheme of the humid permeation test apparatus (re-adapted from Ref. [53])

When the water sorption reaches the equilibrium, the upstream side of the membrane is washed with the humid stream previously created, closing the bypass valve and opening the valves V02 and V03. Simultaneously the acquisition software is started, in order to monitor the downstream pressure variation over time. A typical output obtained from the apparatus is reported in figure 3.9.

The initial transient phase undergone by the system is usually related to the slight differences between the R.H. value of the feed stream and the activity at which the membrane has been equilibrated. Hence, the initial pressure variation cannot be attributed specifically to any gaseous species present in the system. However, as soon as the water concentration within the membrane matrix will reach the real equilibrium condition with the activity of the feed stream (the time required is different for every single test), the H_2O chemical potential (μ_{H_2O}) will be equal on both sides of the membrane and the variation of the downstream pressure can be attributed only to the incondensable species. When the pressure variation over time reaches a constant value the permeability at the particular water activity can be calculated by means of the same formula used for the dry gas permeation apparatus (Eq. 3.1).

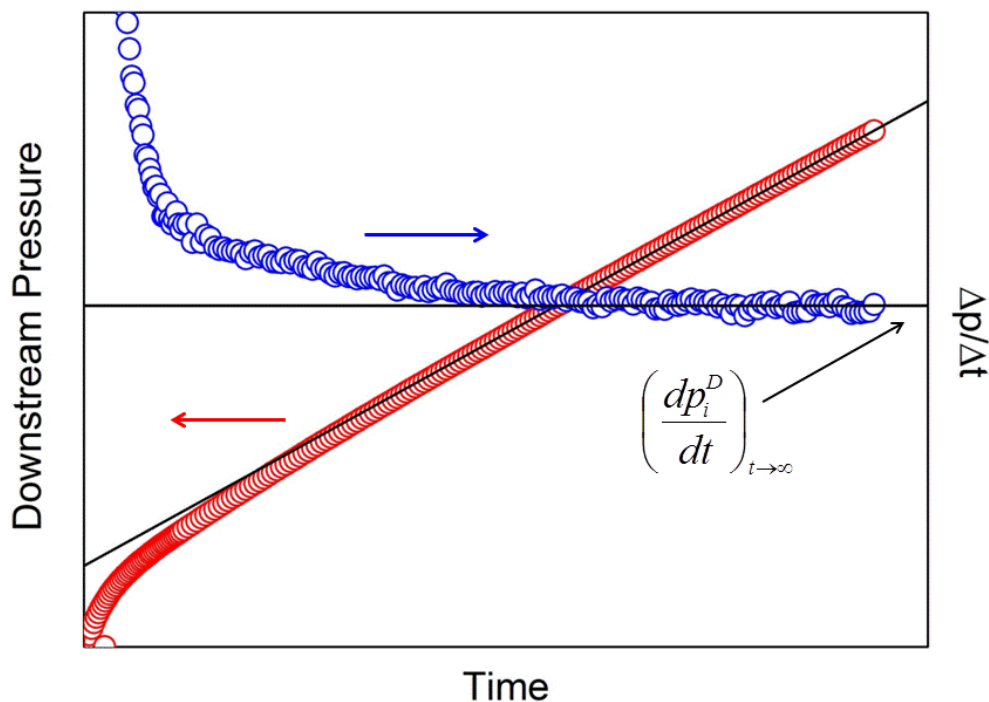


Figure 3.9 - Humid gas permeation experiment output

The scattering of the data showed by the flux (blue curve) at the steady state are mainly related to the vapor pressure adjustment due to very small and uncontrollable temperature fluctuations in the system, which affect necessarily the R.H. of the gaseous stream.

Both the dry and humid permeation apparatus have been used for the characterization of the Matrimid transport properties.

3.2.3 Mixed gas permeation

To characterize the performance of the facilitated transport membranes mentioned in the first paragraph of the present chapter, a mixed gas permeation apparatus has been used. Differently from the previous permeometers, permeability is evaluated measuring the gaseous streams concentrations by means of a gas chromatograph (GC). Indeed, the sample is continuously washed on the upstream side (feed gaseous mixture with different composition) and on the downstream side (sweep gas, Argon). After the sample holder, the obtained retentate and permeate streams concentrations are constantly analyzed for the entire duration of the test. In Figure 3.10 the layout of the apparatus is showed [96].

The membrane sample was held in a circular stainless steel cell with an active area of 5.7 cm^2 and tested with countercurrent flow pattern between the feed and the sweep sides in order to maximize the driving force across the membrane. The whole system was placed inside an oven with a very accurate temperature control (BEMCO Inc.). The dry gas flow rate was obtained by means of highly precise flow meters (Brooks Instrument) and set equal to $60 \text{ cm}^3/\text{min}$ and $30 \text{ cm}^3/\text{min}$ in the feed and sweep side respectively.

Both the feed-side and the sweep-side relative humidities were controlled by highly precise water pumps (Varian ProStar, Model 210). The liquid was mixed with the feed and sweep lines inside the humidifiers, previously packed with filling material in order to increase the mixing and ensure the achievement of the calculated R.H. values in the streams. The water flow rate was set differently according to the temperature, pressure and relative humidity conditions fixed for the specific test and they will be specified during the results description.

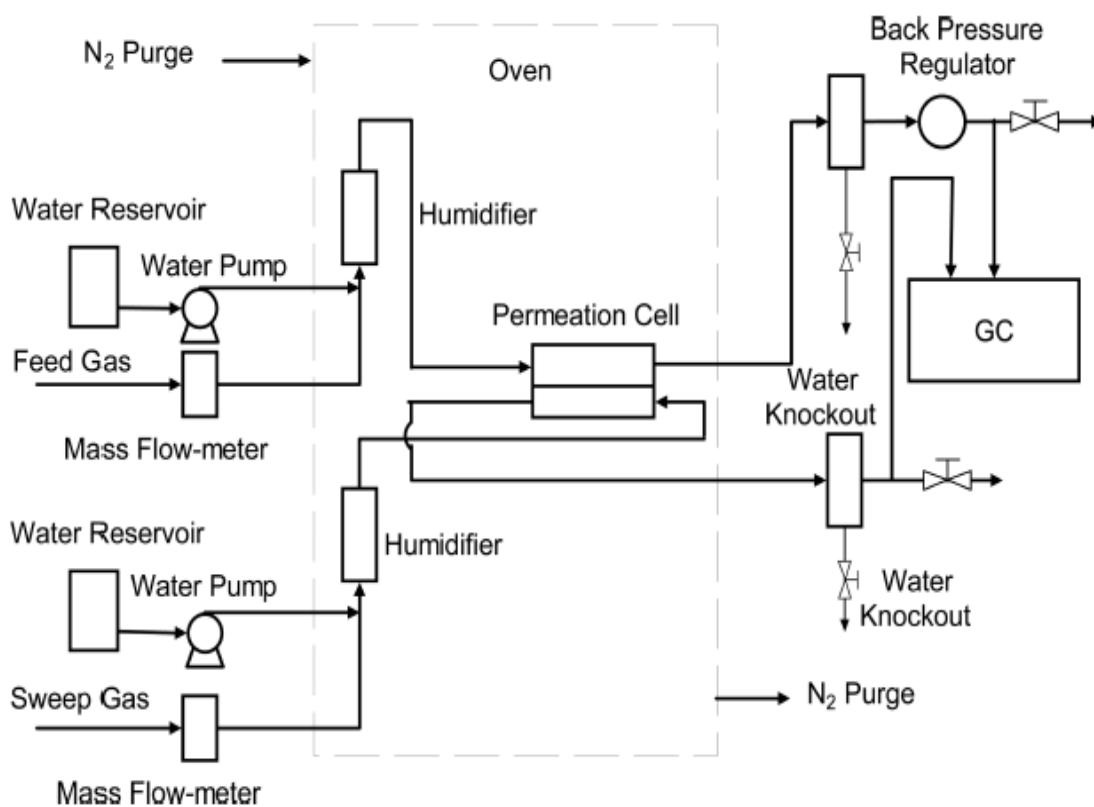


Figure 3.10 - Mixed gas permeation apparatus layout (originally drawn from Dr. Jian Zou)

The retentate and permeate side gas samples were analyzed by online gas chromatograph (Agilent 6890N) [18,69,78], using a micro-packed column Supelco Carnoxen 1004 (Sigma Aldrich).

For the permeability calculation, the logarithmic mean method (Eq. 3.2) was used to calculate the average pressure jump across the membrane:

$$\Delta p_i = \frac{(p_{i,feed\ in} - p_{i,sweep\ out}) - (p_{i,feed\ out} - p_{i,sweep\ in})}{\ln(p_{i,feed\ in} - p_{i,sweep\ out}) - \ln(p_{i,feed\ out} - p_{i,sweep\ in})} \quad (3.2)$$

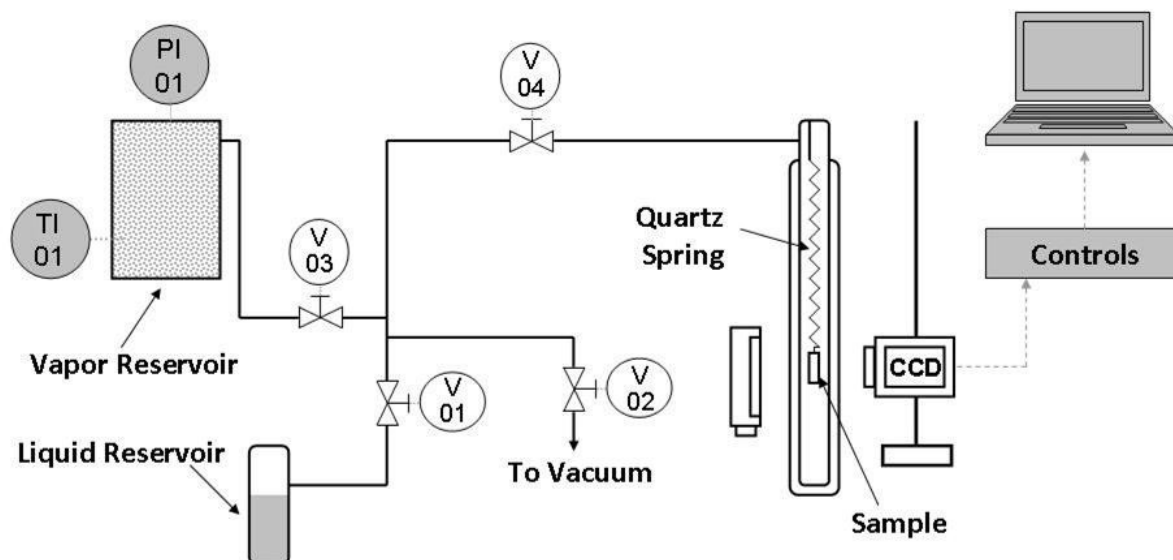
where the different gas partial pressure were obtained from GC measurements.

3.3 Sorption

The vapor sorption experiments are performed using the quartz spring microbalance apparatus (QSM), whose sketch is showed in Figure 3.11. The quartz spring is mounted inside a glass column endowed with a water jacket for temperature control. The sample is hanged on the spring hook by means of a sample holder obtained with an aluminum sheet wrapped with a copper wire. Before starting the test, the sample is evacuated overnight to ensure the complete removal of penetrants within the specimen matrix. To this purpose, a vacuum pump (Edwards, Model RV3) is used and a liquid N₂ trap is inserted on the vacuum line to avoid vapor condensation in the pump oil.

The liquid penetrant is stored in a 500ml volume and vaporized into a 4 L reservoir (vapor reservoir, Fig. 3.11) up to the desired pressure. Stainless steel tubes and valves allow connections between the different parts of the apparatus and to the vacuum system. A heating tape wrapped all around the manifold prevents the penetrant from condensing along the tubes. The spring, purchased from Deerslayer, has a sensitivity of 1 mm/mg and can hold a maximum load of 100 mg.

The sample behavior is monitored through a CCD Camera (Series 600 Smartimage sensors) manufactured by DVT Corporation equipped with additional lenses (25 or 35 mm) and some extenders to optimize magnification and focal distance during different experiments. A strobe led array illuminator, model IDRA-6, has been placed behind the glass column to achieve the optimal illumination and the maximum image contrast.



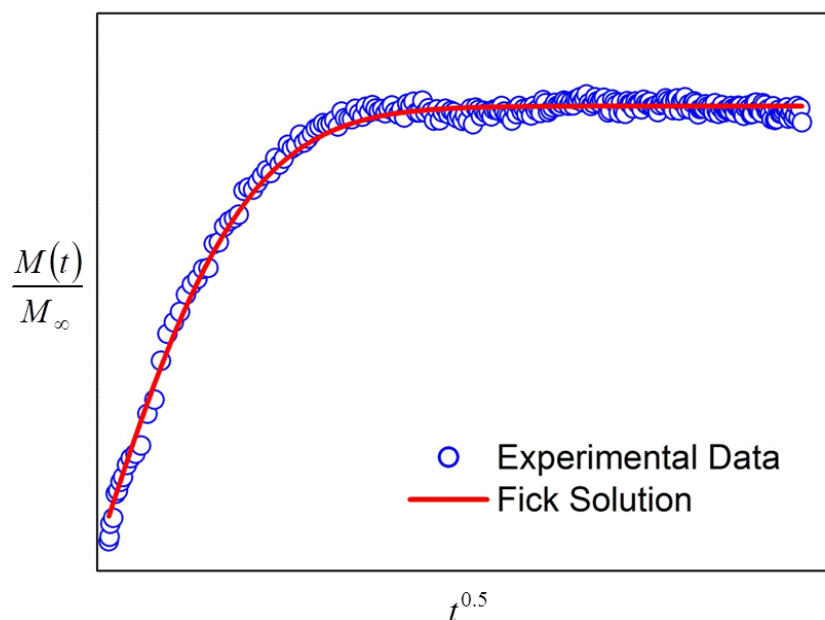
3.11 - Quartz spring microbalance layout

After a vacuum test is performed to ensure the absence of leaks, a certain penetrant is vaporized into the vapor reservoir reaching a certain pressure value, with the valve V04 closed in order to prevent sorption before starting the test. Once the vapor pressure is stable, the acquisition is started and the valve V04 is opened. Initially, due to the expansion the penetrant pressure drops down, but after few seconds reached a stable value, which remains usually constant for the entire duration of the single test. Absorbing the penetrant, the sample gains weight producing a spring elongation. Knowing the spring constant and monitoring the spring length variation with the camera, it is thus possible to correlate the number of pixels recorded by the CCD to the amount of vapor sorbed within the polymer matrix.

In Figure 3.12 a typical output of a sorption experiment is reported. The Fickian kinetics of the sorption process is evaluated based on the solution proposed by Crank, described in paragraph 2.1.3. With particular reference to Eq. 2.16, D_i can be directly estimated from the best fitting of the experimental data, obtaining an average diffusion coefficient for the given pressure jump. On the other side, solubility is calculated directly from the equilibrium value M_∞ and the initial mass of sample M_0 . The measure is commonly corrected taking into account the buoyancy, even though its influence in the present study

was generally negligible due to the very low vapor pressure used for the experiments and to the reduced sample size (~ 40 mg) placed on the hook of the spring.

Normally, the sorption isotherm is obtained by successive incremental steps, in which every time the pressure is increased of a certain amount. In addition, starting from the measured solubility and the estimated diffusion coefficient for the pressure increase between two consecutive steps, the permeability value can be calculated, according to the solution diffusion theory.



3.12 - Sorption experiment typical output

3.4 IR Spectroscopy

The IR spectroscopy has been used to detect the residual solvent present in the membrane matrix after different thermal treatment and to investigate the amino-functionalization of the MWNTs used in the facilitated transport membranes as a mechanical reinforcement.

For Matrimid study, absorbance spectra were taken from a Nicolet Avatar FTIR spectrometer (32 scan per spectrum with a resolution of 4 cm^{-1}), present in Bologna's lab. A small amount of polymer solution has been poured directly on the crystal and then the first spectrum has been taken after 24 h in order to reproduce the same conditions obtained before the thermal treatment. Being the FTIR crystal cell equipped with an

accurate PID thermal control, a T ramp (1°C/5 min) has been set to reproduce the heating rate of the oven used for the pretreatment. FTIR spectra were then taken at different T (namely 50°C and 150°C) to verify the presence in the sample of residual solvent.

To confirm and characterize the amino-functionalization of the nanoparticles added to the membrane composition, some functionalized fillers samples have been analyzed with an FTIR spectrometer (Nicolet 470). Due to the significantly high MWNTs absorbance of infrared rays [97], the samples have to be diluted with a certain amount of KBr, which is known to have a negligible absorption in the infrared spectrum. The solid samples of MWNTs and KBr are firstly pulverized and subsequently compressed in a pelletizer, in order to obtain a pellet suitable for the FTIR characterization. A weight ratio of 1:20 (MWNT to KBr) is used.

3.5 Density

The density of several polyimide samples has been determined by means of a buoyancy method, using a Sartorius analytical balance (readability 0.01 mg) and the Sartorius Density Kit YDK01 for density determination (Fig. 3.13).

Basically, the measure exploits the Archimede principle and in particular the polymer density is calculated starting from the specimen weight in air and in a fluid, with a known density. To minimize the errors related to the measurement, a liquid with a negligible sorption within the polymeric matrix must be utilized. In the present case, Dodecane was identified to be the optimal medium to carry out the test. Indeed, it has been showed that Matrimid samples immersed in such solvent displayed a mass variation lower than 0.3% after more than 1 h experiment [98].

The density calculation takes also into account the air buoyancy related to the metal wires composing the hanger, which remain outside the liquid. The formula adopted for the calculation is the following:

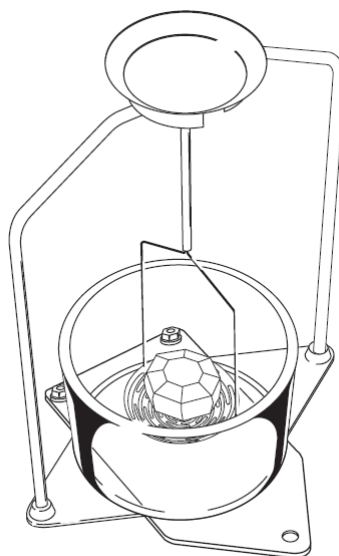
$$\rho_S = (\rho_L - \rho_A) \cdot \frac{W_A}{(W_A - W_L) \cdot CF} + \rho_A \quad (3.3)$$

where ρ_S is the density of the sample, ρ_L is the liquid density, ρ_A is the air density, W_A and W_L are the sample weights in the air and in the liquid respectively and CF is the

correction factors which takes into account the air buoyancy of the wires composing the hanger [99]. This correction is estimated on the basis of geometrical considerations on the hanging structure and is calculated as follow:

$$CF = 1 - 2 \frac{d^2}{D^2} \quad (3.4)$$

where d is the wires diameter and D is the becher diameter, which for the specific configuration are equal to 0.7 mm and 76 mm respectively.



3.13 - Sartorius Density kit layout

4. Results

In the present chapter, the experimental characterization obtained for the two considered materials will be reported. In the first part, the results observed, during a period of 6 months, for the different thermal treatments of polyimide samples will be presented. Subsequently, the protocol showing the best performance in terms of separation and stability will be adopted and the effect of water vapor on the gas transport properties will be illustrated for different gaseous species (CO_2 , CH_4 , N_2 and He). In order to achieve a throughout characterization, humid gas permeability tests and pure H_2O sorption experiments will be carried out. Finally, the CO_2 separation performance of the synthesized facilitated transport membranes will be examined, highlighting the key parameters able to ensure the membrane stability under high pressure conditions and to maximize the separation efficiency.

4.1 Aging and thermal treatment effect in Matrimid

As previously described, the structure of polymeric materials in glassy state is kinetically packed in a non-equilibrium condition, determining the presence of an excess free volume (Fig. 4.1), with respect to the real thermodynamic equilibrium [38]. Due to kinetic constraints, the additional free volume cannot rapidly rearrange to facilitate molecule transport, and for the diffusing penetrants it results as a sort of rigid nanoporous structure. The distance from the true thermodynamic equilibrium, however, is only a pseudo-stable condition, since it involves the presence of a driving force, which leads the structure to evolve over time towards the fully relaxed configuration. The molecular chains rearrangement, which are very fast in rubbers, are now hindered and they take place on a very long time scale with respect to normal experimental conditions.

The rearrangements rate obviously depends on the distance from the equilibrium, and in particular on the energy available to activate the chain motion. In this view, the process time scale can be accelerated by increasing the system temperature, due to the enhancement of the energy available for relaxation phenomena. As a consequence, the

physical properties of glassy polymers are thus affected by thermal history [41,50,100–102] and physical aging [39,44–46,103,104], which influence the amount of free volume of the polymer and necessarily also its transport properties, according to the FVT. In particular high temperature treatments and aging usually cause a densification of the polymer matrix, thus affecting negatively the membrane permeability, although a slight improvement of selectivity is usually observed. However since the increase of α is usually not enough to offset the productivity loss, the overall effect of such phenomena is a reduction of membrane performances. Understanding the effect of aging and thermal treatment on membranes materials is thus needed to evaluate their real potential for industrial applications.

In order to investigate the effect of thermal treatment and physical aging on polyimide materials, the gas transport properties of Matrimid ($T_g \sim 300^\circ\text{C}$) have been characterized after different curing temperature (50,100, 150 and 200°C) and aging time (48, 1000, 2000 and 3000 h). In particular CO_2 and CH_4 permeability and diffusivity have been measured at different operative temperature (35, 45 and 55°C) by means of a dry gas permeometer apparatus, allowing also the calculation of solubility coefficient, according to the solution diffusion theory.

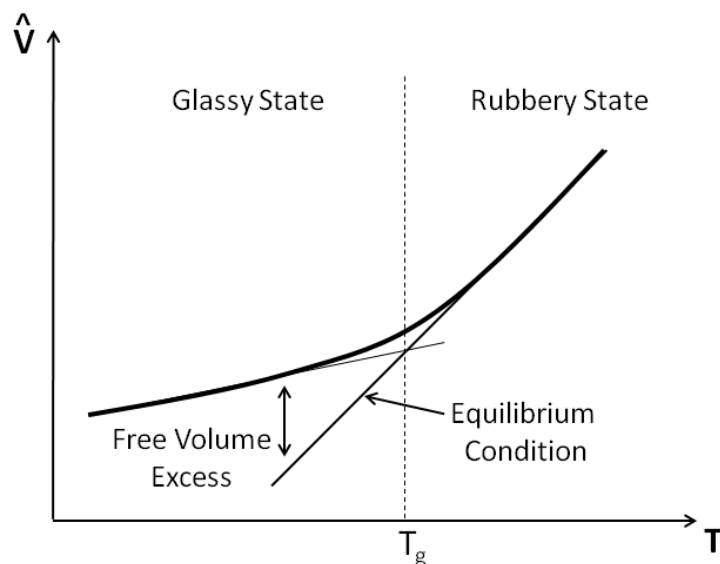


Figure 4.1 - Polymeric material specific volume as a function of temperature

4.1.1 Thermal treatment

The results obtained for un-aged samples, cured with different thermal protocols, are reported in Figure 4.2 and 4.3 for CO₂ and CH₄ respectively. The data show that the thermal history is clearly affecting the polymer transport properties: at 35°C, the CO₂ permeability drops from 17.9 Barrer observed in Ma50, to 11.8, 9.7 and 9.5 Barrer measured in Ma100, Ma150 and Ma200, respectively (Appendix, Table A.1). Permeability is thus constantly reduced by increasing the curing temperature up to 150°C, showing a 50% drop (Fig. 4.2). However, a further T increase (Sample Ma200) does not show any significant variation, suggesting that a sort of plateau for CO₂ permeability is achieved. As expected, by increasing the test temperature (45 and 55°C), permeability values increase for each pretreatment temperature considered. Clearly, similar trends were obtained at the three operative conditions as a function of pretreatment temperature. Analogous behavior was also observed for CH₄ permeability: at 35°C, the permeability of Ma50 sample was 0.46 Barrer, and decreased to 0.30 Barrer for Ma100 and to 0.24 Barrer for Ma150. Similarly to what observed for CO₂, also methane showed no significant changes between Ma150 and Ma200, at 35°C as well as at other test temperatures. Both CO₂ and CH₄ permeability of Ma150 and Ma200 samples are in good agreement with literature data, for those cases in which similar thermal pretreatment and casting procedures of the samples were carried out [105–108]. Indeed, it must be taken into account that also solvent used to obtain the casting solution can affect the transport properties [109] and DCM is reported to produce Matrimid samples with the highest permeability with respect to the use of other solvents such as dimethylformamide, dimethylacetamide or tetrahydrofuran. Indeed, due to its rather low boiling point, evaporation rate is faster for DCM than for the other solvents, resulting likely in a higher amount of free volume in the matrix, compatible with faster penetrant diffusion.

The diffusivity values obtained from time lag measurements (Eq. 2.12) are showed in Figure 4.4 and 4.5. All values are in the order of 10⁻⁹ cm²/s and are in good agreement with data usually observed in glassy polymers and in particular with those already available for carbon dioxide and methane in Matrimid [106]. As expected, the penetrant with the larger kinetic diameter (CH₄) showed lower value of diffusivity with relative differences even higher than those which could be observed for permeability, confirming

that the change in permeability due to thermal pretreatment or aging is mainly driven by the evolution of diffusivity rather than solubility coefficient.

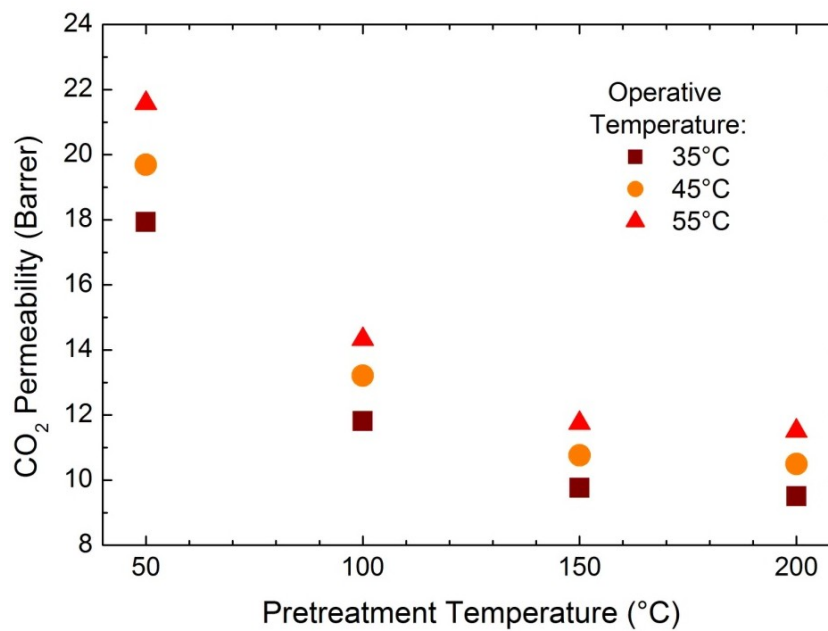


Figure 4.2 - CO₂ permeability of Matrimid for different thermal treatments ($p^u = 2$ bar)

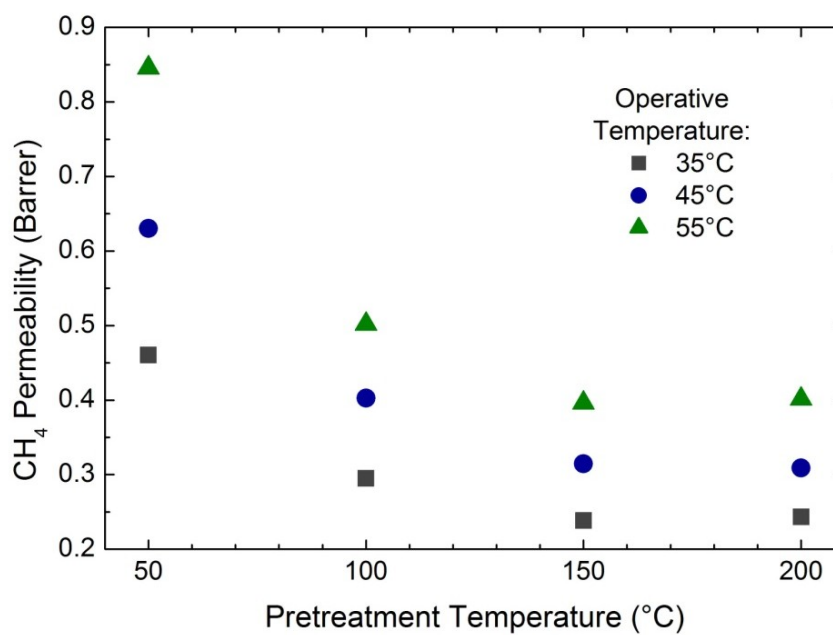


Figure 4.3 - CH₄ permeability of Matrimid for different thermal treatments ($p^u = 2$ bar)

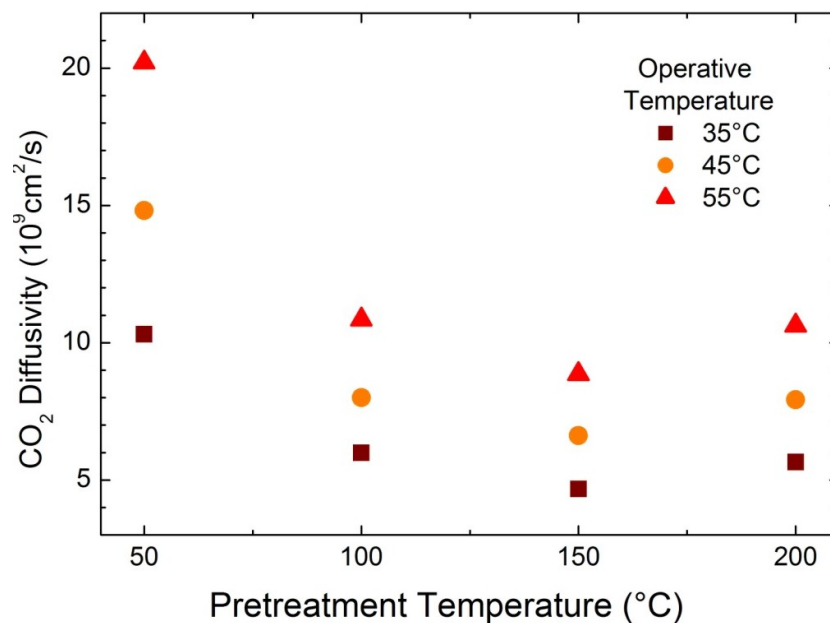


Figure 4.4 - CO₂ diffusivity coefficient of Matrimid for different thermal treatments ($p^u = 2$ bar)

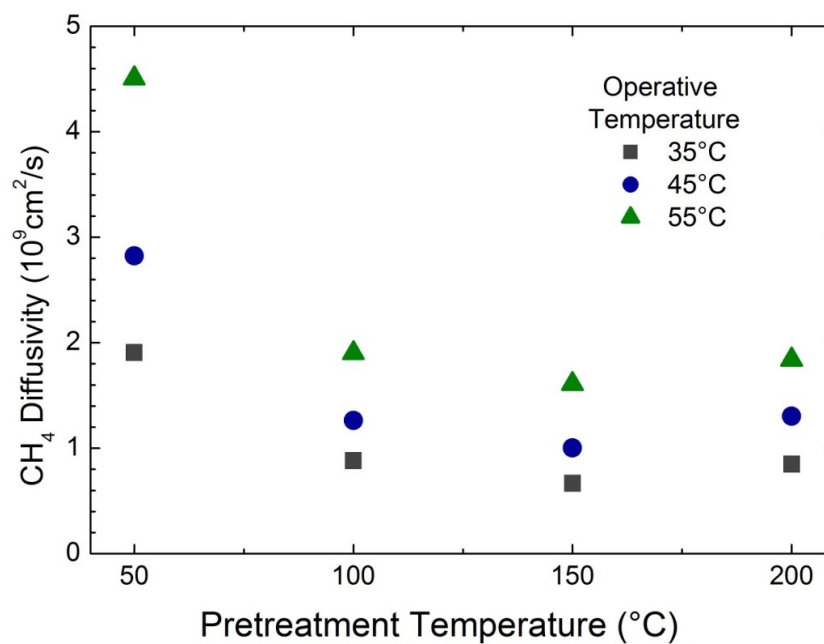


Figure 4.5 - CH₄ diffusivity coefficient of Matrimid for different thermal treatments ($p^u = 2$ bar)

The relative variation of diffusivity and permeability due to thermal pretreatment is reported in Figure 4.6 for the different sample inspected. The behaviors showed by diffusivity and permeability are very similar, with a large variation between from Ma50 and Ma100 and a generally minor changes between Ma100 and the samples treated at higher temperatures.

The experimental data set is particularly interesting because it shows substantial differences in the polymer properties even though the pretreatment was always conducted below the polymer glass transition temperature, where the relaxation phenomena are usually considered slow. However differences are definitely evident and suggest a well defined evolution of polymer free volume with the pretreatment conditions. The high flux observed in samples treated at the lower temperature seems thus to be related to a larger fractional free volume available in these specimens, which decreases when higher pretreatment temperatures are considered. In this concern, it is interesting to notice that Comer et al. [110] identified a secondary relaxation for Matrimid at 80°C, which can be responsible of the observed variation of transport properties with thermal treatment; the fact that the maximum changes in transport properties are observed between Ma50 and Ma100 samples therefore is fully consistent with that interpretation.

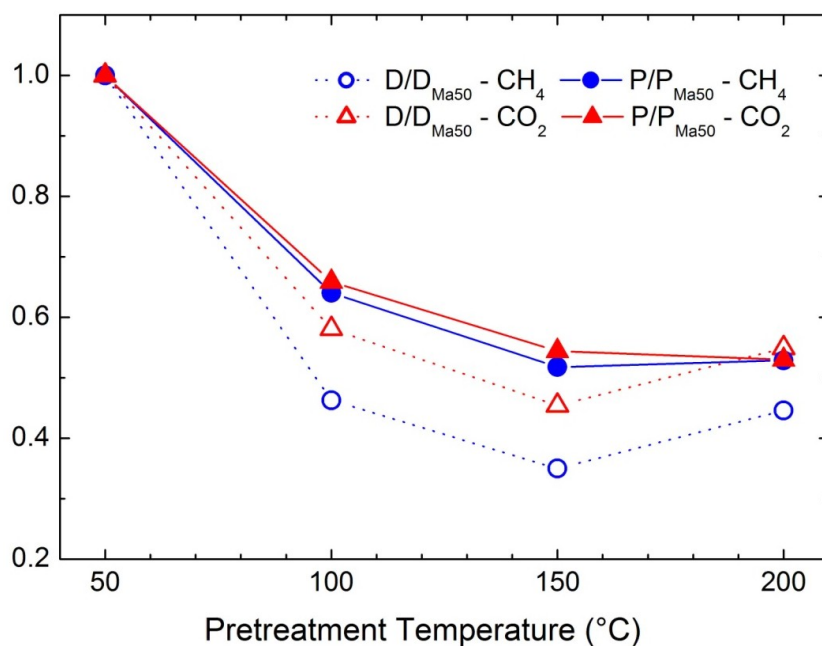


Figure 4.6 - Relative diffusivity and permeability as function of the treatment T (Operative temperature = 35°C)

As a possible alternative motivation for the observed behavior one could also consider that the solvent might not have been fully evaporated from the as-cast samples and is progressively removed as the pretreatment temperature is increased. Joly et al [111] disclosed that the gas transport properties of polyimides can be greatly affected by the presence of residual solvent within the polymer matrix. FTIR analysis has been carried out to investigate the presence of residual solvent within the matrix and the results are showed in Figure 4.7. At first, a spectrum of the solvent has been taken (black line). Afterwards, a Matrimid sample was casted on the FTIR crystal, as described in paragraph 3.4. A spectrum of the polymer was taken after 24 hours from casting, to reproduce the experimental condition after solvent evaporation (red line). Subsequently, a temperature ramp was set up to 50°C and a spectrum was taken after 24 hours treatment, in order to re-create the oven condition (blue line). The same procedure was repeated for a higher temperature (150°C), to evaluate possible differences between the two thermal treatments (green line).

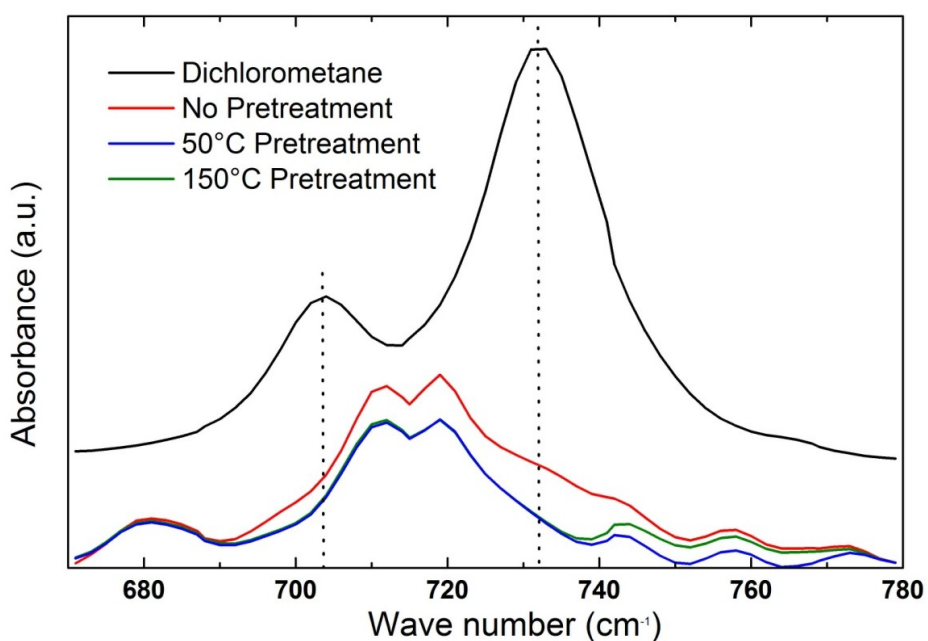


Figure 4.7 - FTIR spectra of DCM and untreated, Ma50 and Ma150 samples

Comparing the spectra of the untreated and the 50°C cured polymer in the DCM characteristic region (680–770 cm^{-1}), it is evident that a considerable amount of solvent

has been removed by the considered thermal treatment from the polymer matrix, as could be expected considering the boiling point of the solvent (39.6°C). Indeed, the Ma50 spectrum shows a marked decrease in correspondence to the DCM characteristic peaks wavenumber. Increasing the treatment temperature to 150°C, no further solvent removal was detected via FTIR measurements. Thus the decrease of permeability with increasing the thermal treatment conditions suggests that relaxation phenomena dominate over any possible effect related to the residual solvent removal.

In Figure 4.6 it is also noted that the decrease of the diffusion coefficients of both CO₂ and CH₄ is larger than the parallel decrease in the permeability values, so that an increase of the solubility coefficient is also associated to the thermal treatments. The observed effects on diffusivity and solubility as well as the differences between CO₂ and CH₄ are not simple to rationalize and to relate univocally to well identified structural variations. Many authors [49,102,112] reported for different polymers that the variation of the permeability value due to a reduction of fractional free volume is related to a decrease of both the diffusivity and the solubility coefficients. However, while this behavior is completely general for diffusivity, in case of solubility several exceptions have been reported and usually related to the decrease of free volume associated to a more complex relaxation phenomena: e.g., Laot et al. [50] presented a decrease of diffusion coefficient and a simultaneous increase of the solubility in polycarbonate samples subject to different cooling rate, attributing the behavior to a change of the molecular chains mobility. Furthermore, Vaughn et al. [47], studying the annealing effect on a polyamide-imide membrane, suggested the occurrence of a thermally activated planarization process of polymer chains. In particular, they reported the overcoming of the rotation energy barrier for the bond between a phenyl group and the imide group, which happens to be present also in the chemical structure of Matrimid. The different configuration leads to a redistribution of the fractional free volume inside the polymer matrix, affecting the transport properties of the material in a way which resembles the one here reported. It is therefore possible that in the present work the structural relaxation suggested by the data is not just related to a decrease of free volume but to a more complicated rearrangement and to a stiffening of the polymeric chains.

Comparing the behavior of the two gases, the different pretreatments always induce higher variations, i.e. decrease in permeability and diffusivity, for methane than for CO₂. As a consequence, the ideal selectivity of CO₂ vs CH₄ is slightly enhanced at higher pretreatment temperature, as it can be seen in Figure 4.8 where selectivity is reported in the Robeson's plot for all sample and test temperatures investigated. The samples pretreated at the lower temperature are closer to the upper bound curves and thus exhibit the best performance for the CO₂/CH₄ separation; the increase in selectivity at higher pretreatment temperature, indeed, is not high enough to counterbalance the permeability drop observed for those samples [30,31,113,114].

From Figure 4.8 it is also possible to notice that CO₂/CH₄ selectivity is not favored by the increase of the operative temperature, similarly to what reported for other polymers and polyimides [115]. Indeed, a T increase corresponds commonly to an enhancement of gas permeability, due to the positive effects on the diffusion coefficient related to a higher molecular chains mobility. However, methane, endowed with the larger kinetic diameter, undergoes a larger increment compared to CO₂, determining a decrease of α_D (diffusivity selectivity, Eq. 1.15); simultaneously, the CO₂ solubility coefficient is reduced by the T increase to a larger extent if compared to CH₄ [82], with a consequent decrease of α_S (solubility selectivity, Eq. 1.15). The negative variation of the two factors (α_D and α_S) results in the lowering of the overall membrane selectivity.

As a consequence of the two simultaneous effects (on permeability and on selectivity), the T increment corresponds to the reduction of the membrane separation performance, inasmuch as the increase in permeability is not enough to offset the loss in selectivity of the membrane.

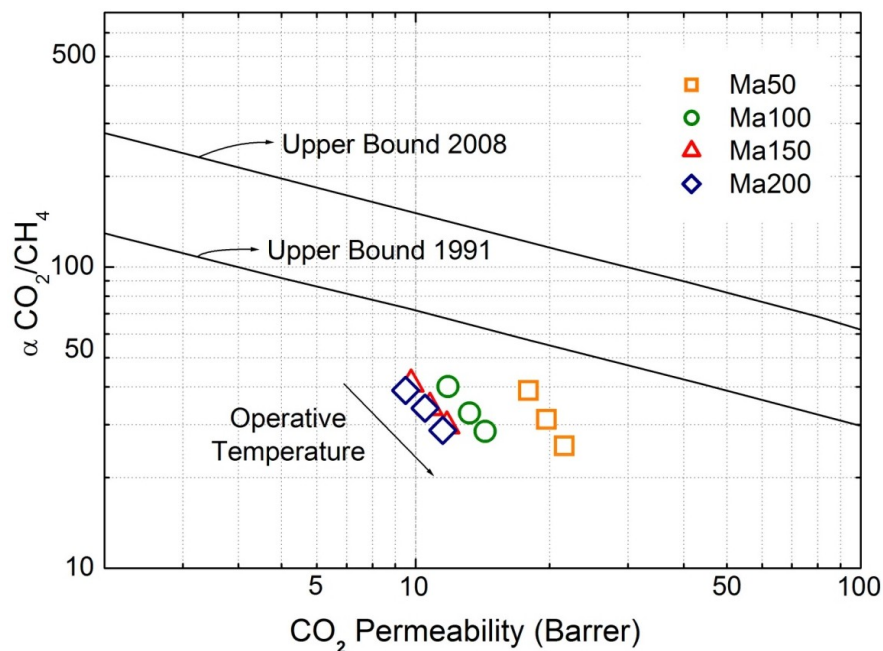


Figure 4.8 - Robeson Plot of Matrimid pretreated at different temperatures

The permeability values obtained at the three operative temperatures follow a clear Arrhenius-type of behavior (see Chapter 1, Eq. 1.5) for each thermal treatment, with a coefficient of determination of the linear regression always larger than 0.99 (Fig. 4.9 and 4.10). The activation energies and the Arrhenius pre-exponential factors for CO₂ and CH₄ obtained at different thermal pretreatment are reported in Figure 10. As expected, the penetrant endowed with the larger kinetic diameter shows the higher activation energy values. The activation energy of CO₂ permeation is not significantly affected by the thermal treatment, with an average value of 7.9 kJ/mol, while a slight activation energy decrease is observed for methane with increasing pretreatment temperature. For the latter penetrant E_p varies from 25.6 kJ/mol for Ma50 sample to 21 kJ/mol for the specimen treated at the higher temperature. The pre-exponential factor, on the other hand, shows more pronounced decrease for both penetrants; for CO₂, in particular, a decrease of 41% is observed between the samples pretreated at 50°C and at 200°C, whereas for CH₄ the change is even more significant, close to one order of magnitude. Consistently with the free volume theory, the decrease in P_0 is associated to a free volume decrease (see Chapter 1, Eq. 1.4), which affects to a higher extent the penetrants with the larger kinetic diameter.

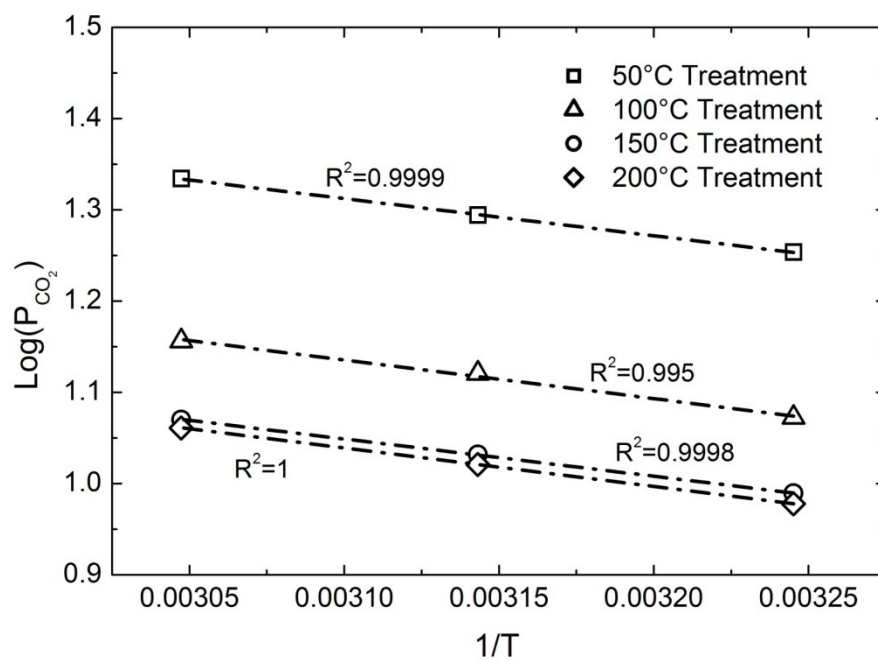


Figure 4.9 - Temperature influence on the CO₂ permeability for the samples pretreated at different T

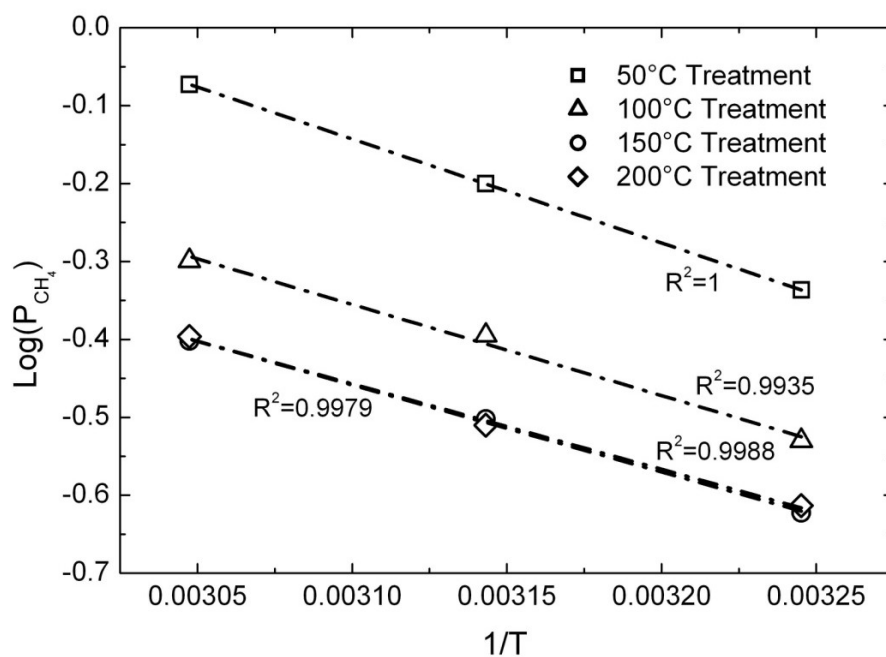


Figure 4.10 - Temperature influence on the CH₄ permeability for the samples pretreated at different T

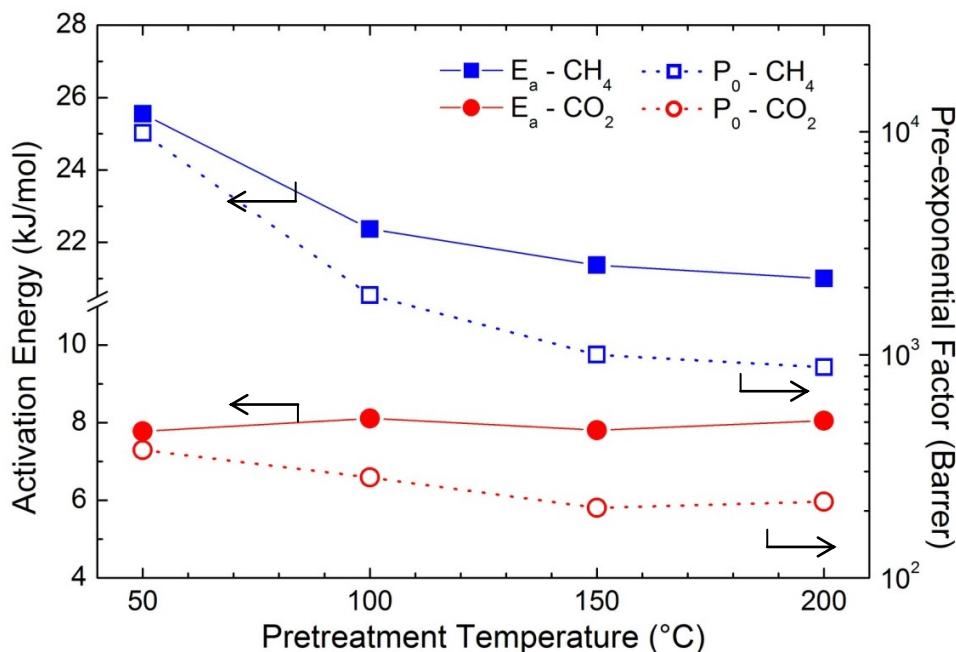


Figure 4.11 - Activation energy of permeation and pre-exponential factor vs the pretreatment temperature.

4.1.2 Aging

The effect of aging on the gas transport properties of Matrimid was monitored for more than 3000 hours repeating the permeation experiments about every 1000 h from the sample casting. The variation of CO_2 and CH_4 permeability at 35°C is showed in Figure 4.12 and 4.13 as function of aging time, for the four different pretreatments; the complete set of data obtained during the experimental campaign is reported in Table A.1. The Ma50 sample exhibits a faster aging rate compared to the other specimens, with an overall permeability decrease of 25% during the investigated period. Conversely, a different behavior is observed for the samples treated at higher temperature: a limited decrease in permeability was obtained for Ma100 specimen, whereas no significant variation of the transport properties was detected for Ma150 and Ma200 membranes for the entire duration of the aging study. Similar trends were also obtained for the other two test temperatures of 45 and 55°C .

These results are in agreement with the general interpretation, previously presented, for the behavior of permeability and diffusivity of un-aged samples. The samples with the larger departure from equilibrium conditions is subject to the faster aging; its evolution

over time leads to a configuration progressively closer to those initially obtained by higher temperature pretreatments, which in turn results more stable during the investigated period of time. Indeed, after almost 3000 hours the CO₂ permeability of the Ma50 sample ends up very close to the value observed for the un-aged (tested within the 48 hours after their thermal treatment) Ma100 sample which, on the other hand, shows much more stable transport properties. The permeability measured in Ma150 and Ma200 samples appears as the long time asymptotic value for aged Matrimid.

In parallel, the aging protocol seemed also to affect materials mechanical properties, beyond permeability and diffusivity. More precisely, the different samples became progressively more fragile and some of them even broke before the end of the study. In particular Ma100 samples could be studied only until 2208 hours, since all of the specimens fractured after the second and third set of tests (1000 and 2000 h) and no samples were left to proceed with further tests at longer times.

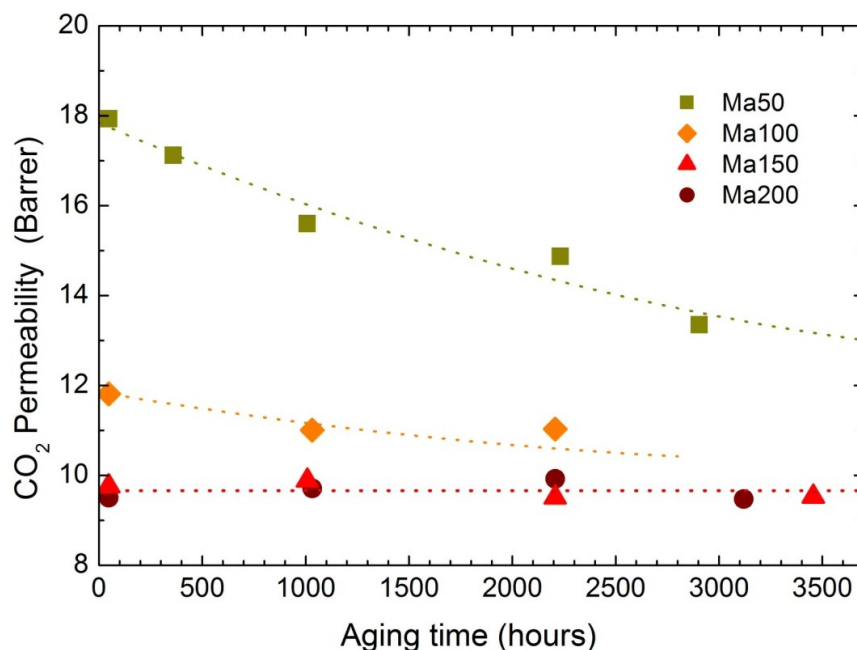


Figure 4.12 - CO₂ permeability for different thermal treatments as function of aging time (35°C, 2 bar). The dashed lines do not represent any analytical model, they are just use as guidelines

By comparing the behavior of different gases, it can be noticed that also with aging time the variation of CH₄ permeability is more marked than that of CO₂, for the samples treated at the lower temperature, which shows a 34% decrease for methane but just a 25% decrease for CO₂. As a consequence, a slight increase of the CO₂/CH₄ selectivity is

observed for the aged sample treated at 50°C. Therefore, the evolution induced by aging time and the changes induce by the different pretreatment temperatures follow a parallel path in the polymer structures, which cause in both cases a decrease in permeability and a slight increase in selectivity.

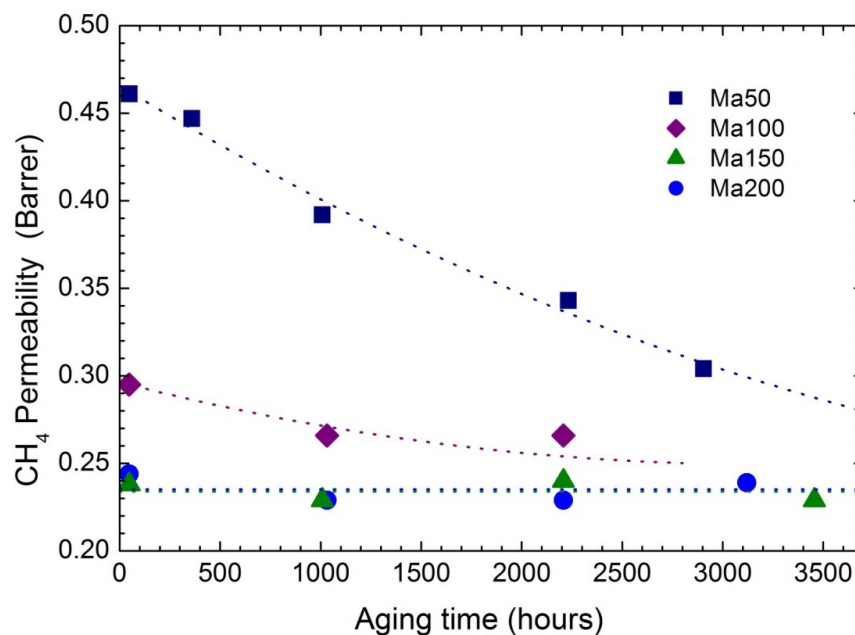


Figure 4.13 - CH₄ permeability for different thermal treatments as function of aging time (35°C, 2 bar). The dashed lines do not represent any analytical model, they are just use as guidelines

Also the behavior of diffusion coefficient undergoes significant changes (Appendix, Table A.1) similar to those observed for permeability, but it is more affected by aging time than permeability. Indeed, in case of CO₂, D decreases by 52% after 3120 hours aging, whereas for CH₄ an even more significant decrement is observed, with a reduction of 68% of the initial value. Analogous results were detected also at the other inspected temperatures. Therefore, also for gas diffusivity in Ma50 samples the effects of physical aging are similar to those induced on the polymer matrix by the thermal treatment. The similar relative decrease observed for both permeability and diffusivity suggests that thermal treatment and aging time have an analogous effect on the structural properties of the polymer, related to the reduction of the fractional free volume.

Likewise in the case of aged samples, the temperature dependence of gas permeability follows rather closely an Arrhenius-type behavior, with a coefficient of determination

always higher than 0.988, allowing a reliable evaluation of permeability activation energy and pre-exponential factor. The time evolution during the aging period of the activation energy and the pre-exponential factor in Ma50 sample are showed in Figure 4.14. The value of E_p for CO_2 is not significantly influenced by the aging phenomenon, since no change was observed during the whole time period investigated. Conversely, as in the case of the thermal treatment, the CH_4 activation energy showed a slight decrease over aging time, varying from an initial value of 25 kJ/mol to 23 kJ/mol after 2904 hours aging.

Results in line with what observed in the case of the effect of thermal treatment were obtained also in case of the pre-exponential factor for permeability, P_0 , of Ma50 samples which decreased significantly over time. In particular, similarly to what already observed for different thermal treatments, the effect transport properties are more relevant for CH_4 than for CO_2 . A reduction of P_0 of about 75% of the initial value (from 9900 to 2500 Barrer) is detected for methane permeability, while for the CO_2 the decrease is limited to a less than 35%, from 370 to 250 Barrer. Again, the marked decrease of the pre-exponential factor is a clear indication that the fractional free volume is reducing inside the polymer matrix, due to polymer chains rearrangement.

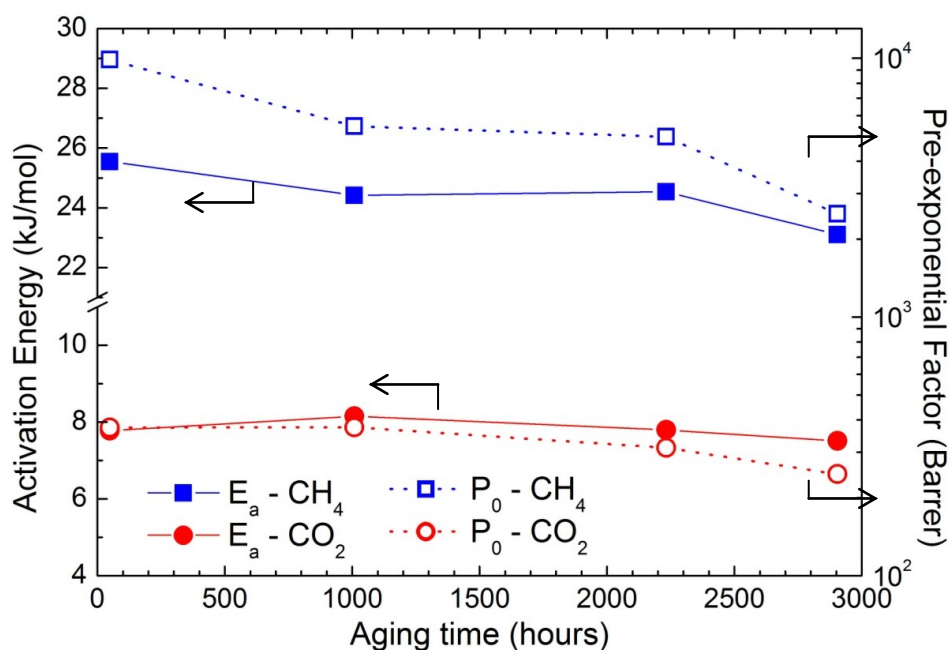


Figure 4.14 - Activation energy of permeation and pre-exponential factor vs of aging for Ma50

4.2 Water vapor effect on gas permeability in Matrimid

Water is a minor compounds frequently present in several separation processes and, as previously discussed, it can affect the permeation of small penetrants across the membrane in different ways. So, the study of H₂O influence on the gas transport properties is a fundamental aspect which must be investigate at the lab scale for a further scale up of the membrane separation process.

Aromatic polyimides are known to be hydrophobic or weakly hydrophilic polymers, since the molecular chain groups present generally a low affinity for polar compounds. Lokhandwala et al. [116] reported the water sorption in 4 different 6FDA-based membranes, varying the diamine moiety. Even if appreciable differences have been observed related to the different diamine nature, the water uptake at high activity has always been reported to be lower than 3.2 wt%. A similar behavior has been observed for 6FDA-TMPDA [60], with a water concentration in the polymer matrix of 3.7 wt% obtained for an activity of 0.8, whereas 6FDA-ODA showed an even lower water concentration (2.2 wt%) for an R.H. value equal to 85% [57]. The main reason for the poor water sorption of 6FDA-based polyimide may be related to the hydrophobic character of the CF₃ groups of the dianhydride moiety. However, the water uptake remains low even for other dianhydrides: a PMDA-based commercial polyimide from Dupont, Kapton[®], absorbs a water amount equal to 2.7 wt% [117] at saturation conditions, and this quantity increases slightly for BPDA-based polyimides even though it is reported to be always lower than 5.6 wt% for a T range between 25 and 50°C [57,118].

Despite the low water uptake, frequently polyimides exhibit relevant variation of gas permeability at increasing the water concentration within the membrane [60–62]. Hence, the characterization of Matrimid performance under humid conditions has been deeply investigated, coupling permeation tests at various water activity with pure water sorption experiments. Combining the results obtained from both experiments, it has been possible to correlate the permeability for a given R.H. of the gaseous flow in the upstream side of the membrane directly with the water concentration within the membrane matrix. Indeed, as previously described in the experimental chapter, the permeability under humid conditions is measured for a water concentration in the membrane at the equilibrium with

the humid stream. This particular measurement is not frequently reported in literature, since normally in mixed permeation tests with water vapor, the R.H. values are different on the two sides of the membrane [60,63].

In addition, a systematic approach will be adopted for the investigation of water vapor influence on permeability in Matrimid, exploring different penetrants and thermal conditions. Hence, the study aims at pointing out the physical phenomena related the variation of the transport rate, enhancing the understanding of the involved fundamental mechanisms.

4.2.1 Water Vapor Sorption

The sorption experiments have been carried out by means of the quartz spring microbalance apparatus at three different operative temperatures (25, 35 and 45°C) and the obtained results are showed in Figure 4.15. As expected, the mass ratio Ω_{H_2O} , measured in g_{H_2O}/g_{pol} , is found to decrease at increasing T for a given water vapor pressure of the bulk phase. The experimental data at 35°C are in line with previous literature results for Matrimid [60,82] and a substantially linear behavior of the sorption isotherms is showed, as already reported for other polyimides [59,116].

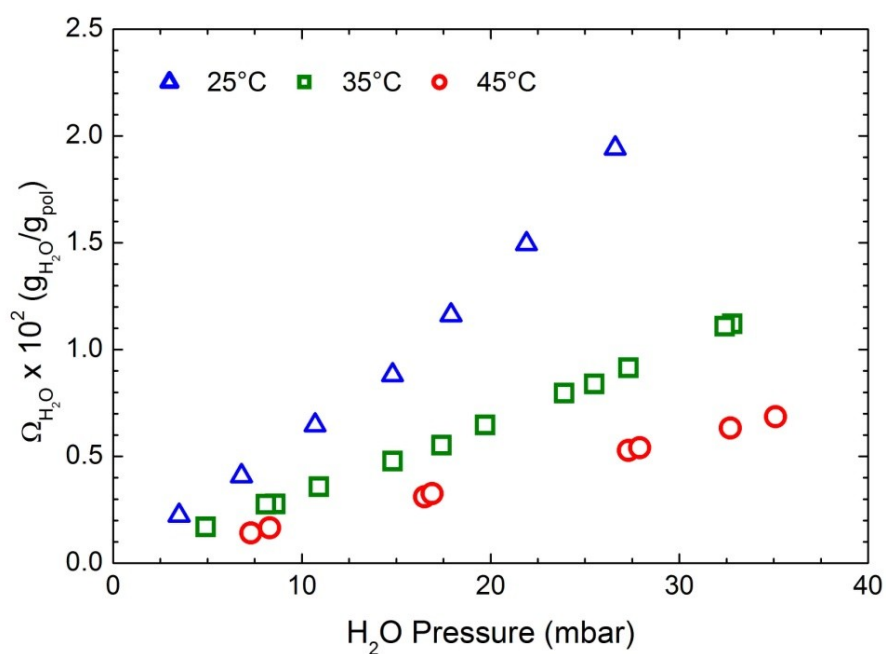
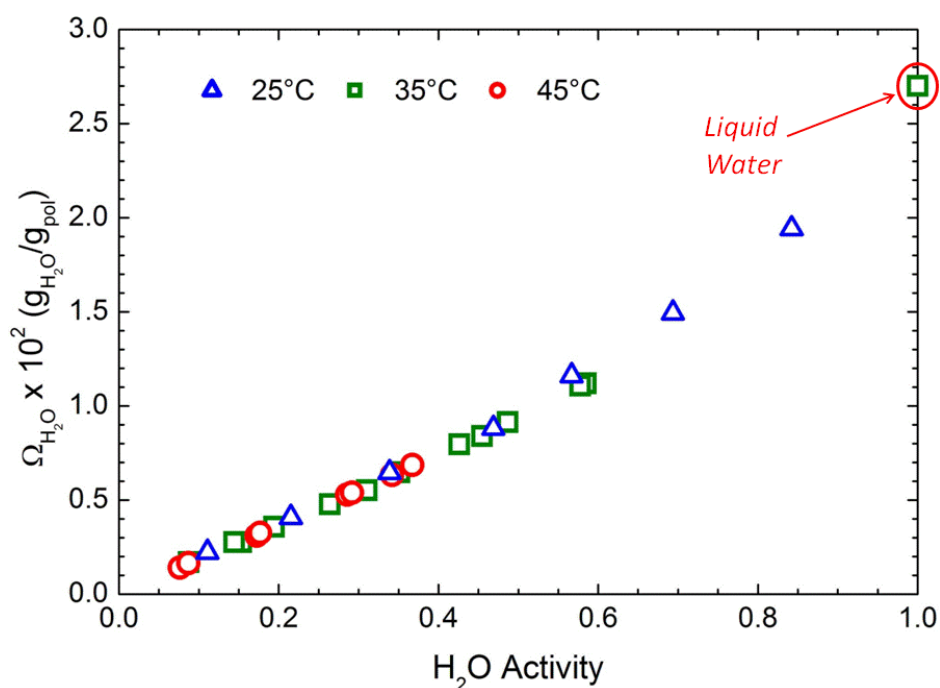


Figure 4.15 - Water sorption isotherms for Matrimid as function of H₂O pressure

However, when the H₂O solubility is plotted as a function of driving force of the absorption process, i.e. water activity, the sorption isotherms tend to merge into a single curve (Fig. 4.16). The activity is approximated here by the relative vapor pressure p/p^* where p^* is the saturation pressure at the given temperature. In the plot, the water uptake corresponding to the unitary water activity has been obtained by immersing a Matrimid sample directly into the liquid at 35°C and it is in good agreement with the results obtained from the vapor tests. In the low activity range, a linear trend of the sorption isotherms can be observed, but at higher values a clear upturn is displayed, likely related to the clustering phenomena, as reported for other polyimides [58,59,117]. A more detailed analysis of the sorption isotherms will follow in the modeling part of the present thesis (Chapter 5).



4.16 - Water sorption isotherms for Matrimid as function of R.H.

As reported in paragraph 3.3, the experimental setting allows also the evaluation of the sorption process kinetics, from the best fitting of the single incremental step curves through Eq. 2.16. In this framework, the estimated value of the diffusion coefficient is obtained for a driving force corresponding to the pressure variation within the single step of the sorption experiment. Diffusion process showed a Fickian behavior, no relaxation

were observed during experiments, and in all case a more than satisfactory description of the experimental data was obtained considering a constant diffusivity along the step. Figure 4.17 shows the H₂O diffusion coefficient for Matrimid, evaluated at different T as a function of water mass fraction in the membrane, calculated as the mean value between the initial and final mass fraction of the single sorption step. The obtained data are in the range of 10⁻⁸ cm²/s, typical for H₂O vapor in polyimide materials [57,116,117] and, as expected, the diffusivity is found to increase along with the operative temperature. A negligible dependence of *D* is observed over the studied water concentration range within the membrane matrix, for the three experimental conditions (25, 35 and 45°C). Similar behavior has been observed also for Kapton [119], whose water sorption behavior is similar to the one observed for Matrimid.

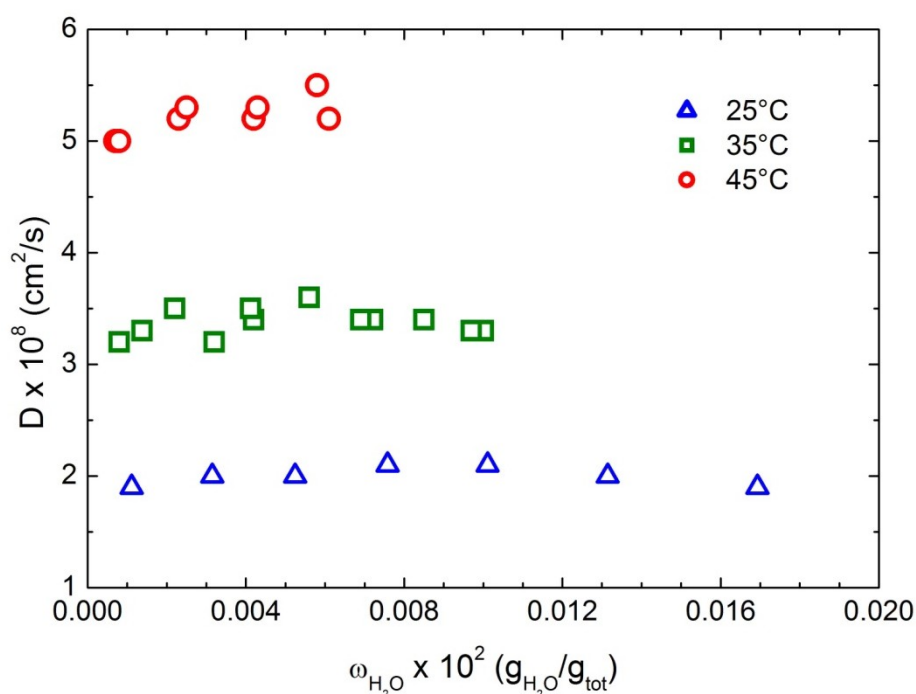


Figure 4.17 - Diffusion coefficient of water vapor in Matrimid as a function of water vapor mass fraction within the polymeric matrix

Moreover, the evaluation of the kinetic and the thermodynamic parameters of water transport in Matrimid films allows the calculation of H₂O permeability, in the framework of solution diffusion mechanism. Figure 4.18 shows the outputs for the investigated

thermal conditions. Despite the data scattering, mainly related to the estimation of the diffusion coefficient for such a hydrophobic matrix, it appears that the permeation coefficient tends to increase along with the water concentration within the membrane, as reported for polyimides [116]. In addition, the observed diffusion coefficient values are similar to literature data, reported for Matrimid [120]. However, conversely to what is normally found for incondensable species, the H₂O transport rate is showed to decrease at increasing the operative T. This effect has been documented for other polyimide-based copolymer [121] and it may be mainly related to the fact that for condensable penetrants the solubility coefficient has a dominant role on the H₂O permeability. Hence, at increasing the operative temperature, the increase of the diffusion coefficient is not large enough to contrast the solubility reduction, resulting in an overall decrease of the transport rate across the membrane.

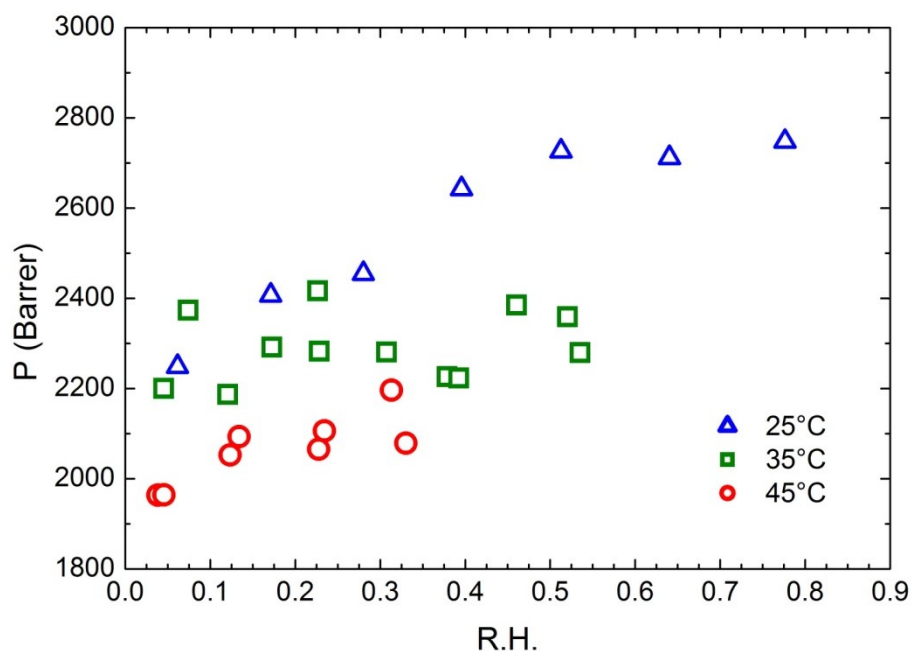


Figure 4.18 - Permeability of water vapor in Matrimid as a function of the R.H. in the feed side

4.2.2 Gas permeability under humid conditions

The transport properties of different gaseous penetrants (CH_4 , N_2 , CO_2 and He) have been investigated in a wide range of water activity (0 - 75% R.H.) for different thermal conditions (25, 35 and 45°C). The penetrants choice was made in order to investigate different gas characteristics, in terms of kinetic dimensions and condensability (Table 1.1), which affect diversely the diffusion and solubility coefficients. The results are showed in Figure 4.19 - 4.22. The dry gas permeability obtained is in good agreement with literature data for all the investigated species [105–107,122,123] and also with the permeability obtained for Ma200 samples, showed in the previous paragraph. The data set suggests a diffusion controlled permeation process, as usually encountered in glassy polymers, because the permeability scales qualitatively with the kinetic size of the penetrating molecules ($P_{\text{He}} > P_{\text{CO}_2} > P_{\text{N}_2} > P_{\text{CH}_4}$ with $d_{k,\text{He}} < d_{k,\text{CO}_2} < d_{k,\text{N}_2} < d_{k,\text{CH}_4}$).

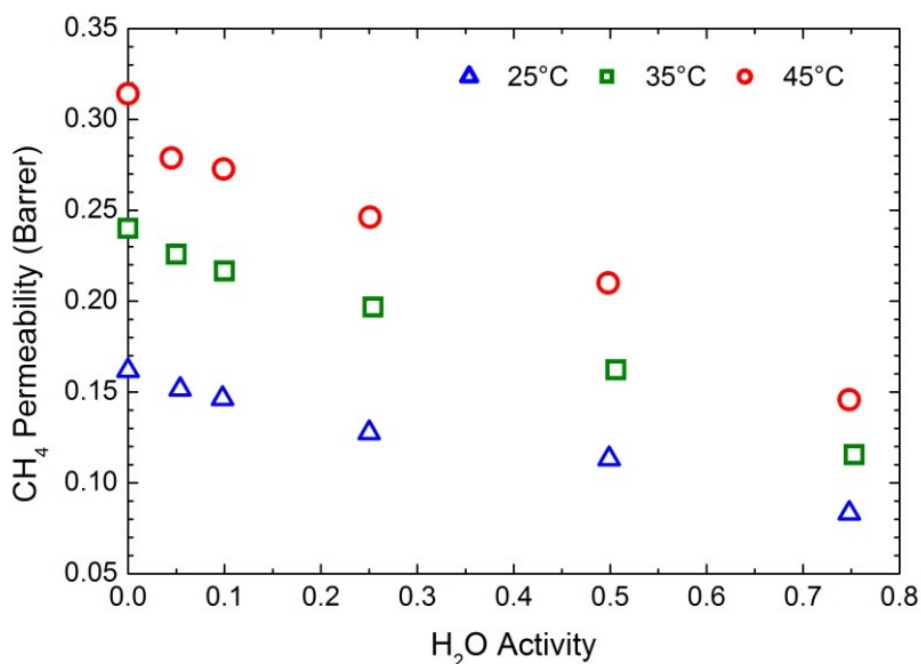


Figure 4.19 - CH_4 permeability vs R.H. at the 3 operative T (25, 35 and 45°C) and $p_u = 1$ bar

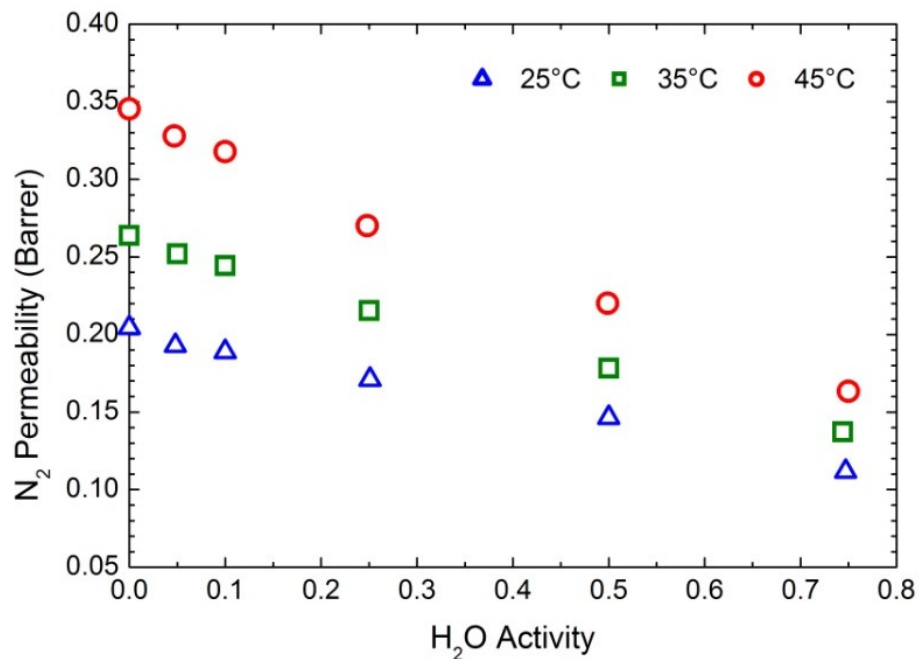


Figure 4.20 - N_2 permeability vs R.H. at the 3 operative T (25, 35 and 45°C) and $p_u = 1$ bar

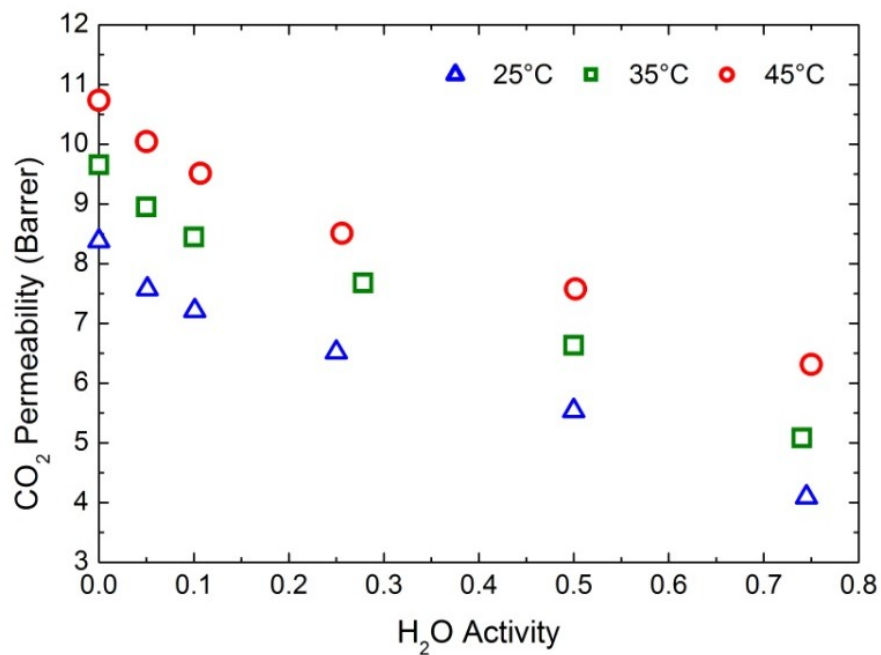


Figure 4.21 - CO_2 permeability vs R.H. at the 3 operative T (25, 35 and 45°C) and $p_u = 1$ bar

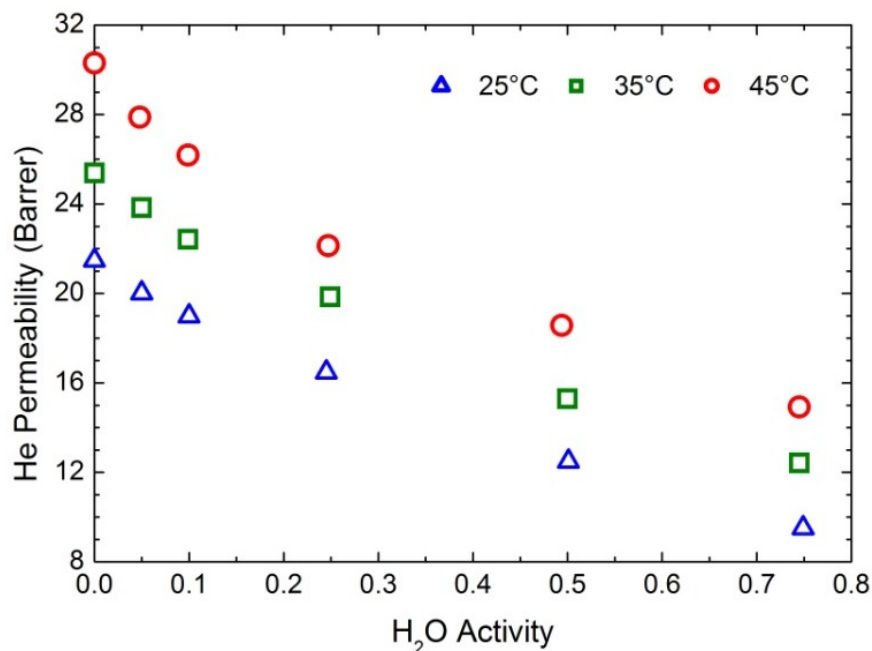


Figure 4.22 - He permeability vs R.H. at the 3 operative T (25, 35 and 45°C) and $p_u = 1$ bar

Among the different gases, helium is the most permeable one, with pure dry gas permeability ranging from 21.5 to 30.3 Barrer for the different thermal conditions inspected, followed by CO₂ (P ranging from 8.4 to 10.7 Barrer), N₂ (0.20 - 0.35 Barrer) and CH₄ (0.16 - 0.31 Barrer). As usually observed for diffusion-controlled processes, the permeability of the incondensable gaseous species considered increases monotonously with T; on the contrary, gas permeability is reduced by the presence of water, as often reported for hydrophobic materials as well as for Matrimid® [60] and other polyimides such as Kapton® [124], non-sulfonated CARDO/ODA copolyimide [125] and (6FDA-TMPDA) [24].

Interestingly, for all the gases inspected a very similar permeability decrease has been obtained as a function of R.H., as showed in Figures 4.23 - 4.25, in which the ratio between humid gas (P) and dry gas permeability (P_0) is reported for all gases at a temperature of 35°C. On the average, the gas permeability was decreased by 6% of the dry value at 0.05 of water activity, and then further lowered: 10% at 0.1 activity, 20% at 0.25, 34% at 0.5, and finally about 50% at 0.75 R.H.. The same trend is common to all gases, including CO₂, which is known as a plasticizing agent for Matrimid (although in the high pressure range, ~ 10 bar) and has the higher affinity to water with respect to the other penetrants considered.

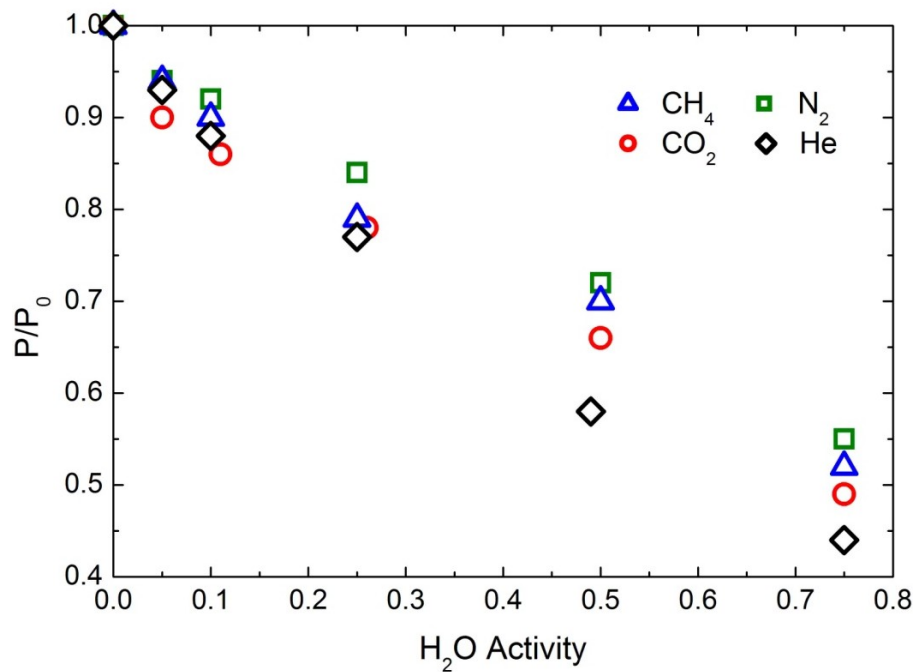


Figure 4.23 - Ratio P/P_0 between permeability under humid conditions, P , and dry gas permeability P_0 for the investigated gases at 25°C ($p_u = 1$ bar)

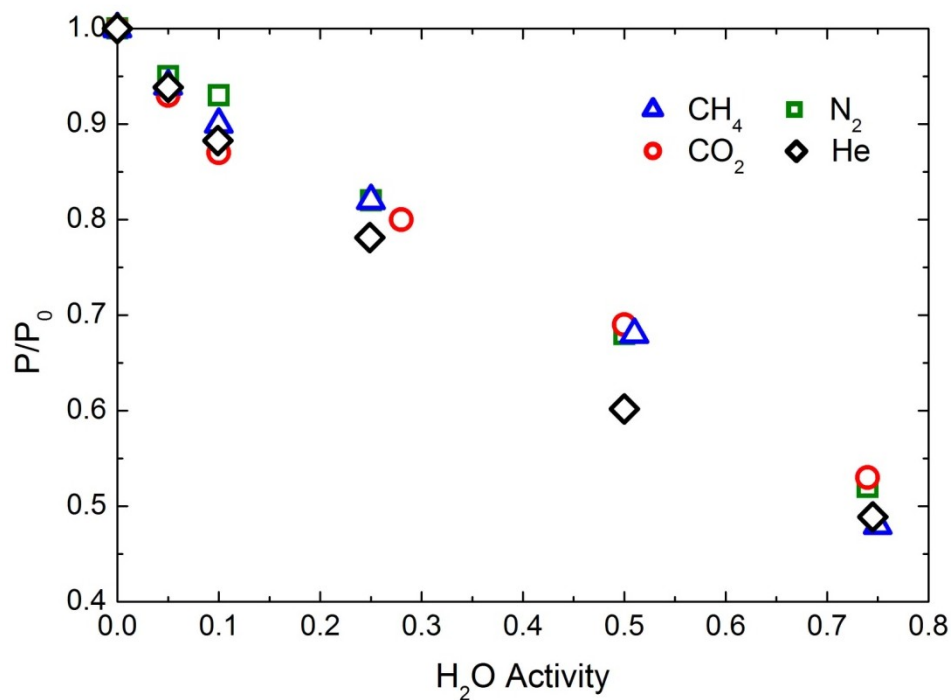


Figure 4.24 - Ratio P/P_0 between permeability under humid conditions, P , and dry gas permeability P_0 for the investigated gases at 35°C ($p_u = 1$ bar)

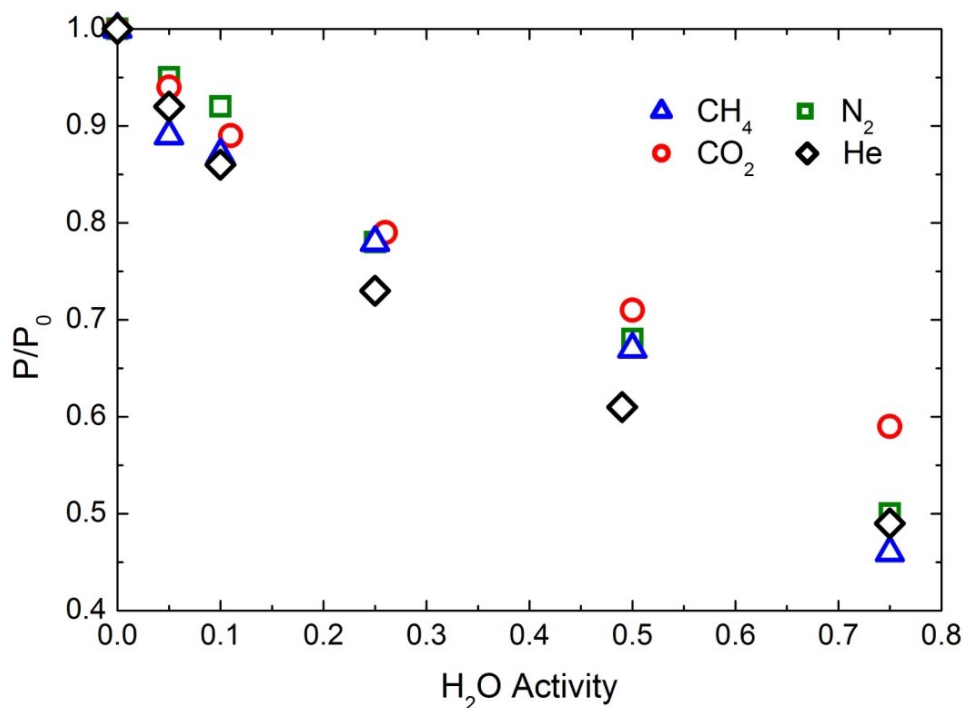


Figure 4.25 - Ratio P/P_0 between permeability under humid conditions, P , and dry gas permeability P_0 for the investigated gases at 45°C ($p_u = 1$ bar)

Chen *et al.* [60] reported a similar qualitative behavior for gas permeability in humid conditions for Matrimid, at various water activities. Quantitative comparison with the data reported in ref. [60] is not simple due to the different experimental setup used in that work, in which water vapor is present only on the feed side and is a permeating species, with a water concentration profile established across the membrane. However, a substantial agreement is obtained by comparing, as a first approximation, the data at the same average water content within the membrane in the different experiments. In this way, the decrease in permeability reported in Chen's work is only slightly lower than the one here presented for CH_4 (about 25% of the dry value at 35°C for water activity of the feed side close to 1), whereas it is rather comparable for the case of CO_2 .

By varying temperature at constant R.H., the permeability under humid conditions increases with trends similar to those observed for the dry gas permeability, and the same effect of R.H. on permeability is observed at 25, 35 and 45°C . Indeed, the analysis of P/P_0 (Fig. 4.26 - 4.28) for all the penetrants shows a very similar trends at the investigated three temperatures, as the curves substantially overlap with one another at

least at activity values up to 50% and shows only limited differences at the higher R.H. investigated. However, it must be noticed that at increasing the water content in the feed stream, the uncertainty related to the measurement tends to increase (Appendix, Table A.2), affecting more significantly the low permeable gases.

To better understand the observed behavior it is worthwhile to recall the slight dependence on temperature of water solubility in Matrimid, previously described. As water solubility is not thermally affected, the same amount of water is present within the membrane at different temperatures for any given R.H., resulting in a reduction of humid gas permeability very similar for all gases and at all temperatures investigated.

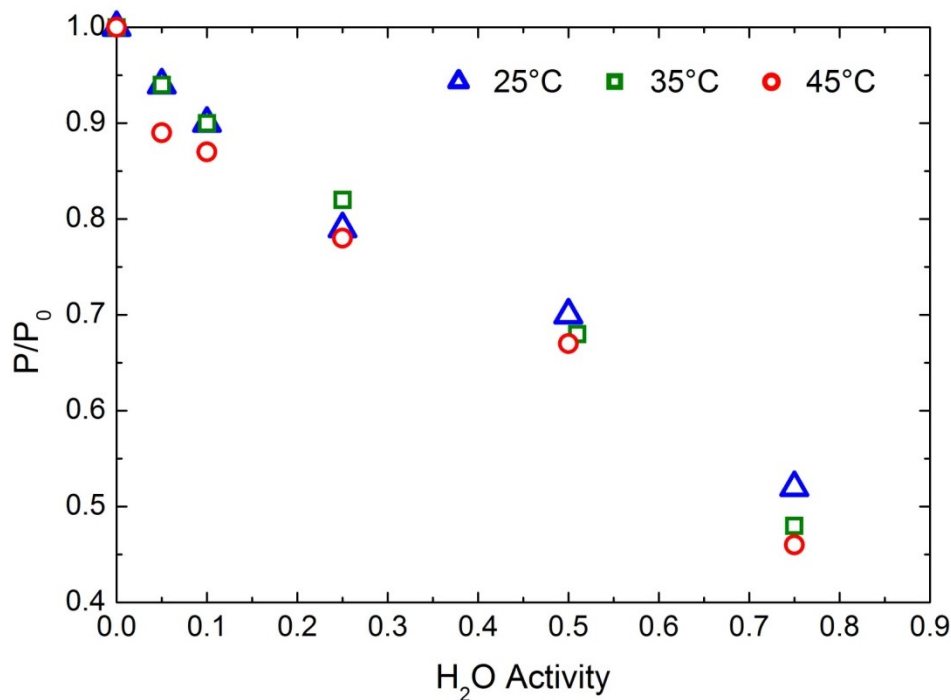


Figure 4.26 - P/P_0 for CH_4 at different temperatures (25, 35 and 45°C) as a function of R.H.

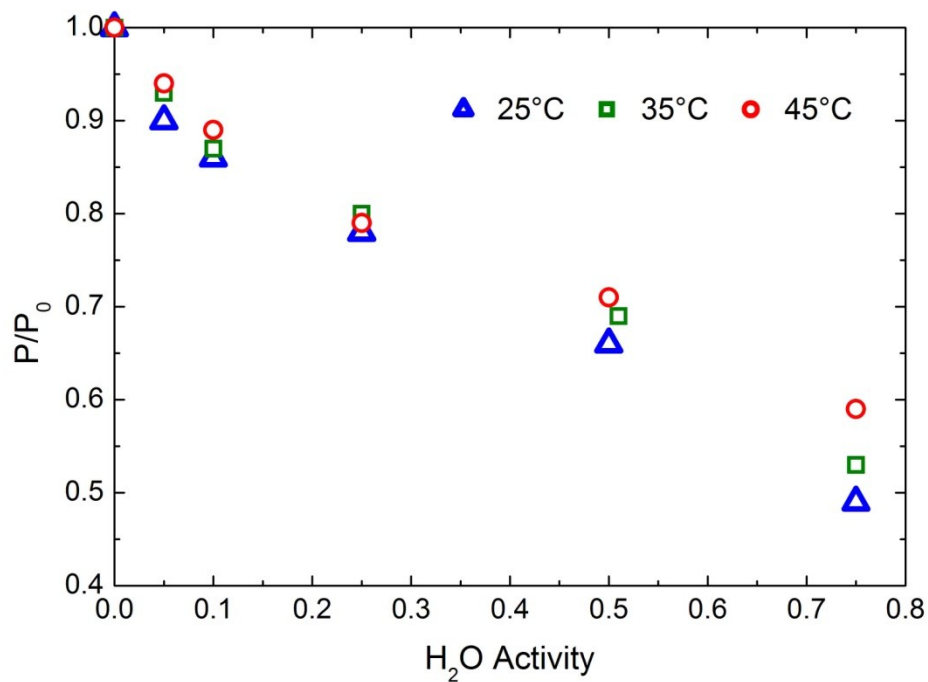


Figure 4.27 - P/P_0 for N_2 at different temperatures (25, 35 and 45°C) as a function of R.H.

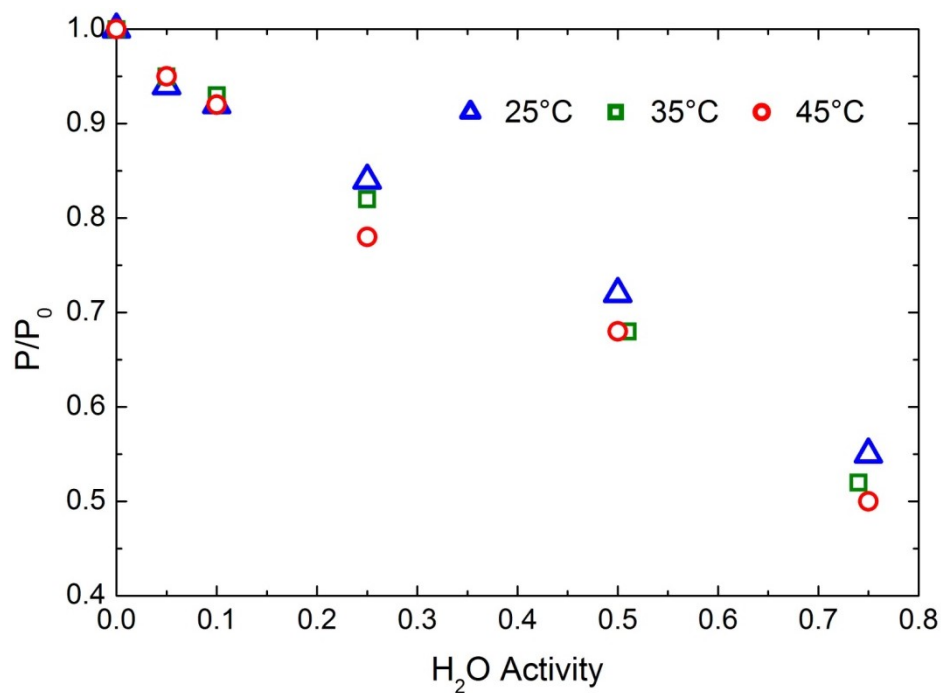


Figure 4.28 - P/P_0 for CO_2 at different temperatures (25, 35 and 45°C) as a function of R.H.

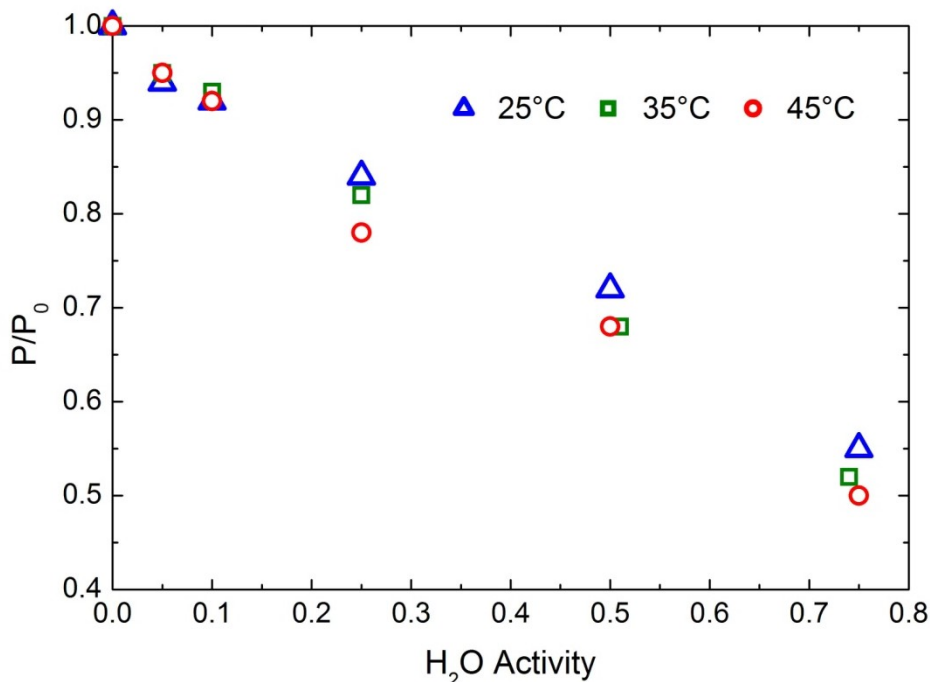


Figure 4.29 - P/P_0 for He at different temperatures (25, 35 and 45°C) as a function of R.H.

Figure 4.30 and Figure 4.31 illustrate the membrane separation performances in a Robeson plot [30,31] reporting CO_2 permeability along with CO_2/CH_4 and CO_2/N_2 ideal selectivity respectively, at the various water activities and temperatures inspected. Matrimid has properties very close to those of many commercial membrane materials used for gas separations, even though well below the upper bound, and it is thus suitable to be used as membrane for CO_2/CH_4 or CO_2/N_2 separation, at least in low pressure processes, so that CO_2 -induced plasticization is prevented. As it often occurs in polymer membranes, with increasing temperature the permeating flux increases, while selectivity is reduced. On the contrary, in the presence of water, the permeability in Matrimid decreases by almost the same extent for all gases, while the separation factor is not significantly influenced by the presence of H_2O , thus leading to a decrease of the overall membrane efficiency in terms of distance from the upper bound. This is apparent e.g. from the experimental data at 25 °C for the CO_2/CH_4 in which the ideal selectivity is constant at different water concentrations in the membrane and CO_2 permeability is reduced with increasing R.H. At 35 and 45 °C similar results are obtained, with a slight

increase in selectivity at the higher activities, related to a difference of the factor P/P_0 of CO_2 with respect to the other gases.

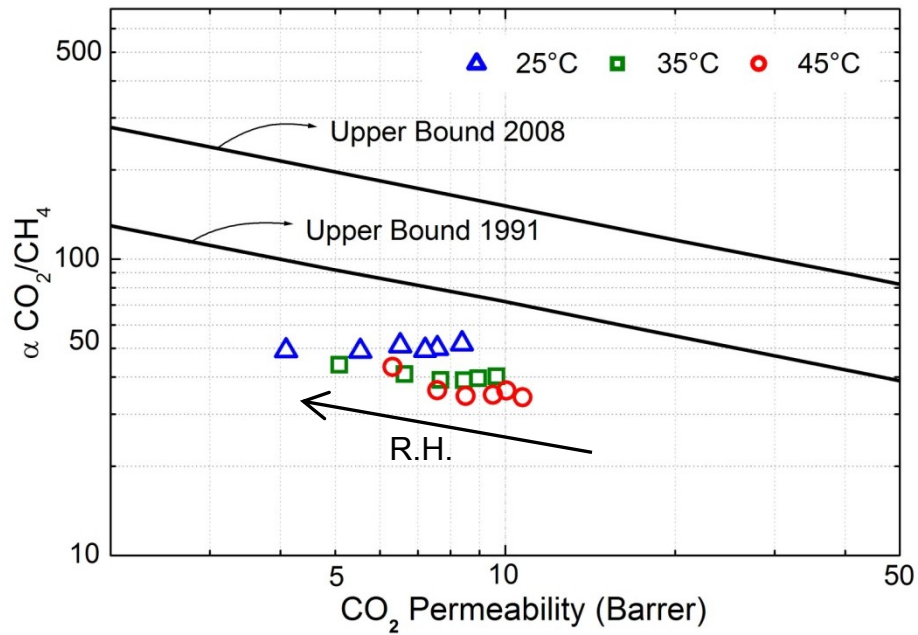


Figure 4.30 - Robeson Plot for CO_2/CH_4 selectivity as function of R.H.

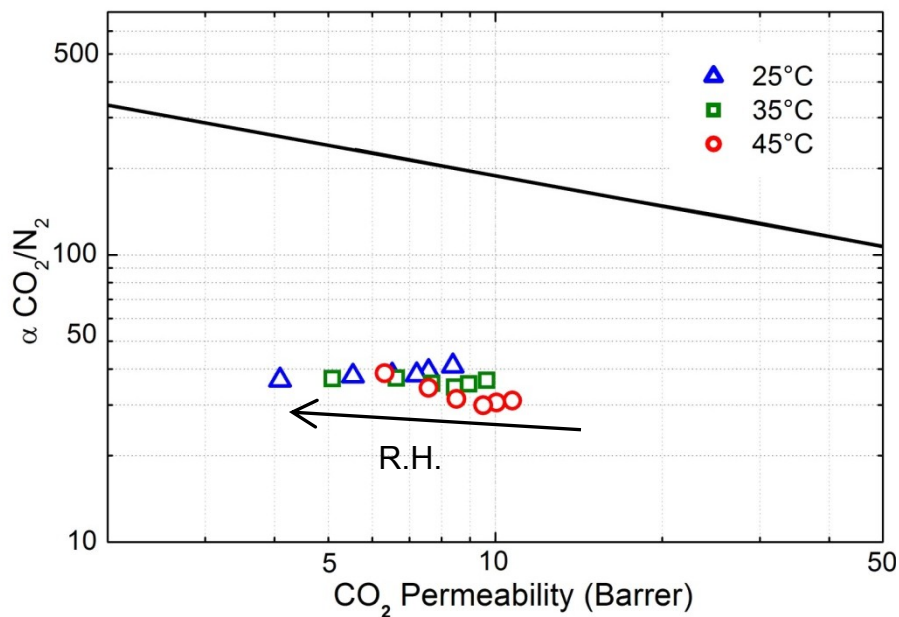


Figure 4.31 - Robeson Plot for CO_2/N_2 selectivity as function of R.H.

4.2.2.1 Activation Energy

The analysis of temperature effect on gas permeability confirms that the experimental P values follow an Arrhenius behavior (correlation coefficient always higher than 97%) both in dry conditions, as well as at any fixed R.H. Therefore, the activation energy of permeation process ($E_{P,i}$) for penetrant i can be evaluated over the entire water vapor activity range throughout the following relationship:

$$\frac{E_{P,i}}{R} = - \left(\frac{\partial \ln P_i}{\partial (1/T)} \right)_{R.H.} \quad (4.1)$$

Equation 4.1 defines an effective quantity, since the activation energy is calculated at constant relative humidity in the external gas rather than at constant composition in the membrane, as already pointed out by a previous work of our research group [32]. However, no significant differences are observed in the water solubility isotherms at different temperatures [126]. Consequently, at constant R.H., the overall composition inside the membrane is substantially the same for the investigated thermal conditions, and $E_{P,i}$ provides a meaningful estimation of the actual activation energies for permeation in Matrimid at various water activities.

Figure 4.32 shows the trends of the activation energies versus R.H. measured for the four different penetrants. The $E_{P,i}$ values calculated in dry conditions agree quite well with literature data [106,127,128], and for the less condensable gases such as He, N₂ and CH₄, they increase with the kinetic diameter, as is often the case for glassy polymers. In fact, for these penetrants the permeation process is controlled by diffusion and at increasing the kinetic size a higher energy barrier must be overcome to allow the single molecule to jump from one available site to another one. On the other hand, CO₂ showed the lowest $E_{P,i}$ value among the gases considered, likely in view of the larger contribution of solubility to the permeation mechanism.

As one can see in Figure 4.32, the effect related to the presence of water vapor on the activation energy of permeation is rather limited up to approximately 25% R.H. for all the gases investigated. At the highest R.H. values (50% and 75%), E_P shows different trends, decreasing in case of N₂ and CH₄ and increasing for CO₂ and He. However, the behaviors displayed are likely related to the intrinsic uncertainty of the measurement (Appendix,

Table A.2). Hence, a small variation on the permeability values, may have a higher influence on the calculated activation energy value.

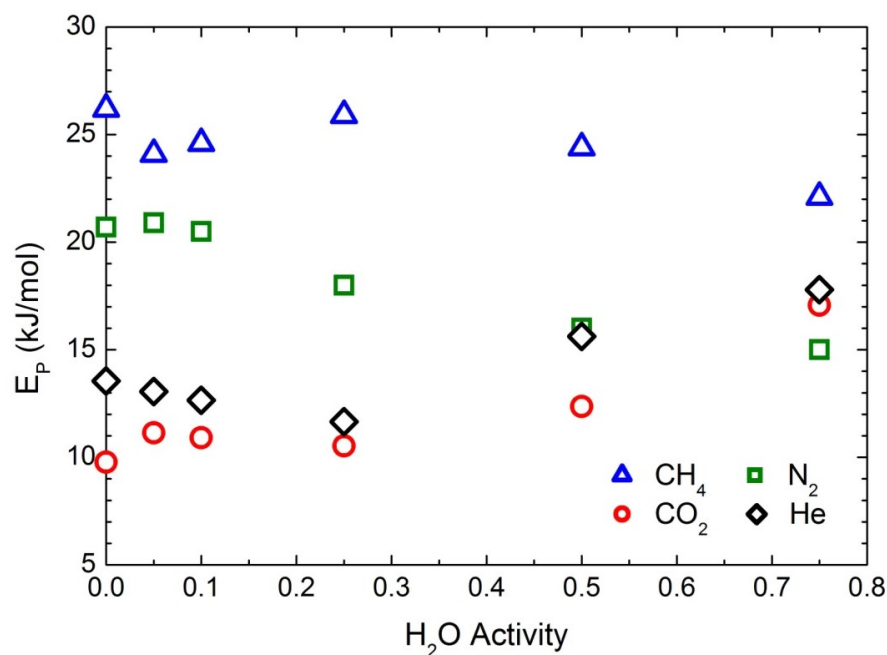


Figure 4.32 - Activation energy for CH₄, N₂, CO₂ and He as function of R.H.

4.3 Facilitated transport membranes

The main issue of facilitated transport membranes, together with the carrier saturation phenomena, is related to the separation performance stability under high pressure conditions. Bai [75] reported that the selective layer of these composite membranes undergoes a relevant compaction after being exposed at high pressure (15 atm) for more than 500 h (Fig. 4.33).

In order to overcome the limit of these promising membranes, multi-walled carbon nanotubes (MWNTs) have been used as mechanical reinforcement, due to their outstanding mechanical property [129,130], embedding them in the polymer matrix and producing mixed matrix membranes (MMMs). The nanoparticles were amino-functionalized in order to increase the hydrophilicity of the graphene structure, thus the affinity with the polymeric matrix. In addition, three different long chain amines were used as fixed carriers and their effect on the membrane performance at 15 atm has been

studied, disclosing the importance of the high molecular weight species amount in the membrane composition for high pressure (up to 28 atm) conditions.

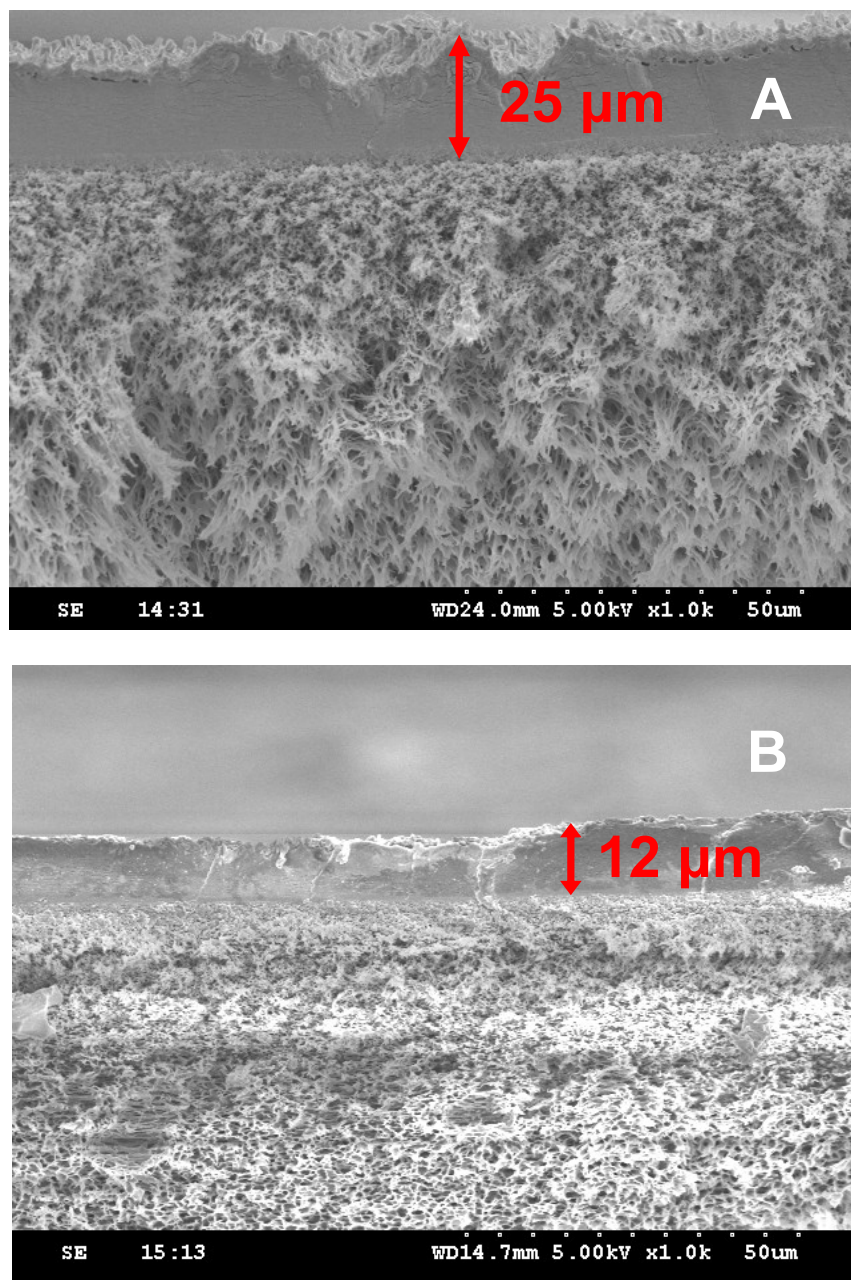


Figure 4.33 - SEM images of the cross-section of amine-based facilitated transport membranes before (A) and after the stability test at 106°C and 15 atm (B) [75]

Two different gas compositions have been used for the membrane characterization, in order to fully investigate the potential of these materials with particular reference to

natural gas sweetening and H₂ purification. The effect of different chemical and physical parameters have been highlighted in order to achieve a more comprehensive understanding of the transport mechanism and to optimize the separation process. In particular, the influence of the inorganic loading, water content of the sweep stream, the operative temperature and of the selective layer thickness has been inspected.

4.3.1 MWNTs characterization

Figure 4.34 depicts the FTIR spectra of raw MWNTs and the two functionalized MWNTs, i.e., AT-MWNTs and AF-MWNTs. The spectrum of raw MWNTs is presented in Figure 4.34a, which identifies two groups of peaks: (1) the C=C bond peaks at 1632 cm⁻¹ and 1500 cm⁻¹ and (2) the C–H alkyl bond peaks in the region of 2923 – 2850 cm⁻¹ [131]. The first group of peaks shows the typical carbon skeleton in MWNT structure, whereas the second group is in correspondence to the presence of defects in the nanotubes walls and end parts generated from the fabrication process.

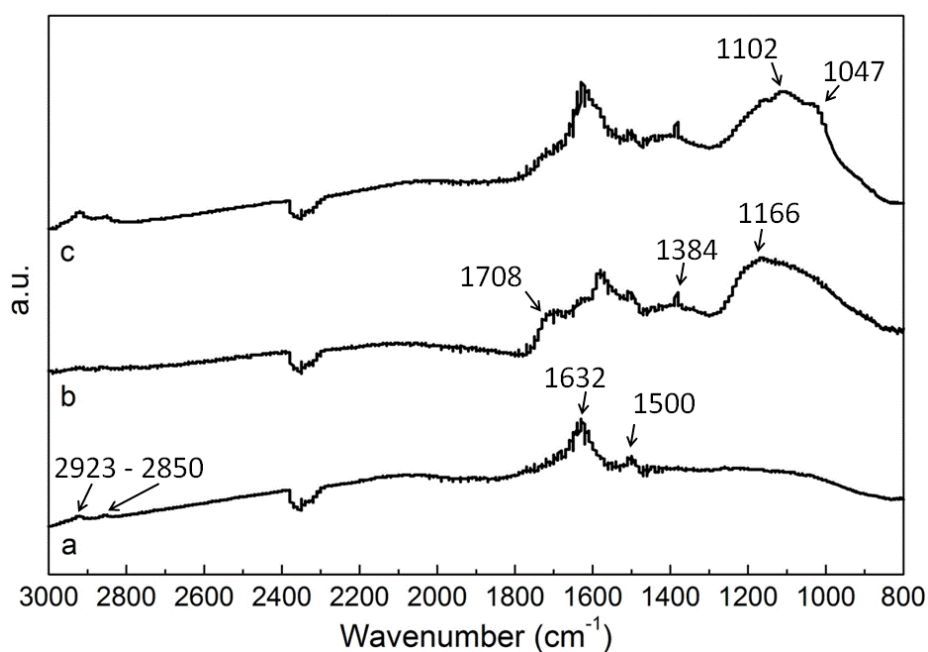


Figure 4.34 - FTIR spectra of raw MWNTs (a), AT-MWNTs (b), AF-MWNTs (c).

The treatment by strong acid oxidation introduced carboxylic acid groups and hydroxyl groups on raw MWNTs. As showed in the FTIR spectrum of AT-MNWTs (Fig. 4.34b),

new peaks appear at 1708 cm^{-1} relating to C=O stretching vibration of –COOH, 1384 cm^{-1} in correspondence to O–H bending deformation of –COOH and/or –OH, and 1166 cm^{-1} for C–O stretching in –COOH [87,90,132]. The presence of these new chemical groups confirms the effective surface functionalization for the nanotubes.

Figure 4.34c shows the spectrum of MWNTs after the amine functionalization. Compared with Figure 4.34b, the peak at 1166 cm^{-1} representing C–O stretching in –COOH decreases. Meanwhile, two new shoulders, at 1047 cm^{-1} corresponding to the Si–O–C bond and 1102 cm^{-1} corresponding to the Si–O–Si bond [78], raise on this wide peak. The above evidence affirms that the condensation of hydroxyl groups took place between the AT-MWNTs and APTES as well as the aminosilane molecules themselves [89,90]. Thereby, the amino groups from APTES were successfully grafted on MWNT surface.

4.3.2 Membrane performance at 15 atm

Facilitated transport membranes are known to be able to couple high CO_2 trans-membrane flux and very good selectivity versus other gaseous species, thanks to the chemical reaction mechanism, described in Chapter 1. In the open literature [69,71], different fixed carriers, such as polyallylamine (PAA) and polyethylenimine (PEI), have been used coupled with mobile carriers for facilitated transport membranes synthesis. Nevertheless, the use of polyvinylamine (PVAm) was always limited on the fixed-site-carriers membrane applications [74,133]. Theoretically, the higher N/C atoms ratio of PVAm compared to PAA and PEI should increase the reactive site availability per unit volume of the selective layer, enhancing the CO_2 facilitation factor and, hence, the membrane performance. Therefore, in the synthesis of the first samples, the PVAm was used as fixed carrier adding Lupamin as received in the casting solution composition (Samples S-01, S-02, S-03, Table 3.1).

Initially, low pressure tests were carried out for a membrane containing 22.3 wt% Lupamin (Sample S-01, Table 3.1). The operative conditions were chosen according to the research group know-how and the membrane performance are reported in the Appendix (Table A.4). The CO_2 permeability of 3157 Barrer is similar to the one obtained using unhindered PAA [18], even though a better CO_2/H_2 selectivity is achieved. Also Zou et al. [73] reported a comparable permeability value for similar

operative conditions, but a higher CO₂/H₂ selectivity, likely related to a thicker selective layer, compared to the one used in the present study. Furthermore, Figure 4.35 shows the Robeson Plot [31] for the CO₂/CH₄ separation and it is possible to appreciate the remarkable results achieved by these membranes, with respect to the state-of-art of solution-diffusion-based membranes. In particular, the capability of facilitated transport mechanism to overcome the typical solution-diffusion trade-off may be observed, thanks to the CO₂ transport rate chemical enhancement.

Despite the good results obtained for low pressure conditions, when the total feed pressure was increased to 15 atm, stability issues arose. In particular, the carbon dioxide flux across the selective layer was found to decrease soon after the steady state was reached (Fig. 4.36, the CO₂ GC peak area is proportional to the CO₂ permeability) and the CO₂/H₂ selectivity turned out to be significantly lower if compared to previous results obtained in the research group [78]. In addition, with respect to the low pressure tests, when the membrane was removed from the sample holder, brownish spots were found in the back of the support, giving evidence of a weak membrane integrity.

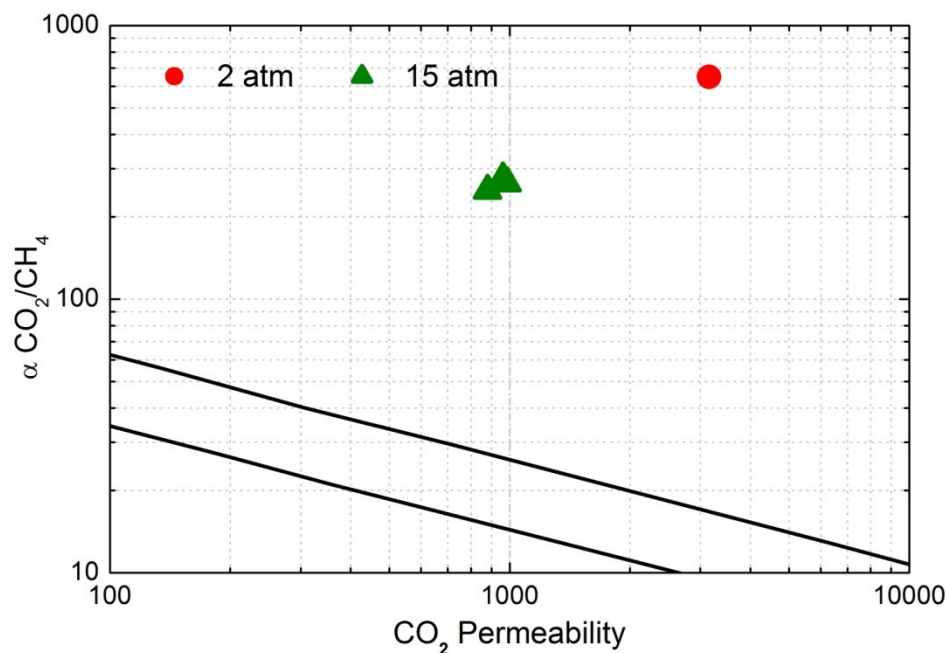


Figure 4.35 - Robeson Plot for the CO₂/CH₄ separation, for the MMM at 2 atm (●, S-01, Table 3.1) and 15 atm (▲, S-08, S-09, S-10, Table 3.1)

In order to solve the problem, the total solid composition of the investigated samples was finely analyzed. In particular, the high molecular weight species (HM_{wS}) amount, identified as the sum of the crosslinked PVA-POS network and the polyamines, has been calculated for several tested samples (in Table 3.1 only 2 samples containing Lupamin are reported for brevity sake). Due to the presence of sodium formate in Lupamin commercial composition (66.6 wt%, solid matter base), the HM_{wS} amount was found to be low (< 35 wt%, Fig. 4.37) and likely responsible for the poor membrane performance. In view of keeping the right balance between the species present in the total solid composition, a purification of Lupamin was carried out [86] and using a specific purification procedure, previously mentioned, the long chain polymer concentration of the PAm solution increased up to 66.6 wt%.

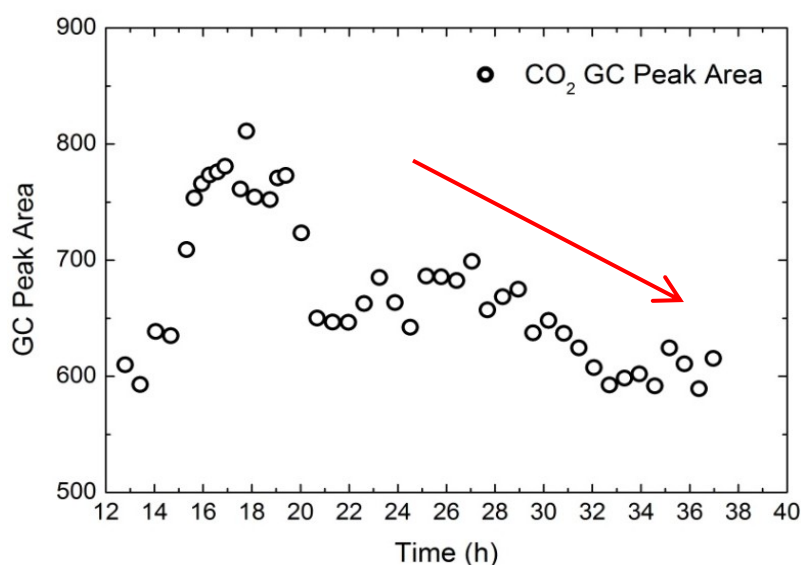


Figure 4.36 - CO_2 GC peak area of the permeate stream over time using Lupamin as fixed carrier ($p^u = 15$ atm)

After purification, new tests were performed on samples produced with slightly different protocols in order to maintain a similar PVAm amount in the final membrane. However, the PVAm refinement did not improve the membrane performance (Sample S-04 and S-05, Fig. 4.37 and Table A.4), neither in terms of stability nor selectivity. On the other hand, when polyallylamine was used as fixed carrier, a sudden results increase was achieved (Fig. 4.37). Due to the higher PAA purity grade, it was possible to reach higher

values of the HM_{wS} amount in the total solid composition ($> 55\text{wt}\%$, Fig. 4.37), improving both the membrane stability (Fig. 4.38) and doubling the CO_2/H_2 selectivity values obtained for Lupamin or purified PVAm. The results for samples from S-06 to S-11 are summarized in the Appendix (Table A.4): averagely a CO_2 permeability of 957 Barrer, CO_2/N_2 selectivity of 384, CO_2/H_2 selectivity of 56 and CO_2/CH_4 selectivity of 264 are achieved. Likely, an increased of the amount of long chain polymers in the membrane composition helps in obtaining a more stiff polymeric matrix. The water-induced swelling was hence reduced, preventing any possible carrier leakage for the investigated conditions.

Compared to the low pressure results, an evident decrease of the membrane performance was observed (Fig. 4.35), which may be attributed to the carrier saturation phenomenon [96]. Indeed, the concentration of carriers molecules per unit volume of the selective layer is fixed for a given composition, hence, the amount of available sites for the CO_2 -carrier complexes formation is limited.

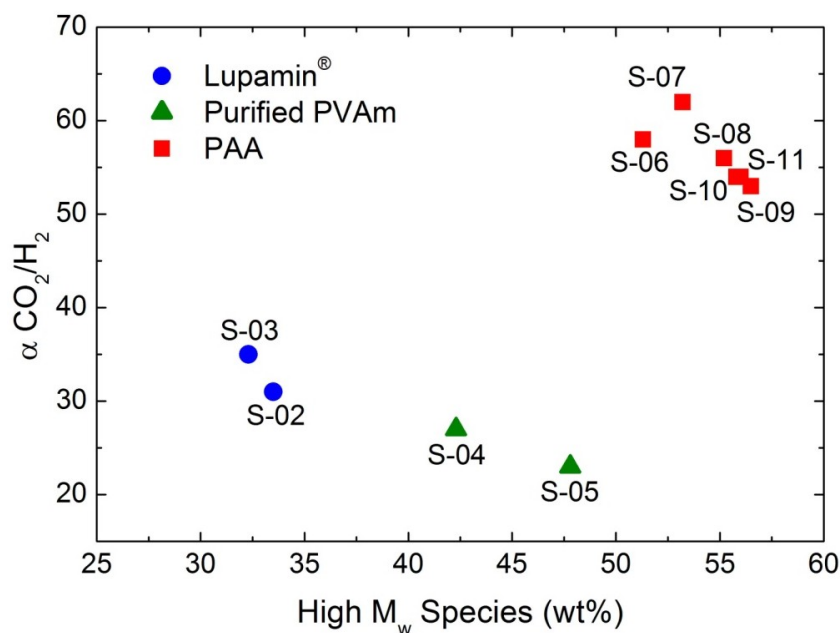


Figure 4.37 - CO_2/H_2 selectivity as a function of the high molecular weight species amount present in the membrane total solid composition for different PAM used as fixed carrier ($p = 15$ atm, $T = 107^\circ\text{C}$).

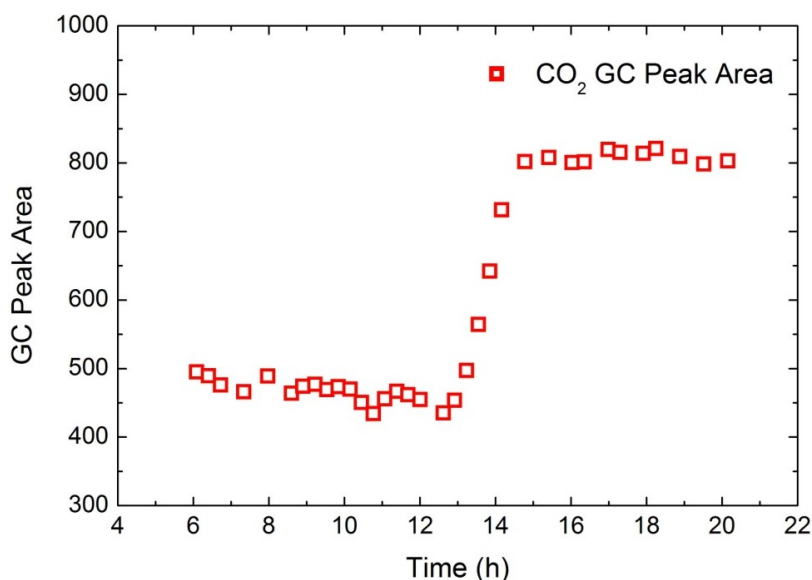


Figure 4.38 - CO₂ GC peak area over time using PAA as fixed carrier ($p^u = 15$ atm)

Increasing the CO₂ pressure on the feed side of the membrane, an upper bound is reached by the complexes, so that the CO₂ flux related to the chemical reaction becomes constant. Hence, the total CO₂ flux increases only due to the physical transport, reducing the CO₂ permeance [76], thus its permeability. On the other hand, the solution-diffusion flux of other penetrants increases linearly with pressure, so that carrier saturation affects negatively also the separation factor.

Despite the carrier saturation influence on permeability and selectivity, Figure 4.35 shows that the performance of the samples obtained using PAA as fixed carrier remain still relevantly above the Robeson upper bound for the CO₂/CH₄ separation for the high pressure conditions. The achieved results at 15 atm feed pressure make these membranes particularly attractive for natural gas sweetening. Additionally, considering that water catalyzes the facilitated transport mechanism, no dehydration step is needed before the membrane module, simplifying the whole purification process.

4.3.3 Membrane performance at 28 atm

After the attainment of the best membrane performance at 15 atm, the feed pressure was increased up to 28 atm. Once again, the higher pressure generates a reduction of both permeability and selectivity together with instability issues on the sample which showed

the best results at 15 atm conditions. Several attempts have been carried out in order to improve the membrane performance and the most effective outcomes were obtained reducing dramatically the small molecules amount in the membrane composition (Samples S-14, S-15, S-16).

At the beginning, the amount of KOH and AIBA-K was decreased to 10.6 wt% and 10.8 wt% respectively in the final membrane composition. Simultaneously the long chain amine content was increased up to 46 wt% (Sample S-14), in order to improve the mechanical stability of the selective layer by incrementing the HM_{wS} percentage. Similarly for the 15 atm pressure conditions, the strategy was found to be successful, returning stable separation performance. A permeability of 224 Barrer and a selectivity of 16 for CO_2/H_2 separation and 139 for CO_2/N_2 (Appendix, Table A.4) were achieved. In a second stage, in order to check the mobile carrier influence on the membrane performance under these pressure conditions, the AIBA-K was removed from the membrane composition, increasing the KOH content up to 21.4 wt% (Sample S-15). The separation performance increased consistently in terms of CO_2 flux across the selective layer, with a permeability of 326 Barrer (Appendix, Table A.4), whereas the CO_2/H_2 and CO_2/N_2 selectivity remained constant, suggesting a more efficient carrier ability of KOH compared to AIBA-K. An additional increment of the KOH amount to 26.8 wt% to the detriment of the PAA content (Sample S-16), hence of the HM_{wS} amount, corresponded to a further improvement of the membrane performance, in particular of the CO_2 permeability, which showed an increase to 440 Barrer, with no significant influence on CO_2/H_2 and CO_2/N_2 selectivity and without instability problem for the duration of the tests.

Figure 4.39 shows the variation of membrane performance along with the feed pressure over the investigated pressure range. The permeability and selectivity decrease is mainly attributable to the carrier saturation effect, previously described, and the trend is showed to be exponential with pressure for both permeability and selectivity. The CO_2/N_2 selectivity is the only one which seems not to follow this tendency, but the reason may be attributed to the uncertainty on the detection of the N_2 peak in the sweep side, due to the very low concentration achieved in the permeate stream for the 2 atm pressure tests. In

the end, Figure 4.40 highlights the outstanding results achieved by the MMM presented in this work, even under such severe pressure conditions.

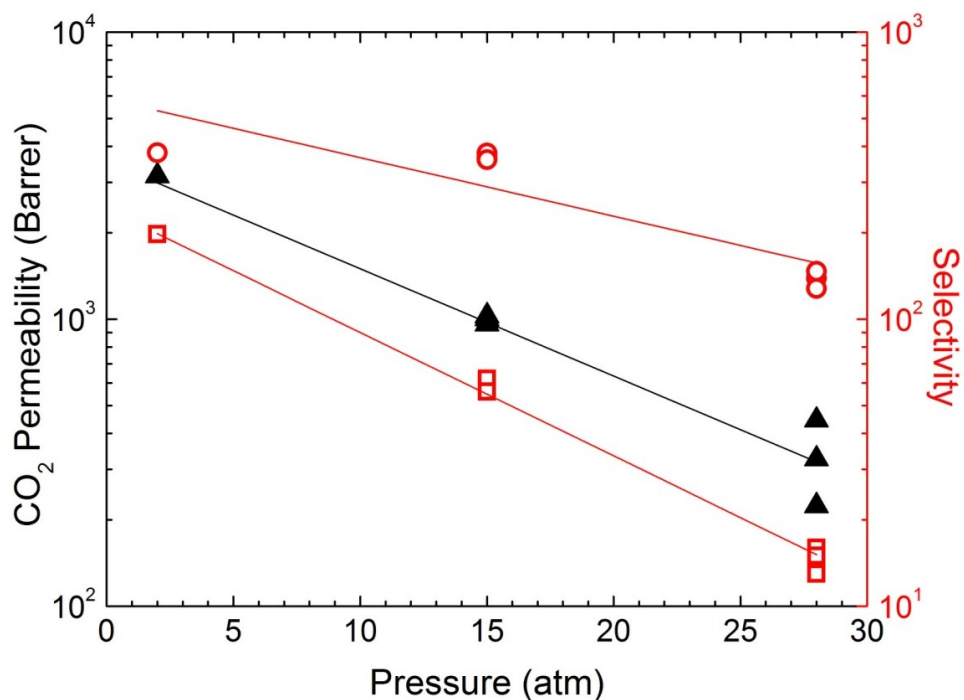


Figure 4.39 - Effect of feed pressure on the CO₂ permeability (▲) and on the CO₂/N₂ (○) and CO₂/H₂ (□) selectivity of sample.

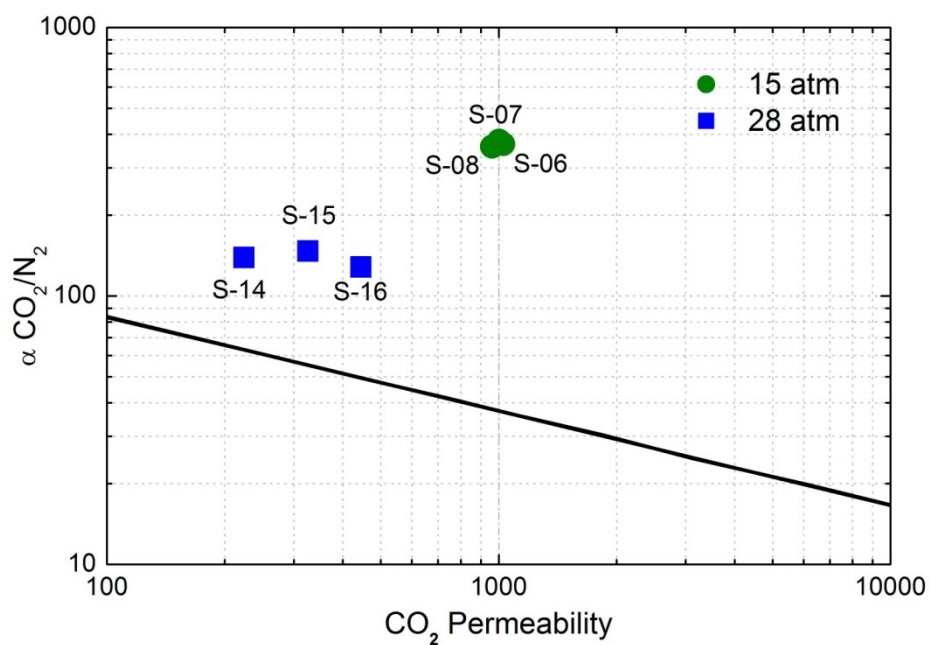


Figure 4.40 - Robeson Plot for CO₂/N₂ separation for the MMM at 15 and 28 atm

4.3.4 Effect of the inorganic loading

In literature, several attempts have been reported to incorporate carbon nanotubes in polymeric matrixes, in order to enhance both their mechanical and transport properties. Kim *et al.* [134,135] reported a significant increase (up to 70%) of the storage modulus after the addition of 5-15 wt% of octadecyl ammonium-modified SWNTs. In addition, they showed also an increase of the permeability of all the investigated gaseous probes, which was more evident for the less permeable species. Hence, the separation factor was usually reduced with increasing the inorganic loading content in the membrane composition. A similar effect have been obtained by Choi *et al.* [136] on pervaporation MMMs using acid treated MWNTs. Incrementing the functionalized MWNTs amount, they reported a significant increase of the solute flux across the selective layer along with a simultaneous decrease of water/ethanol selectivity.

Analyzing the variation of gas transport properties of MMMs based on PES and functionalized MWNTs, Ge *et al.* [137] disclosed that the additional gas diffusion, compared to the pure PES, does not take place inside the hollow nanotubes cavities but likely through the voids between the MWNTs surface and the polymer chains, called nanogaps. As theorized by Cong *et al.* [132], the size of nanogaps plays a key role for separation performances of mixed matrix membranes: if the nanogaps dimensions are increased because of a poor compatibilization between the nanoparticles and the polymeric matrix, the selectivity of the gas separation system could be adversely affected. The use of raw MWNTs or AT-MWNTs has been reported [19,138] to determine a decrease of membrane selectivity at increasing the inorganic loading, likely related to the formation of nanogaps at the polymer-filler interface. Hence, in the present work an amino-functionalization of MWNTs was carried out in order to increase the affinity between the hydrophobic nanofillers and the hydrophilic polymeric structure in order to improve membrane properties both in terms of transport and mechanical stability. As showed in Figure 4.41, the compatibility enhancement was achieved by means of AF-MWNTs: no relevant variation of transport properties was obtained for an inorganic loading up to 6 wt% (2 wt % AF-MWNTs loading values are obtained as average of S-09, S-10 and S-11, whereas the other values are obtained from sample S-12 and S-13). As reported, varying the MWNTs amount in the membrane composition between 0 and 6.4

wt% the permeability deviates of a values lower than 4%, whereas the CO_2/H_2 remains equal to 54. Only the CO_2/CH_4 selectivity decreases slightly after the particles addition, but the variation is still not really significant. At the same time, membrane permeability did not show any relevant variation at increasing the fillers loading, despite the presence of amino groups on the MWNTs walls. However, the amount of reactive groups added by embedding the fillers is negligible compared to the total amount present on the membrane composition, hence they cannot contribute considerably to the total CO_2 transport rate.

The amino-functionalization produced hence an appreciable improvement in filler embedding compare to raw MWNTs [19], enhancing the separation performance. Presumably, the presence of $-\text{NH}_2$ groups on the nanotubes surface reduced the nanogaps formation, thanks to a reduced repulsion interactions between the nanofiller and the hydrophilic polymers chains. In addition, amine moieties could also react during the thermal curing, when the crosslinking reaction is brought to completion, chemically bonding the nanoparticles to the matrix.

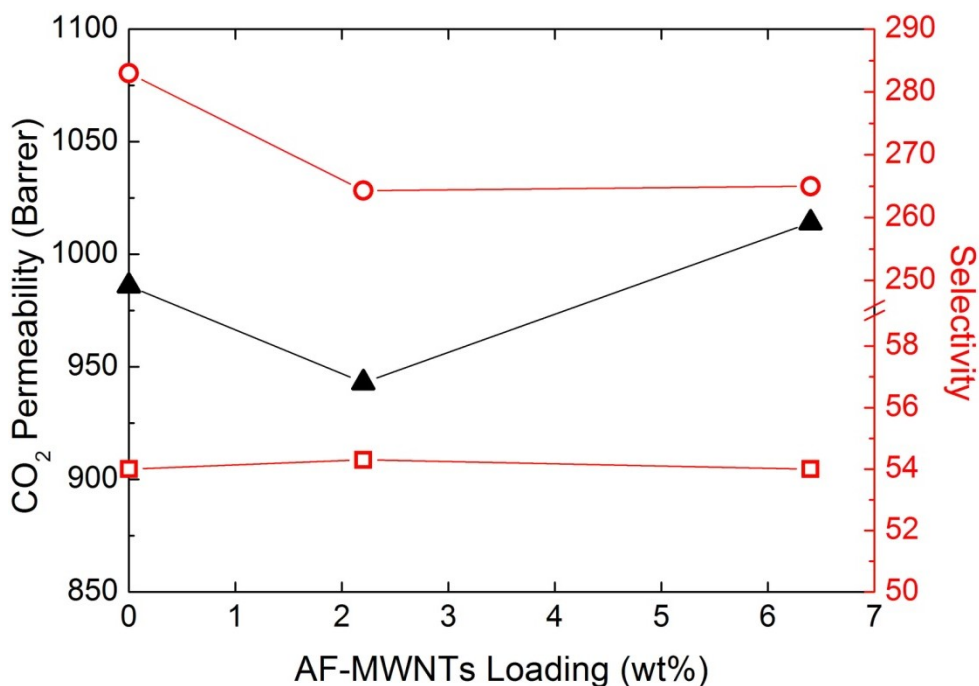


Figure 4.41 - Influence of AF-MWNTs loading on the CO_2 permeability (▲) and the CO_2/CH_4 (○) and CO_2/H_2 (□) selectivity

4.3.5 Effect of sweep side RH

Due to its participation in the reversible CO₂-amine reaction (i.e., the hydrolysis of zwitterion and carbamate ion), the presence of water is crucial for the facilitated transport process. In addition, due to the highly hydrophilic characteristics of PVA and long chain amines, the membrane matrix is largely swollen by water [74]. Hence, the mobility of ions and small gas molecules is relevantly affected if compared with dry conditions.

From this point of view, the membrane performance have been characterized at different water concentration within the polymeric matrix varying the relative humidity in the sweep side. In fact, due to the chosen experimental conditions (dry stream flow 60 cm³/min) and because of the lower limit for the water flow of the piston pump (0.01 cm³/min), the R.H. in the feed side could not be set lower than 100% for 15 atm feed pressure. On the other hand, the output rate of the water pump for the low pressure sweep side was adjusted to 0.03, 0.06, 0.15 and 0.52 cm³/min to obtain respectively a relative humidity equal to 47%, 60%, 72% and 80%. The outcomes are plotted in Figure 4.42.

As previously reported [18,73,78,96], the CO₂ permeability is found to increase monotonously with increasing the water content in the polymeric matrix. Using the sweep gas of 80% RH, the CO₂ permeability reached a high value of 1147 Barrers, almost 5 times of that at 47% RH (234 Barrers). The above results demonstrated the dramatic enhancing effect of water retention on CO₂ facilitated transport. Indeed, the increase of water concentration within the membrane matrix simultaneously enhances the mobility of ions and CO₂ across the selective layer and also the CO₂ reaction rate with amine carriers [18,96].

On the other hand, the membrane selectivity is differently influenced by the sweep side water activity and the effect is confirmed by both the investigated gas pairs. Indeed, the CO₂/H₂ and CO₂/CH₄ selectivities increased along with the CO₂ permeability up to a 72% R.H. reaching a maximum and then they started to decrease. Despite CO₂ plasticization may occur, the behavior can be mainly related to the water-induced swelling, since the CO₂ partial pressure didn't change for the different tests. After a certain H₂O concentration within the membrane matrix value is overcome, the polymeric chains mobility is enhanced to such an extent that their barrier properties efficiency is reduced, allowing an enhancement of the solution-diffusion permeable species flux.

Similar trend has been reported from Xing & Ho [78] for facilitated transport membranes containing silica at 15 atm pressure conditions. Conversely, a monotonous increase of selectivity along with CO₂ permeability has been observed for low pressure conditions [18,73,96], suggesting that the negative effect on selectivity after a certain water concentration in the membrane matrix is mainly associated to the drastic enhancement of non-reacting species driving force under such severe pressure conditions.

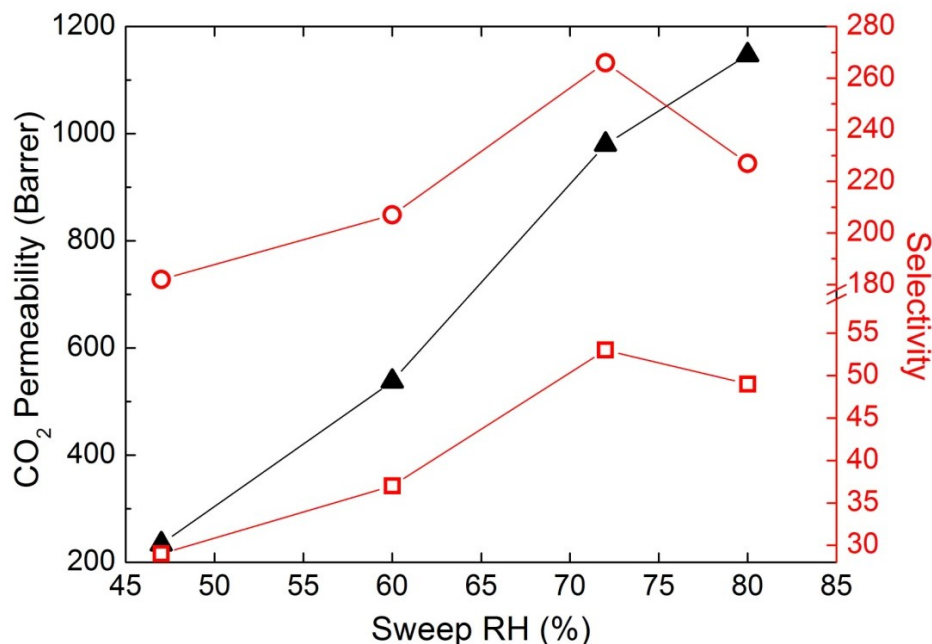


Figure 4.42 - Influence of sweep side R.H. on the CO₂ permeability(▲) and the CO₂/CH₄ (○) and CO₂/H₂ (□) selectivity (sample S-09). Operative conditions: T = 107°C; p = 15 atm; dry gas flow rate = 60/30 cm³/min (feed/sweep)

4.3.6 Effect of temperature

Membranes for industrial gas purification are expected to be operated at high temperatures above 100°C from the energy efficiency point of view. However, few data on membrane performance at such severe conditions could be found in the literature. As a supplement, this work investigated the membrane transport properties including CO₂ permeability and CO₂/H₂ selectivity of the MMMs developed in this work at different high temperatures ranging from 103°C to 121°C at a feed pressure of 15 atm. All the other operating conditions are showed in Table 4.1.

Temperature affects the facilitated transport mechanism in two competing ways. On one hand, higher temperature accelerated the chemical reaction between CO₂ molecules and amine carriers and the diffusion of the reaction products across the membrane. On the other hand, keeping constant the water flow rate injected in the humidifier, the R.H. of the streams contacting the membrane decreases by increasing the operative temperature. As showed in the previous paragraph, the R.H. influence on the CO₂ transport across the selective layer is significant, hence a decrease of the water amount in the gaseous streams determines a reduction of the separation performance of the membrane.

Sample	T (°C)	R.H. (Feed)	R.H. (Sweep)	CO ₂ Perm (Barrer)	CO ₂ /H ₂ -	CO ₂ /N ₂ -	CO ₂ /CH ₄ -
S-11	103	100%	86.3%	691	32	225	-
	105	100%	86.2%	817	47	370	-
	106	100%	77.8%	882	52	403	-
	107	100%	72.5%	828	53	451	-
	110	100%	67.9%	828	53	451	-
S-10	107	100%	72.5%	880	54	-	250
	114	100%	57.2%	583	50	-	242
	121	100%	45.6%	432	48	-	251

Table 4.1 - Gas transport properties of mixed matrix membranes with 2.2 wt% AF-MWNTs tested at different temperatures. Dry gas flow rate = 60/30 cm³/min (feed/sweep)

Figure 4.43 illustrates the influence of the operative temperature on two samples, S-10 and S-11. Varying T from 103°C to 107°C the CO₂ permeability increases significantly, and the variation can be mainly related to the increase of the chemical reactions rate and the products diffusivity across the selective layer. Interestingly, the effect on the reaction kinetics dominates any other possible impact related to the water retention variation: the CO₂ permeability increase takes place along with a decrease of the water concentration within the membrane, even if the R.H. variation is reduced (Table 4.1). At the same time, the monotonous decrease of the H₂ permeability at increasing T determines the CO₂/H₂ selectivity enhancement, suggesting that the H₂ transport rate is mainly related to the

water-induced swelling of the membrane matrix, which dominates over any possible kinetic effect associated with an increase of thermal conditions. A maximum is reached at 107°C, showing a CO₂ permeability of 886 Barrers accompanied with a CO₂/H₂ selectivity of 54. Similar behavior has been obtained for N₂ (Fig. 4.44), with the CO₂/N₂ selectivity increase even more marked compared to CO₂/H₂. Indeed, the mobility reduction, related to the decrease of water concentration, affects more severely the larger-size penetrant, N₂, compared to the smaller one, H₂, (Table 1.1.).

Beyond 107°C, the temperature increase (up to 121°C) corresponds to a substantial reduction of CO₂ permeability value. This decrease is consistent with the influence of water retention on the membrane performance described in the previous paragraph. With less water retained in the membrane matrix at higher temperature (owing to the reduced relative humidity), the fast reaction between CO₂ and carriers as well as the mobility of CO₂-amine reaction products and mobile carriers was hindered significantly, resulting in a consequent decrease of membrane performance. Simultaneously, H₂ permeability kept decreasing along with the water content: the reduction of water-induced swelling of membrane matrix affects negatively the hydrogen transport rate. As a consequence, the CO₂/H₂ selectivity decreased slightly when the operative temperature was increased. On the other hand, different behavior is observed for CH₄ which showed a negligible variation of the related separation factor the T range 107 - 121°C (Fig. 4.44). Such behavior may be related to the higher critical temperature and to the higher partial pressure in the feed stream of CH₄ compared to H₂ and N₂ (feed gas compositions: 20% CO₂, 59.8% CH₄, 20.2% H₂ and 20% CO₂, 40% N₂, 40% H₂), which determine a reduced impact of the H₂O concentration on the overall transport properties of this compound.

Thus, for the MMMs developed in this work, 107°C is determined to be the optimal test temperature at a feed pressure of 15 atm. Similar results are reported in literature for other facilitated transport membrane: for example, the optimal test temperature was 100°C for sulfonated polybenzimidazole copolymer-based membranes [72], 107°C for crosslinked PVA-POS/fumed silica MMM [78], and 110°C for the chitosan-based membranes [139]. For facilitated transport membranes with a similar composition, the optimal test temperature varied according to the operating conditions. For example, the

optimal temperature was 110°C for the crosslinked PVA/amine membrane tested at a feed pressure of 2 atm [96], but changed to 106°C when operated at 15 atm [77].

The above results show that the membrane performance are very sensitive to some parameters such as temperature and relative humidity, and the operative conditions which maximize the separation performance are limited to a narrow range. Reduced changes of the operative conditions may lead to relevant variations in permeability or selectivity and a very accurate control would be needed in case of further scale up of this technology.

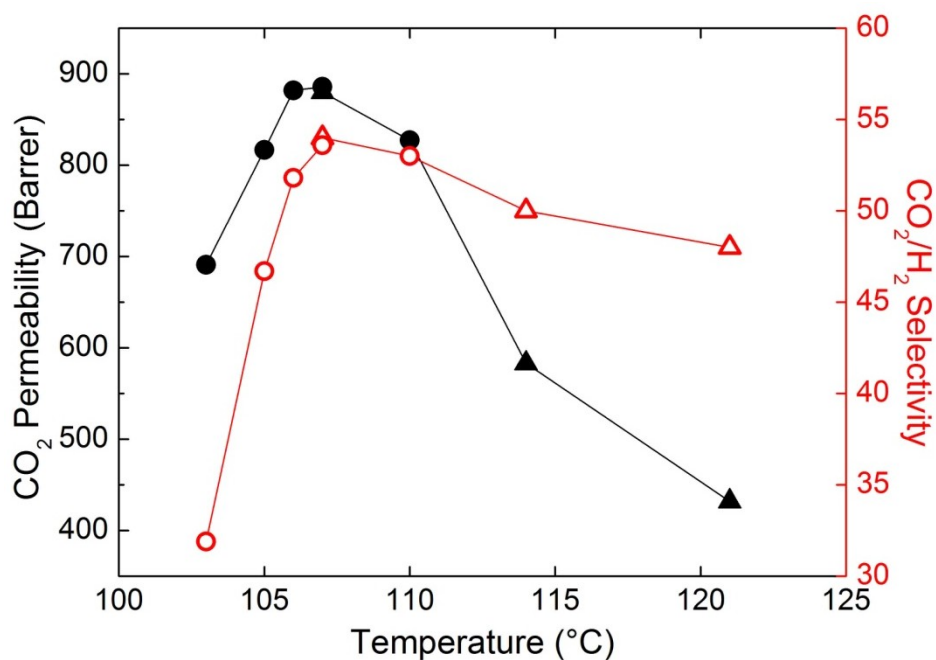


Figure 4.43 - Effects of operating temperature on the separation performances of MMMs with 2.2 wt% AF-MWNTs at a feed pressure of 15 atm: (1) CO₂ permeabilities of Membrane S-10 (▲) and S-11 (●); (2) CO₂/H₂ selectivities of S-10 (Δ) and S-11 (○).

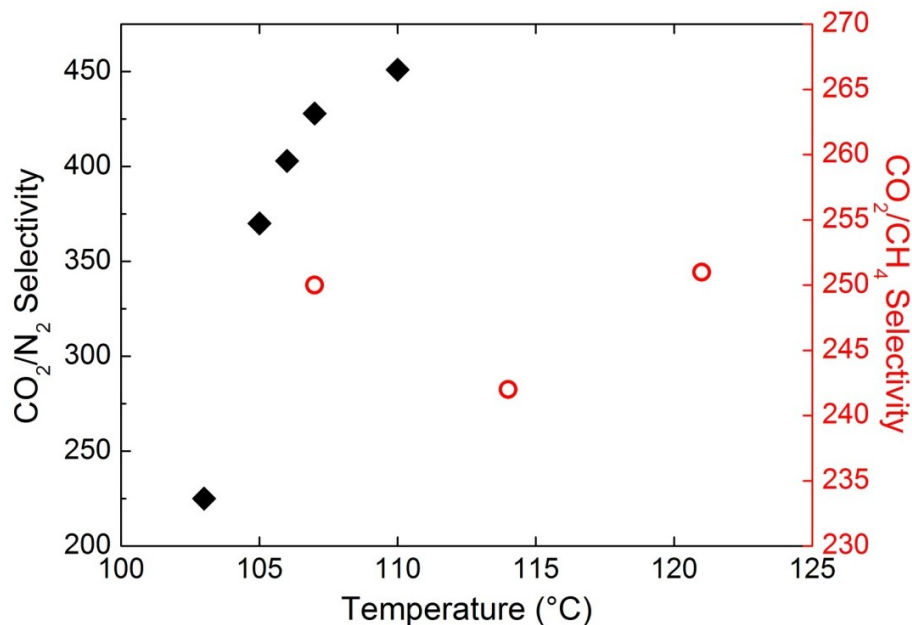


Figure 4.44 - Effects of operating temperature on the CO₂/N₂ and the CO₂/CH₄ selectivity of MMMs with 2.2 wt% AF-MWNTs at a feed pressure of 15 atm

4.3.7 Effect of membrane thickness

Different samples of the mixed matrix membrane of the same composition (composition reference: Sample S-08, Table 3.1) with different thicknesses were also tested under similar operative conditions in order to investigate the influence of the selective layer thickness on the membrane gas transport properties. In particular, a series of permeation experiments were performed maintaining feed pressure and temperature at 15 atm and 107°C, respectively. The test results including CO₂ permeability, permeance, selectivities vs. H₂ and CH₄ are depicted as a function of selective layer thickness in Figures 4.45 and 4.46.

Figure 4.45 reports the variation of CO₂ transport rate along with selective layer thickness: as expected, the CO₂ permeance was found to decrease incrementing the membrane thickness, but interestingly the CO₂ permeability increased. This phenomenon, which is seldom reported in the open literature [71,140], can be explained by the complex gas transport mechanisms in the facilitated transport membrane, which involves the sorption and diffusion of CO₂ molecules and the CO₂-carrier complexes, created by the reaction with the mobile and fixed carriers.

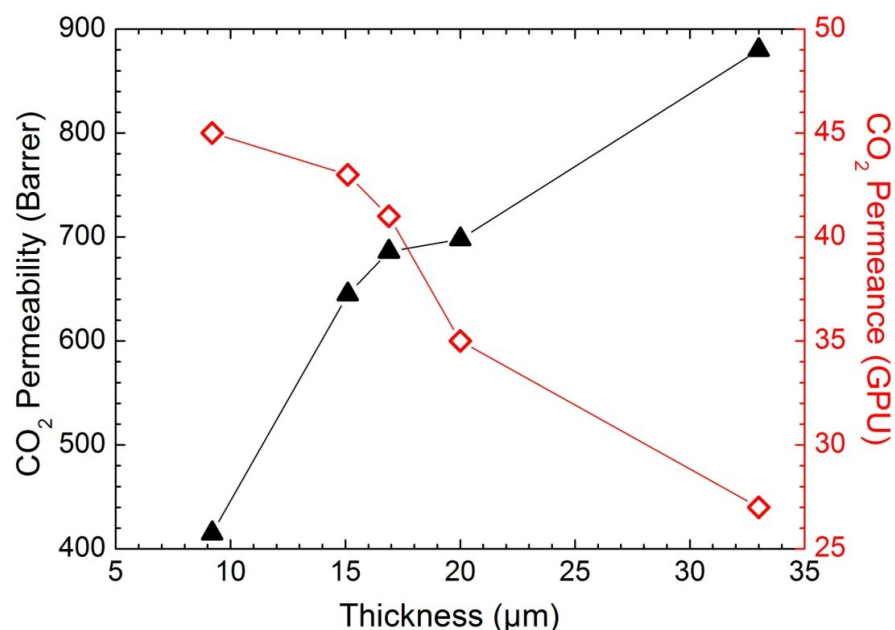


Figure 4.45 - Effect of selective layer thickness on the CO₂ permeability (▲) and CO₂ permeance (◇) (composition reference: sample S-10). Operative conditions: T = 107°C; p = 15 atm; dry gas flow rate = 60/30 cm³/min (feed/sweep); R.H.=100%/72.5% (feed/sweep).

The unreacted CO₂ permeating by solution-diffusion mechanism is indeed believed to be a small portion of the total CO₂ flux across the membrane [66] so that facilitated transport is controlling CO₂ permeation across the membrane. In this framework, CO₂ transport starts with the reaction between CO₂ molecules and amine carriers at the feed gas/membrane interface, followed by the diffusion of the formed CO₂-amine complexes along their concentration gradient across the membrane to the permeate side, where the bonded CO₂ molecules are released into the sweep gas via the reversible CO₂-amine reaction. This complex behavior involving both reaction and diffusion cause the transport to be nonlinear (less than linear) with respect to polymer thickness so that different behavior of permeability and permeances can be found for the same membrane. A more detail description will follow in Chapter 5.

In Figure 4.46 the selectivity trend is reported as a function of the selective layer thickness for both gas pairs. As expected, it increased along with the thickness, since the

flux of the gas species permeating by solution-diffusion decreases to a large extent if compared to the CO₂ flux, in agreement with the permeability behavior showed before.

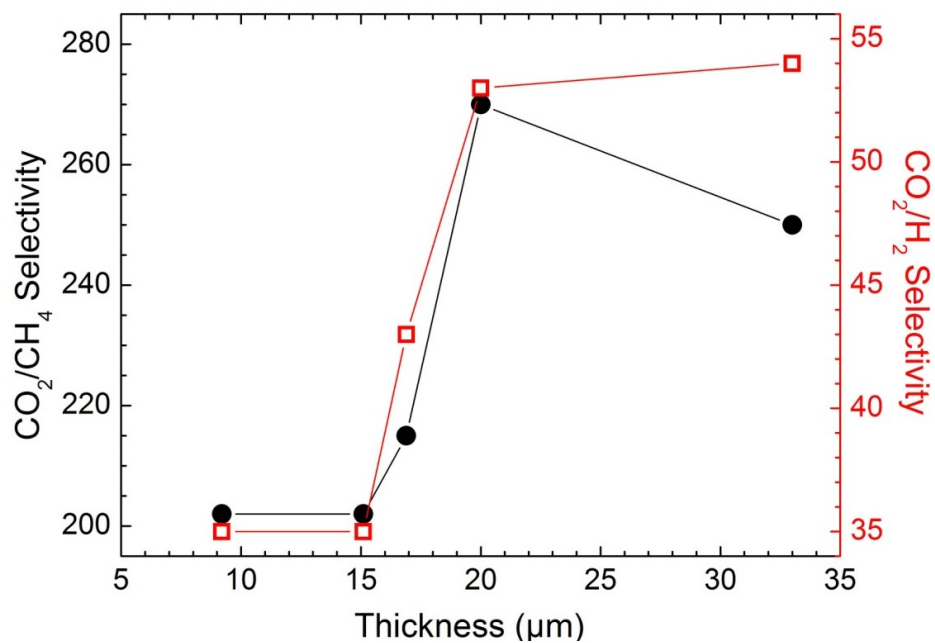


Figure 4.46 - Influence of the selective layer thickness on the CO₂/CH₄ (●) and CO₂/H₂ (□) selectivity (composition reference: sample S-10). Operative conditions: T = 107°C; p = 15 atm; dry gas flow rate = 60/30 cm³/min (feed/sweep); R.H.=100%/72.5% (feed/sweep)

5. Modeling

In this chapter, the experimental data illustrated in the previous sections have been thoroughly analyzed and modeled, aiming at the description of the physical processes that govern the transport mechanisms, and the achievement of a deep insight on the effect of different operative parameters on the materials transport properties.

Therefore, the constitutive equations and the thermodynamic models of interest for the description of the diffusion and the solubility of low molecular weight species in polymeric systems will be briefly presented. Subsequently, these theories will be suited to the particular conditions considered during the experimental characterization considered, and then applied in order to give a theoretical representation of the obtained data sets.

5.1 Free Volume Theory

The diffusion of low molecular weight species in polymer systems can be represented by the well known free volume theory (FVT) [40,46,101,141], considering the motion of small molecules within the matrix as a series of elementary diffusive jumps in the unoccupied volume available for penetrants. The diffusion kinetics are thus strongly correlated with the free volume present in the polymer matrix, as first presented by Cohen & Turnbull [142], who provided a theoretical description of the diffusion coefficient in a liquid composed of hard spheres. They divided the total volume of the liquid in two components: that occupied by the spheres and the remaining free volume. The free volume may be described in terms of voids, created by natural thermal fluctuation, within the framework of the hard spheres. A sphere is able to undergo a single diffusion step when the void size, manifested in its neighborhood, is large enough to host its volume. In this view, they developed a distribution function able to represent the probability of finding a free volume hole of a specific size, relating the kinetic features with the reverse of free volume by means of an exponential equation.

In binary mixtures composed of long molecular chains and small molecule (e.g. solid polymeric matrix with low molecular weight penetrants), the description of the polymer

molecular structure is given by a series of multiple spheres (or jumping units) covalently bonded together. In this case, polymer chains cannot entirely diffuse in a single jump, but their migration is envisioned to be produced by the motion of small elements composing the macromolecules. Small molecules diffusion can take place within these chains fluctuations, which continuously open free volume elements suitable to host the penetrants size, favoring their diffusion across the polymer. Vrentas & Duda [143] divided this quantity in two contributions (Fig. 5.1), to carefully describe the free volume available for small penetrants to diffuse: the *interstitial* free volume, whose redistribution energy is assumed large enough to do not contribute to the molecules motion across the polymeric matrix, and the *hole* free volume, which conversely can redistribute with a negligible energy contribution. Hence the latter term is the free volume fraction accessible for the diffusion process. Starting from these considerations, Vrentas and Duda [27] developed a complex mathematical framework capable to accurately describe the self diffusion coefficient of different penetrants in polymer systems. The model takes into account the energy required by the molecules to overcome the attractive forces holding them to the neighbors, the critical volume required for the polymeric chain displacement and the average hole free volume [27,144].

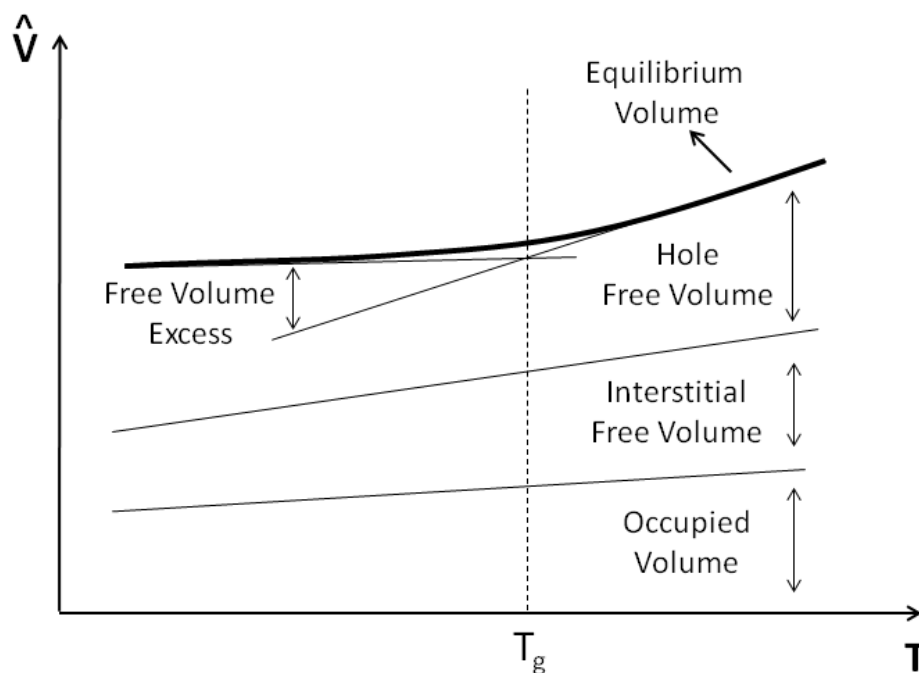


Figure 5.1 - Polymer volume description by Vrentas and Duda (readapted from ref. [145])

The average hole free volume is defined as the difference between the specific volume of the polymers and the specific volume occupied by the polymeric macromolecules themselves, which can be obtained from several schemes reported in literature [146–148]. Despite the original formulation, simpler correlation of experimental diffusion data in polymeric materials have been obtained considering the fractional free volume (FFV), defined as the ratio between the average hole free volume and the specific volume of the polymer. In particular, the FFV is evaluated from the specific volume of the polymer, \hat{V}_{pol} , and the specific volume occupied by the polymeric chains, \hat{V}_{pol}^0 . This last quantity is usually considered correlated to the van der Waals volumes of the various portions of the polymer chains (\hat{V}_{pol}^{vdW}), calculated in the present work through the Bondi's group contribution method [149], by means of the following relationship [150]:

$$FFV = \frac{\hat{V}_{pol} - \hat{V}_{pol}^0}{\hat{V}_{pol}} = \frac{\hat{V}_{pol} - 1.3 \cdot \hat{V}_{pol}^{vdW}}{\hat{V}_{pol}} \quad (5.1)$$

The 1.3 proportionality factor, of general use in FFV calculations, derives from the packing density estimation, and is required to account also for the volume of the polymer phase inaccessible to host molecules [29].

Hence, in the Free Volume Theory simplest formulation, the gas diffusion coefficient is related to the FFV by means of the following equation [151]:

$$D_i = D_{i,0} \cdot \exp\left(-\frac{\beta_i}{FFV}\right) \quad (5.2)$$

where $D_{i,0}$ and β_i are specific parameters for the gas-polymer pair considered. Moreover, as already discussed in the first chapter, a similar dependence from the FFV of the polymeric matrix can be used to describe the permeability coefficient [114,150]:

$$P_i = A_i \cdot \exp\left(-\frac{B_i}{FFV}\right) \quad (5.3)$$

For a given system, the penetrant-free volume interaction parameter, B_i , is practically temperature independent [46], whereas the pre-exponential factor, A_i , can be expressed

by an Arrhenius relationship, which exhibits an exponential dependence with the reciprocal absolute temperature. Eq. 5.2 thus becomes:

$$P_i = A_i(T) \cdot \exp\left(-\frac{B_i}{FFV}\right) = \left(A_{i,0} \cdot \exp\left(-\frac{E_{P,i}}{RT}\right)\right) \cdot \exp\left(-\frac{B_i}{FFV}\right) \quad (5.4)$$

where $A_{0,i}$ is a specific parameter for the gas-polymer pair, substantially temperature independent, whereas $E_{P,i}$ is the activation energy of the permeation process.

Eq. 5.4 can thus provide the evaluation of the gas permeability in the polymeric matrix, using two adjustable parameters, $A_{0,i}$ and B_i , together with the activation energy $E_{P,i}$, once the polymer density is available and several examples are available in literature for permeation data based on dry experimental conditions [46,151–153].

5.2 NELF Model

Several modeling approaches have been proposed in the past decades to describe the thermodynamic behavior of gases and vapors mixture with rubbery materials, but they have been demonstrated to fail in the description of the solubility coefficient below the glass transition temperature, because of the out of the equilibrium nature of glassy polymer systems. Empirical or semi-empirical approaches have been proposed to describe the sorption behavior in glassy polymers (e.g. dual mode solubility model [154], molecular thermodynamic model [155], glassy polymer lattice sorption model [156]), although they do not own any predictive feature.

Doghieri & Sarti [157] in 1996 proposed a rigorous model, based on a thermodynamic approach capable of extending the validity of equation of states in the glassy non equilibrium conditions, aiming at the description of the solubility of fluid penetrants in glassy polymers. This initial model was called, non equilibrium lattice fluid (NELF) model, as it was based on the lattice fluid (LF) theory, originally presented by Sanchez & Lacombe in 1976 [158], which is often employed for the description of phase equilibria of polymer/solute systems, in view of its simplicity and accuracy. The LF theory describes all the system of interest as a lattice, partially filled by different molecules (or macromolecules), whose capability of occupying the lattice sites depends on their structure and molecular weight. The evaluation of the pure component properties is

provided by the LF model with the use of three characteristic parameters, which are in turn related to conditions in the close packed state (the theoretical maximum density condition of the lattice):

- the characteristic density, ρ_i^* , that represents the close packet mass density for the pure component;
- the characteristic pressure p_i^* , related to the cohesive energy density in the same conditions;
- the characteristic temperature, T_i^* , that is a measure of the close packed lattice site energy.

These parameters can be obtained by the best fit of the LF equation of state to pressure volume temperature data (PVT) above T_g for the polymer and to either PVT or vapor liquid equilibrium (VLE) data for the condensable species.

The NELF model adopts the same thermodynamic representation and uses the same parameters of LF equilibrium theory, but extends its validity in the glassy domain through the use of a consistent and physically rigorous approach. The basic hypothesis of NELF model is to consider the non equilibrium structure as a thermodynamic systems endowed with internal state variables kinetically frozen at a value different from that of equilibrium. In particular, the polymer density, ρ_{pol} , was chosen as the internal state variable for the system, as it cannot evolve towards equilibrium conditions due to the kinetics constraint, which hinders polymers relaxation below T_g .

From this initial hypothesis, following rigorous thermodynamic arguments, it has been demonstrated [159] that the chemical potential per unit mass of solute in the glassy state, μ_i^{NE} , coincides with the corresponding property calculated for the equilibrium condition, μ_i^{Eq} , at the same temperature, polymer density and system composition, Ω (vector of the mass ratio of the solutes scaled on the polymer mass), but at a pressure (corresponding to the equilibrium value at the given operative condition) which is different from the experimental one:

$$\mu_i^{NE}(p, T, \rho_{pol}, \Omega) = \mu_i^{Eq}(T, \rho_{pol}, \Omega) \quad (5.5)$$

This result represents the core of NELF theory, and it is independent from the equation of state considered for the free energy calculation. Nevertheless, it must be pointed out that

the ρ_{pol} is a non equilibrium quantity and it cannot be calculated starting from the typical set of variables (i.e. temperature, pressure and composition) but it must be directly measured for the specific conditions in which the NELF model will be used to solve the equilibrium problem. The dry polymer density may be used only assuming a negligible swelling induced by penetrants (e.g. low M_w gases and low partial pressures); in all the other cases, density estimation can be carried out through penetrant-induced dilation data, obtained experimentally, or with a novel version of NELF model [160]. On the basis of the dimensionless equation provided by the LF theory for the Helmholtz free energy of a mixture [158], an expression for the non equilibrium chemical potential can thus be finally obtained:

$$\frac{\mu_i^{NE}}{RT} = \ln(\tilde{\rho}\phi_i) - \ln\left(1 - \tilde{\rho}\right) \left[r_i^0 + \frac{r_i - r_i^0}{\tilde{\rho}} \right] - r_i - \tilde{\rho} \frac{r_i^0 v_i^*}{RT} \left[p_i^* + \sum_{j=1}^{N_p+1} \phi_j (p_j^* - \Delta p_{i,j}^*) \right] \quad (5.6)$$

where:

- $\tilde{\rho}$ is the dimensionless density, calculated as ρ/ρ^* ;
- ϕ_i is the close-packed volume fraction;
- r_i^0 and r_i are the number of lattice cells occupied by the component i in the pure state and in the mixture, respectively;
- v_i^* is the molar volume of the lattice cell;
- $\Delta p_{i,j}^*$ describes the interaction energy between the two species i and j defined as
$$\Delta p_{i,j}^* = p_i^* + p_j^* - 2(1 - k_{ij})\sqrt{p_i^* \cdot p_j^*} ;$$
- k_{ij} is the only binary parameter used to describe the interaction between the two compounds present in the system.

This quantity is then used to define phase equilibria by considering that even in the glassy phase the general equilibrium condition holds, stating that the chemical potential of the same components in the different phases must coincide. In the end, therefore the evaluation of the solubility of the $N_C - I$ gaseous penetrants of the mixture is carried out solving a set of $N_C - I$ pseudoequilibrium equations in order to obtain the mass fraction of

all penetrants in the polymer, giving a direct estimation of their solubility for the given experimental conditions.

5.3 Theoretical consideration on thermal treatment and aging results

As previously examined in paragraph 4.1, the results obtained for gas permeation in glassy polyimides systems pretreated at different temperature and those obtained at different times after such treatment (aging) can be explained in the framework of free volume analysis. Equation 5.1 could be thus used to describe the variation of the diffusion coefficients both for CO₂ and CH₄, as related to changes in the free volume available for penetrant diffusions due to thermal or aging rearrangements of the polymer macromolecules.

In particular, the comparison of the diffusivity at a given state (specific pretreatment or aging time) with that obtained for Ma50, chosen as reference, provides the diffusivity ratio, which is related to the difference in fractional free volumes between the two states as follows:

$$\frac{D_{i,state X}}{D_{i,Ma50}} = \exp \left[\beta_i \left(\frac{1}{FFV_{Ma50}} - \frac{1}{FFV_{state X}} \right) \right] \quad (5.7)$$

For carbon dioxide and methane it is thus possible to write:

$$\left(\frac{1}{FFV_{Ma50}} - \frac{1}{FFV_{state X}} \right) = \frac{1}{\beta_{CO_2}} \ln \frac{D_{CO_2,state X}}{D_{CO_2,Ma50}} \quad (5.8)$$

$$\left(\frac{1}{FFV_{Ma50}} - \frac{1}{FFV_{state X}} \right) = \frac{1}{\beta_{CH_4}} \ln \frac{D_{CH_4,state X}}{D_{CH_4,Ma50}}$$

The left term must be identical for CO₂ and CH₄, producing the following relationship:

$$\ln \left(\frac{D_{CO_2,state X}}{D_{CO_2,Ma50}} \right) = \frac{\beta_{CO_2}}{\beta_{CH_4}} \ln \left(\frac{D_{CH_4,state X}}{D_{CH_4,Ma50}} \right) \quad (5.9)$$

Hence, reporting the two quantities $\ln\left(\frac{D_{CO_2, state X}}{D_{CO_2, Ma50}}\right)$ and $\ln\left(\frac{D_{CH_4, state X}}{D_{CH_4, Ma50}}\right)$ in a plot a linear relationship should hold. Figure 5.2 reports the results obtained for the different thermal pretreatments and, as one can see, a linear relationship well represents the data obtained from experimental diffusivity data (regression coefficient = 0.993), providing further support to the proposed theoretical analysis. A lower regression coefficient is found for the diffusion coefficient measured for the specimen Ma50 as a function of the investigated aging times, although the obtained value remains higher than 0.90, suggesting a satisfying correlation with the proposed theory.

In addition, it should be noted that the slopes of the experimental curves related to the $\beta_{CO_2}/\beta_{CH_4}$ ratio for the two cases, pretreatment and aging, are extremely similar, with differences in the order of 10%, likely related to experimental uncertainty arisen by the completely different processes investigated during the experimental campaign. This feature further support, in a qualitative way, the hypothesis that the effect of aging and pretreatment effect on permeability are both related to variations in the fractional free volume of the polymeric matrix.

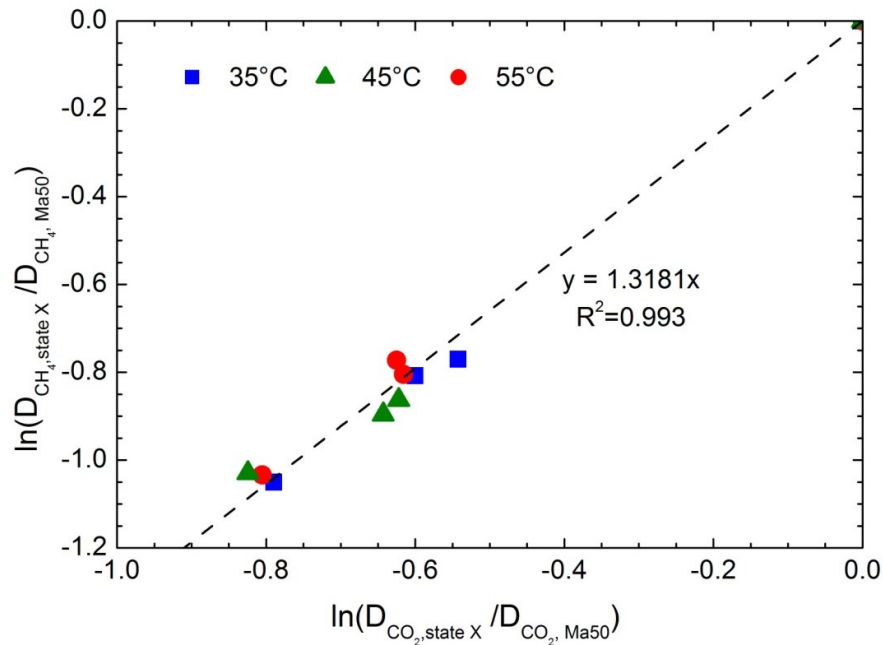


Figure 5.2 - Analysis of different T pretreatments (Ma50, Ma100, Ma150 and Ma200) diffusion coefficient based on the Free Volume Theory

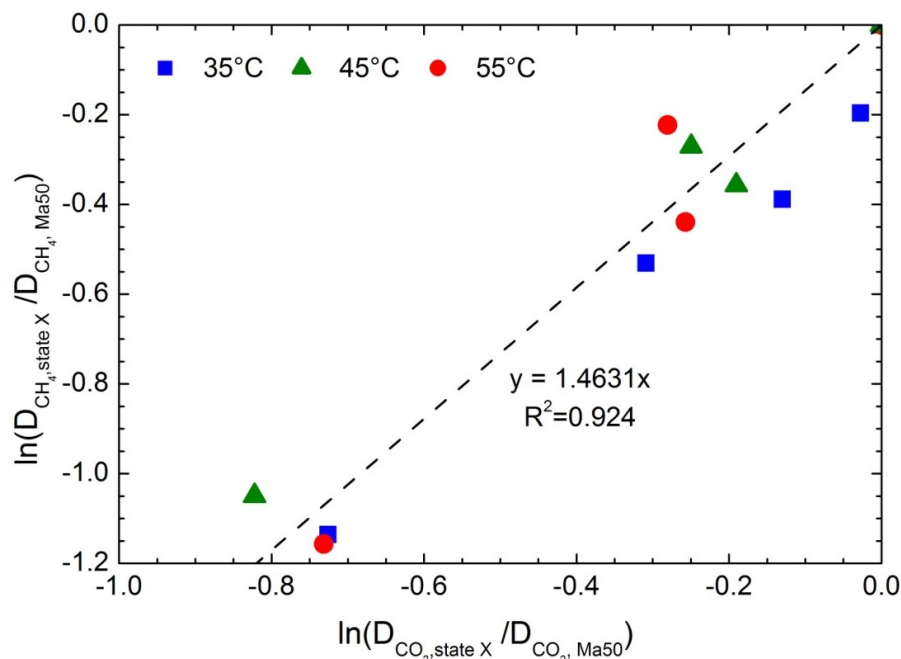


Figure 5.3 - Analysis of Ma50 diffusion coefficient for different aging times based on the Free Volume Theory

5.4 Modeling humid gas permeability

In Chapter 4, it has been showed that the experimental permeability behaviors in presence of water vapor of the different penetrants and at the different temperatures in Matrimid are quite similar, as they decrease as water activity increases by approximately the same extent. This trends may be explained correlating the permeability decrease directly to the water content in the membrane, also in view of a negligible temperature effect on water solubility in Matrimid in the inspected T range (paragraph 4.2.1). In particular, a mechanism of competitive sorption of the gaseous penetrant with the more condensable species (water) is established, leading to the observed permeability reduction. It is thus assumed that water is preferentially absorbed in the polymers occupying free volume sites available for gas diffusion in the glassy matrix, with a consequent reduction of the permeability, as already reported for other polyimides [60,124,125,161]. Such explanation indeed do not consider any preferential or specific interaction between gas molecules and water or polymer, thus explaining why, from an experimental point of view, the permeability of a small gas molecule, like He, is affected by the presence of

H₂O as much as the permeability of CO₂, much larger and definitely more condensable than He.

The decrease of the available free volume induced by the presence of water is expected to affect, in principle, both penetrant diffusion and solubility coefficient in the polymer, thus resulting in an overall permeability decrease for all gases. In this concern, two different approaches will be proposed.

In the first one, a simple empirical model will be used to describe the permeability variation, assuming that the predominant effect of water presence in the matrix may be attributed to the kinetic part of permeation, neglecting, in first approximation, any contribution given by solubility coefficient. These assumptions lead to the behavior observed experimentally with permeability values lower in humid conditions with respect to those in the dry state, as the probability for a gas molecule to find an available site to diffuse inside the membrane is reduced by the presence of water. The larger is the amount of H₂O present in the membrane matrix, the lower is the free volume accessible to other gases, and thus the lower will be their effective diffusivity across the membrane.

In a second modeling scheme, the present free volume approach is combined to a thermodynamic model, capable to predict the solubility coefficient, taking advantage of the concepts proposed in the empirical model. Despite the mathematical complexity, the more rigorous approach will allow the exhaustive description of the physical phenomena associated to the particular studied conditions.

5.4.1 Free volume based empirical model

As previously reported, the presence of stationary water inside the membrane decreases the fractional free volume actually available for gas molecules to diffuse, slowing down the permeation process of incondensable species. This effect is accounted for by the estimation of the FFV in humid condition, $FFV_{humid}(a)$, which is carried out considering that the occupied volume unavailable for diffusion is now due to both the polymer chain contribution, V_{pol} , and the contribution $V_{H_2O}^0$ of the water molecules absorbed in the polymer matrix. Thus we have:

$$FFV_{humid}(a) = \frac{V_{pol} - V_{pol}^0 - V_{H_2O}^0}{V_{pol}} = \frac{V_{pol} - 1.3V_{pol}^{vdW} - 1.3V_{H_2O}^{vdW}}{V_{pol}} \quad (5.10)$$

In the more general case, the value of FFV_{humid} cannot be readily obtained, as accurate measurements of polymer dilation upon water sorption would be required, together with the estimation of the volume occupied by water inside the matrix. However, in the investigated conditions, the polymer swelling associated to water sorption is actually negligible due to the high rigidity of the polymer structure and to the low amount of water absorbed by the polymer. That greatly simplifies the estimation of FFV_{humid} since V_{pol}^0 is the same as for dry conditions.

Regarding the volume occupied by the water absorbed in the matrix, $V_{H_2O}^0$, we will consider two different cases, representing the two limiting conditions for the actual behavior. In particular, we will consider that the volume occupied per unit mass of dissolved water, $\hat{V}_{H_2O}^0$, may be either constant with water activity (case a), or variable with water activity due to ideal water clustering (case b).

Case a) is expected to hold true in the lower activity range, and its use will provide an overestimation of the total occupied volume at higher activity values and thus an underestimation of the value of FFV_{humid} . In this case, the volume of a single water molecule is assumed constant and proportional to its van der Waals volume, over the entire activity range, so that the portion of FFV occupied by water in the membrane matrix is evaluated directly from the water solubility isotherms. Consequently, the ratio $V_{H_2O}^0/V_{pol}$ to be used in Equation 5.10 for the calculation of FFV_{humid} is given by:

$$\frac{V_{H_2O}^0}{V_{pol}} = \frac{1.3V_{H_2O}^{vdW}}{V_{pol}} = \frac{1.3\hat{V}_{H_2O}^{vdW}}{\hat{V}_{pol}} \Omega_{H_2O}(a) \quad (5.11)$$

where $\Omega_{H_2O}(a)$ is the mass ratio of the dissolved water, in g_{H_2O}/g_{pol} , directly given by the water solubility isotherm (Fig. 5.4, solid line).

Case b), on the other hand, allows to account for the variation with water activity of the average volume occupied by water per unit mass, $\hat{V}_{H_2O}^0$, as a consequence of the possible self-association of water molecules, which reduces $\hat{V}_{H_2O}^0$ as the water activity increases.

Self-association and clustering phenomena are indeed known to occur in H₂O sorption in polyimide materials at high R.H., and to affect significantly the average volume of a single H₂O molecule absorbed in the membrane matrix [162,163]. Following Zimm and Lundberg [164], who studied water sorption in many polymer-water mixtures, clustering occurs when, due to mutual interaction (hydrogen bonding), the distance between the centers of two absorbed water molecules becomes lower than one molecular size. Consequently, the volume of n water molecules clustered together is lower than n times the volume of single water molecules, with a clear influence on the actual volume occupied by the water molecules in the polymer. The assumption of no water-induced swelling to the polymer matrix leads to the estimation of the volume actually occupied by water lower than the one calculated in case a) (constant $\hat{V}_{H_2O}^0$), and correspondingly the FFV_{humid} obtained is larger than in case a). In the cases here inspected, this process seems to start at about 60% R.H., at which the water solubility isotherms in Matrimid [47], substantially linear in the low activity region, shows a clear upturn in solubility. This feature is often related to the self-association of water molecules. [56,59,60,116]. The behavior of the solubility isotherms illustrated in Figure 5.4 shows that below about 60% activity, at which water-water interaction are negligible, Henry's law is followed by the experimental data, that is:

$$\Omega_{H_2O}^H(a) = H \cdot a \quad (5.12)$$

where H is the Henry's constant.

On the other hand, at higher activities, at which clustering phenomena occur, a clear deviation from the ideal linear trend is observed. In the ideal clustering behavior, we assume that the total free volume unavailable to other gases is that occupied by the dissolved water molecules which do not interact with one another, whose amount is represented by the Henry's law line of the solubility isotherm. While, on the contrary, the water sorbed in excess to Henry's law line is ideally clustered and occupies the same free

volume already occupied by the non-interacting water molecules, and thus it does not contribute to the free volume unavailable to other gases.

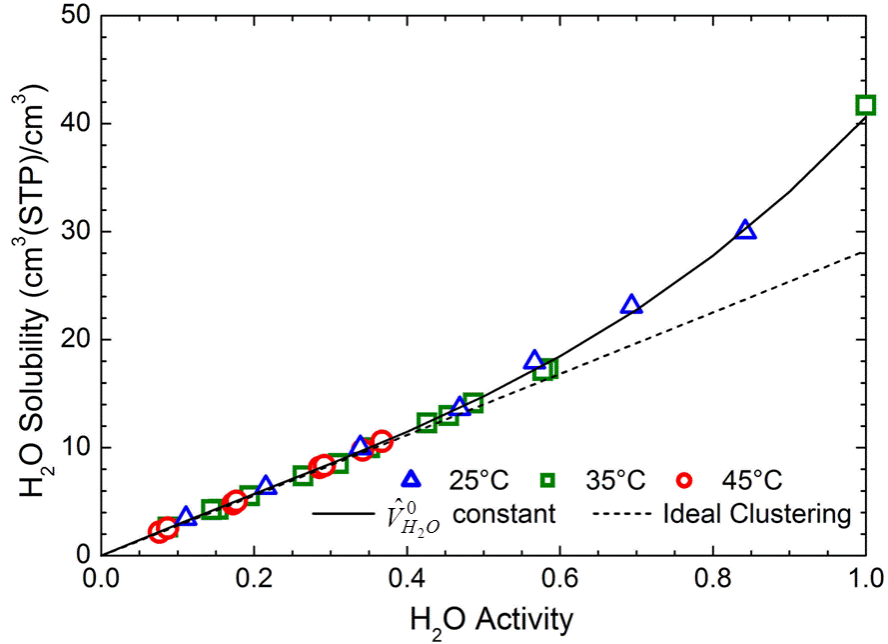


Figure 5.4 - Sorption isotherm theoretical description

This assumption leads to an underestimation of the occupied volume and to an overestimation of the FFV_{humid} value, so that the cases a) and b) here considered reasonably give the lower and the upper limiting values for FFV_{humid} .

According to the assumptions of case b), in the ideal clustering condition one has:

$$\frac{V_{H_2O}^0}{V_{pol}} = \frac{1.3V_{H_2O}^{vdW}}{V_{pol}} = \frac{1.3\hat{V}_{H_2O}^{vdW}}{\hat{V}_{pol}} \cdot H \cdot a \quad (5.13)$$

The FFV_{humid} values calculated in the two limiting conditions considered, case a) and case b), are represented in Figure 5.5. The curves are obtained from the best fit procedure of the actual water solubility isotherm (Fig. 5.4, continuous line), as well as the Henry's law line best described the linear portion of the isotherm (Fig. 5.4, dotted line). The latter curve has been used to calculate FFV_{humid} in the ideal clustering case through Equation 5.13, whereas the actual isotherm is used to calculate FFV_{humid} in the constant $\hat{V}_{H_2O}^0$ case through Eq. 5.9.

All the parameters used to estimate of FFV_{humid} (a) are summarized in Table 5.1.

As expected, both cases a) and b) lead to the same values of FFV_{humid} in the low water activity range as long as the solubility isotherm is actually linear versus R.H. (up to about 60% R.H.), whereas at higher activities, where clustering is likely taking place, case a) would predict a higher free volume decrease with respect to the ideal clustering case b).

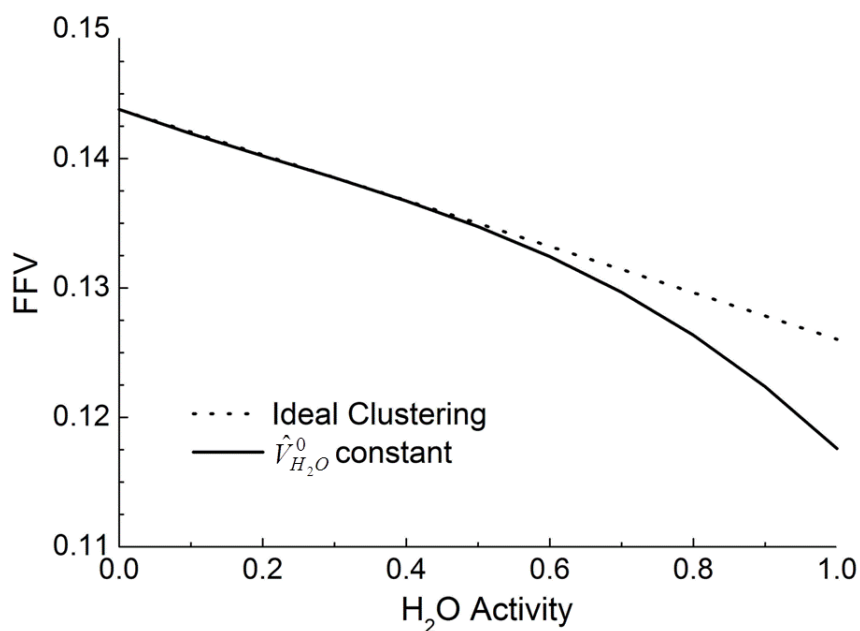


Figure 5.5 - Variation of FFV as a function of R.H. for the two cases considered

ρ (26°C) (g/cm ³)	\hat{V}_{pol}^{vdw} [46] (cm ³ /g)	$\hat{V}_{H_2O}^{vdw}$ [165] (cm ³ /g)	H (g _{H2O} /g _{tot})
1.238	0.532	0.602	0.018

Table 5.1 - Parameters considered for the proposed model

The resulting values of FFV_{humid} at the different R.H. are then used in Equation 5.3 to calculate the permeability of all penetrants, in humid conditions. Two fitting parameters were considered for each gas-polymer pair, namely $A_{0,i}$ and B_i , while, due to a non significant effect of water on the activation energy as discussed in the previous sections,

the $E_{P,i}$, values for all penetrants were considered equal to the ones obtained for the dry conditions and were taken constant over the entire activity range.

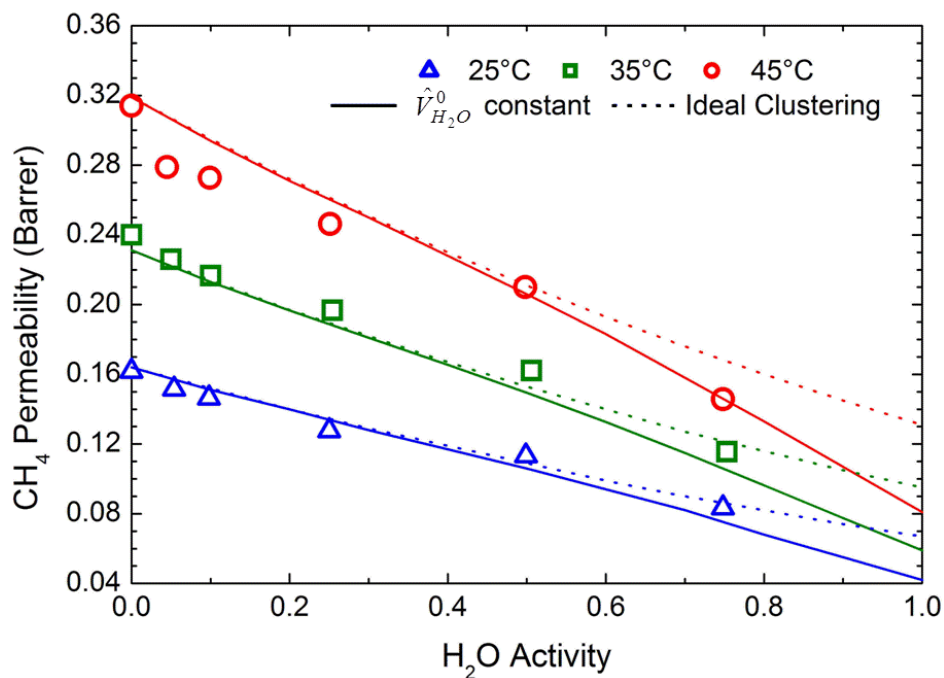
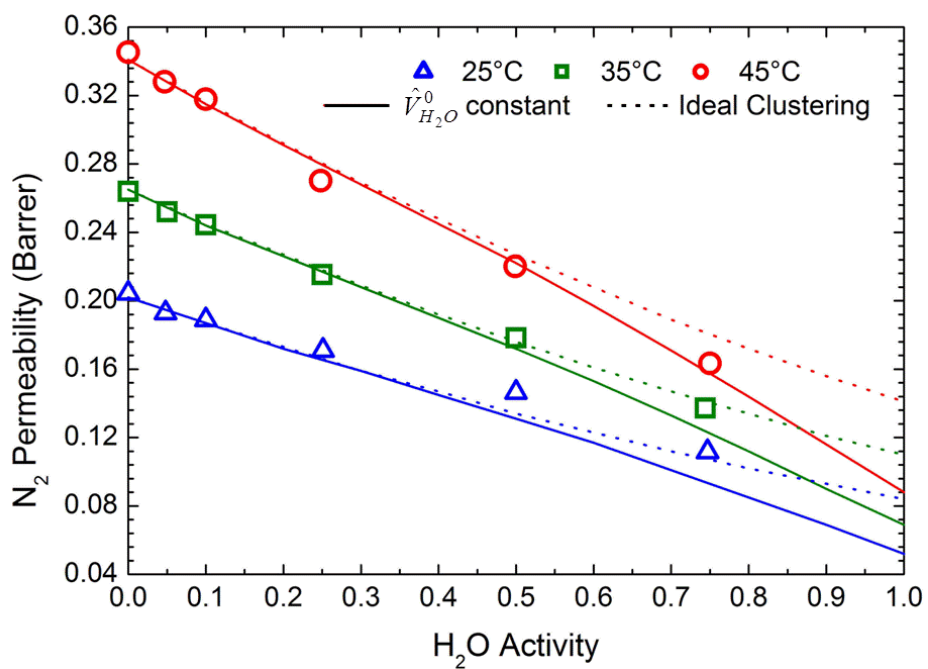
Figures from 5.6 to 5.9 report the comparison between the results of the proposed model and the experimental permeability data of the four different penetrants at the three different temperatures: the solid lines refer to case a) (constant $\hat{V}_{H_2O}^0$), whereas the dotted lines represent the ideal clustering case (case b). As one can see, a remarkable agreement with the experimental permeability is obtained by using for each gas considered only two adjustable parameters, $A_{0,i}$ and B_i , whose values are reported in Table 5.2.

Interestingly, the parameters B_i used in the model calculations, as retrieved from the best fit of the experimental data, are very similar to those already reported in the literature for the different gaseous species, which have been also indicated in Table 3 for the sake of comparison. In particular, the B parameter for CO_2 equal to 0.88, is comparable with the value of 0.86 obtained by Park & Paul [150] based on group contribution methods, whereas the values for N_2 and CH_4 are similar to the ones reported by Rowe et al. [39], obtained by investigating aging effect on the transport properties of Matrimid samples. Likewise, the parameters A_i , calculated by means of Equation 5.3, are comparable with the data available in the open literature: for CH_4 and N_2 for example, at $35^\circ C$, A_i is equal to 128 Barrer and 138 Barrer respectively (case a), very similar to the values of 114 Barrer and 95 Barrer reported by Rowe et al. [39].

In spite of its simplicity, therefore, the model is able to describe rather accurately the experimental permeability behaviors under humid conditions at different temperatures, with only two adjustable parameters per penetrant, suggesting that the physical description presented is highly representative of the real mechanism of the transport process under humid conditions.

	CH_4		N_2		CO_2		He	
	A_0 (Barrer)	B -	A_0 (Barrer)	B -	A_0 (Barrer)	B -	A_0 (Barrer)	B -
<i>This work</i>	$3.5 \cdot 10^6$	0.91	$4.4 \cdot 10^5$	0.90	$1.97 \cdot 10^5$	0.88	$4.60 \cdot 10^6$	0.98
<i>Refs. [39,150]</i>	-	0.967	-	0.914	-	0.86	-	0.701

Table 5.2 - A_0 and B values for the proposed model

Figure 5.6 - Free Volume Theory Model results for CH₄ permeabilityFigure 5.7 - Free Volume Theory Model results for N₂ permeability

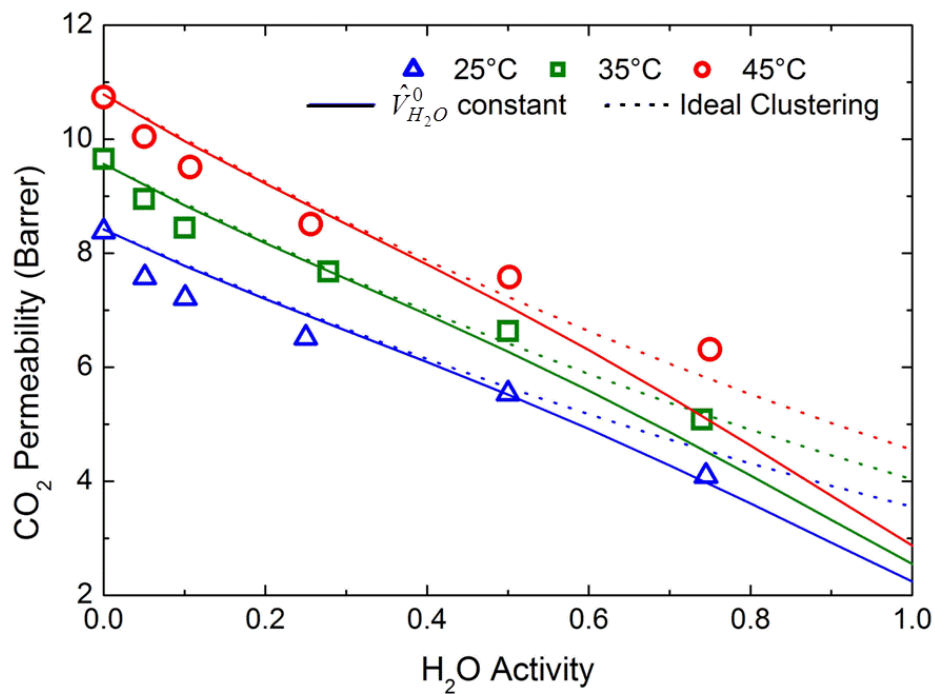
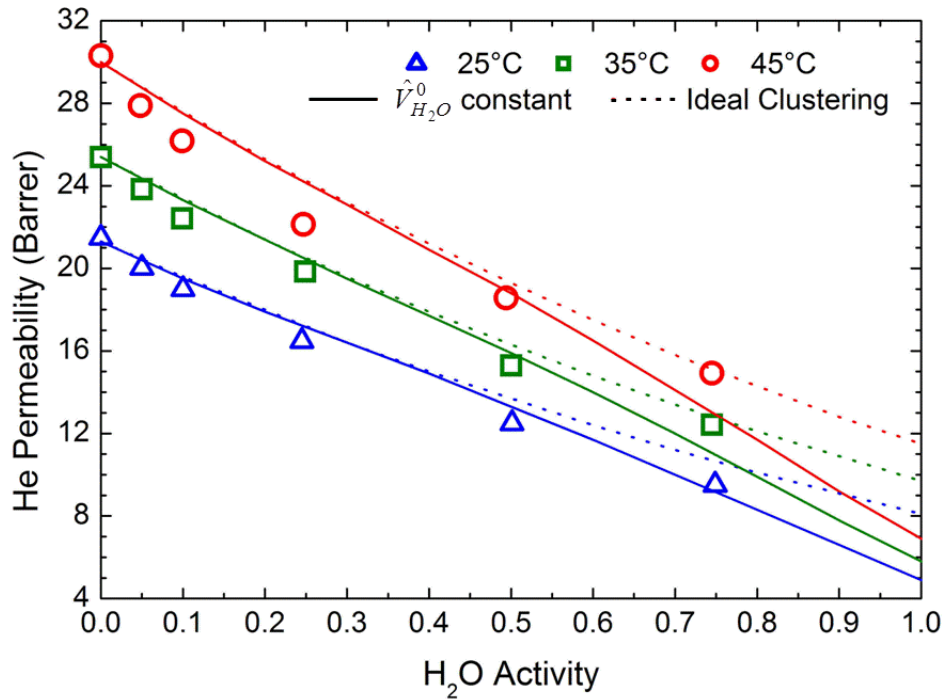
Figure 5.8 - Free Volume Theory Model results for CO₂ permeability

Figure 5.9 - Free Volume Theory Model results for He permeability

5.4.2 Integrated NELF & Free Volume Theory approach

Based on the results obtained from the empirical model reported in the previous paragraph, a more rigorous approach is used to represent the humid permeation process in polyimides, dividing the permeability on the basis of solution diffusion framework. In particular, the ability of NELF approach to predict the solubility of gas mixture in glassy polymers has been coupled with the Free Volume Theory, suitable for the description of the diffusion coefficient, in order to model the permeation process across a selective layer. Indeed, the NELF outcomes will be employed to evaluate both the influence of water vapor on the solubility of incondensable species and to estimate the residual FFV available for them to diffuse across the membrane at increasing the water concentration. The Free Volume Theory will be then utilized for the representation of the kinetic properties in order to describe the permeability data, obtained experimentally. In the present study, only two penetrants have been considered, namely carbon dioxide and methane. The parameters used for the simulation are listed in Table 5.3 and 5.4. In addition a thermal expansion coefficient for the Matrimid polyimide in the glassy state equal to $188.7 \mu\text{m}^3 / (\text{m}^3 \cdot ^\circ\text{C})$ has been considered, obtained from literature [122], and assumed constant in the investigated range of temperature, while a density value at 25°C equal to 1.238 g/cm^3 has been observed experimentally. In the following modeling results, only temperature effect are considered on polymer density, while no swelling is assumed to be induced in the polymer matrix.

	T^* (K)	p^* (MPa)	ρ^* (g/cm ³)
<i>Matrimid</i>	880	450	1.35
<i>H₂O</i>	670	2400	1.050
<i>CO₂</i>	300	630	1.515
<i>CH₄</i>	215	250	0.500

Table 5.3 - Lattice Fluid characteristic parameters for Matrimid and penetrants (Ref. [126])

k_{ij}	H_2O	CO_2	CH_4
<i>Matrimid</i>	-0.093	-0.003	0.072
CO_2	-0.117	-	-

Table 5.4 - Binary interaction parameters as calculated from pure gas sorption data

The H_2O solubility isotherms have been first modeled by means of the NELF for pure and for the mixtures with the two gaseous penetrant at pressure values equal to 0.5 bar, and the results are reported in Figure 5.10. Indeed, in order to mimic the gas concentration within the polymer matrix typical of a permeation experiment ($p^u = 1$ bar), an average concentration has been considered between the upstream and the downstream side, i.e. 0.5 bar. The activity range is showed only up to 60%, as a LF approach can hardly represent the intermolecular forces occurring in the high activity range of vapors, producing association phenomena (e.g. clustering), unless this feature is specifically accounted for by convenient modification in the expression of free energy density. However, in the low activity range, the model provides a satisfactory representation of the experimental data, as documented with the green line (pure H_2O sorption isotherm in Matrimid at $35^\circ C$). Moreover, in the same chart shows also the solubility isotherms in the presence of 0.5 bar of CO_2 or CH_4 , and the results suggest that increasing the condensability of the gaseous compound present in the mixture, the solubility is generally decreasing even though the variation is only to a rather small extent.

The NELF model provides also the information on the influence of water vapor on the incondensable penetrant solubility, and the results are reported in Figure 5.11 and 5.12, at the operative temperatures considered in the present work.

Although, as previously described (paragraph 5.4.1), the experimental data suggested that the presence of water vapor affects mainly the kinetic part of the permeation process, the two figures showed a marked decrease of solubility at increasing the water concentration in the membrane. Interestingly, the more detailed and accurate model, is able to show that, in view of competitive sorption effect, the less condensable penetrant (CH_4) showed the more marked decrease (close to 40% reduction compared to the dry value), as expected considering its critical temperature, whereas CO_2 displayed a decrease up to 26 % if compared to the value obtained in dry conditions. Moreover, increasing the

temperature of the system, this variation becomes more pronounced, although the differences are fairly limited, in the order of 10%. The behavior can be easily explained in view of the temperature influence on CO_2 and CH_4 solubility [82], whose decrease at increasing T is noticeable, compared to the negligible effect observed in case of water uptake process, as previously discussed (paragraph 4.2.1).

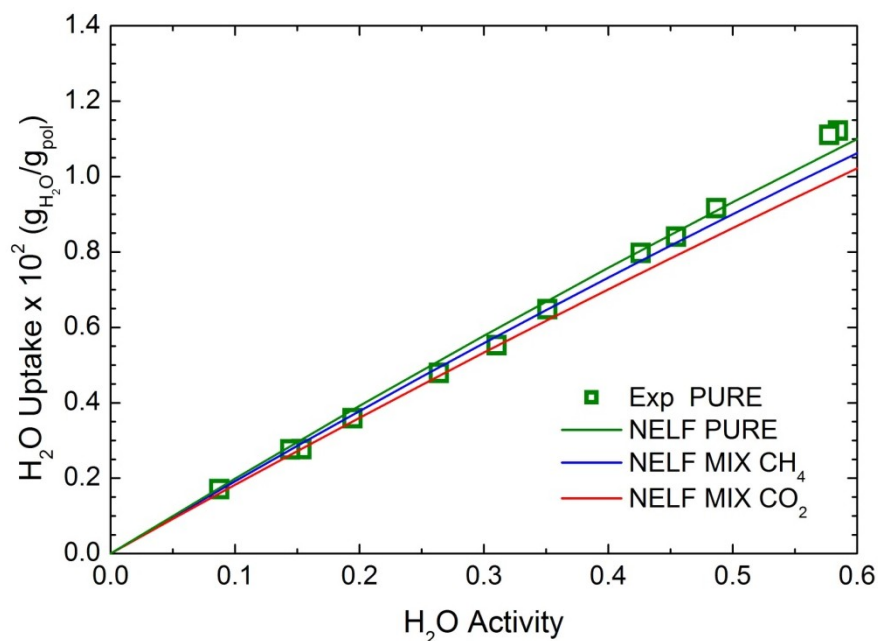


Figure 5.10 - H_2O uptake in Matrimid: experimental data, pure H_2O and mixed $\text{H}_2\text{O}/\text{CO}_2$ and $\text{H}_2\text{O}/\text{CH}_4$ prediction as obtained from NELF Model ($T = 35^\circ\text{C}$, $p_{\text{CO}_2} = p_{\text{CH}_4} = 0.5$ bar)

The free volume theory is applied in this case to the description of the diffusivity only, and to investigate specifically the effect of the presence of water vapor on the D coefficient of the two incondensable species (CO_2 and CH_4). Starting from the H_2O solubility data provided by NELF, the departure of the FFV at increasing the water content in the matrix has been calculated through Equation 5.10, using the same parameters reported in Table 5.1.

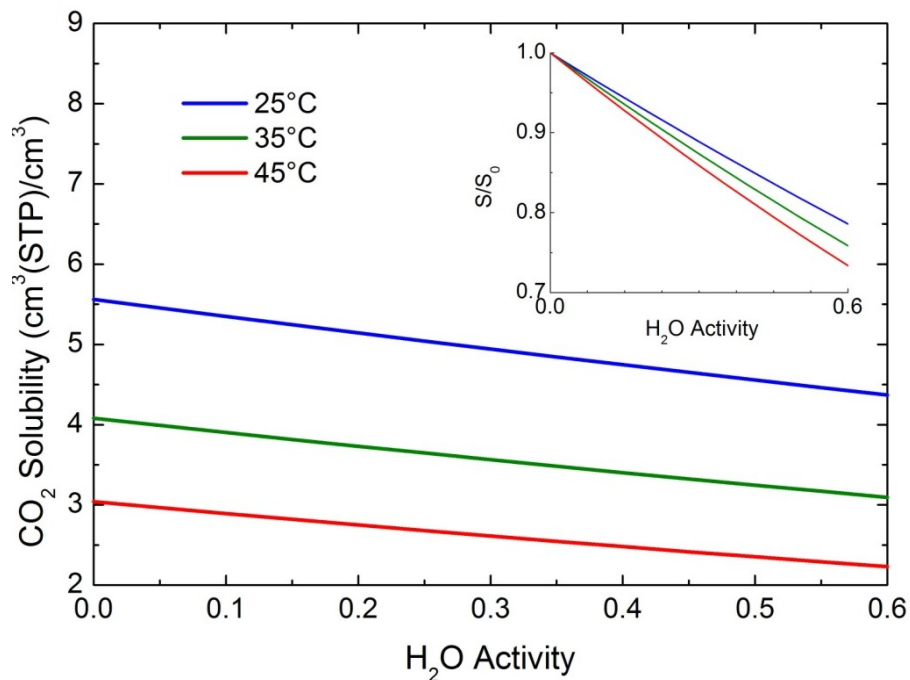


Figure 5.11 - CO₂ solubility variation in the investigated water activity range estimated from NELF ($p = 0.5$ bar)

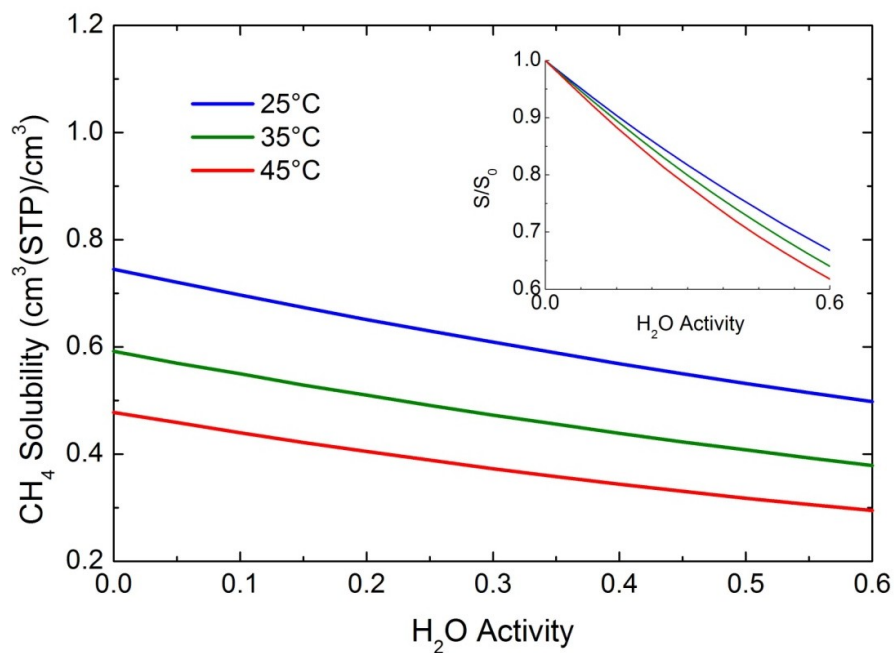


Figure 5.12 - CH₄ solubility variation in the investigated water activity range estimated from NELF ($p = 0.5$ bar)

In particular, this approach describes the approximation of case a), given the unsuitability of NELF model to describe clustering, so that the volume occupied by water molecules has been evaluated as:

$$\frac{V_{H_2O}^0}{V_{pol}} = \frac{1.3V_{H_2O}^{vdW}}{V_{pol}} = \frac{1.3\hat{V}_{H_2O}^{vdW}}{\hat{V}_{pol}} \Omega_{H_2O}^{NELF} \quad (5.12)$$

where $\Omega_{H_2O}(a)$ is now the mass ratio of the dissolved water, estimated for mixture conditions (Figure 5.10, blue and red line for CH₄ and CO₂ respectively). Figure 5.13 illustrates the trends of FFV in the investigated activity range, as obtained at the different temperatures and for carbon dioxide and methane as penetrants. As expected, the free volume available for the penetrant diffusion decreases at increasing humidity, although it is significantly temperature dependent, as it increases at increasing the operative temperature. The present modeling analysis, indeed, accounts also for the thermal expansion of the polymer matrix. Negligible differences are detectable between the behaviors showed by methane at the three operative conditions, whereas in case of CO₂ the reduction in FFV seems to be lower at 25°C, likely due to the capability of the gas to compete strongly with water, which seems to be enhanced at the low temperatures.

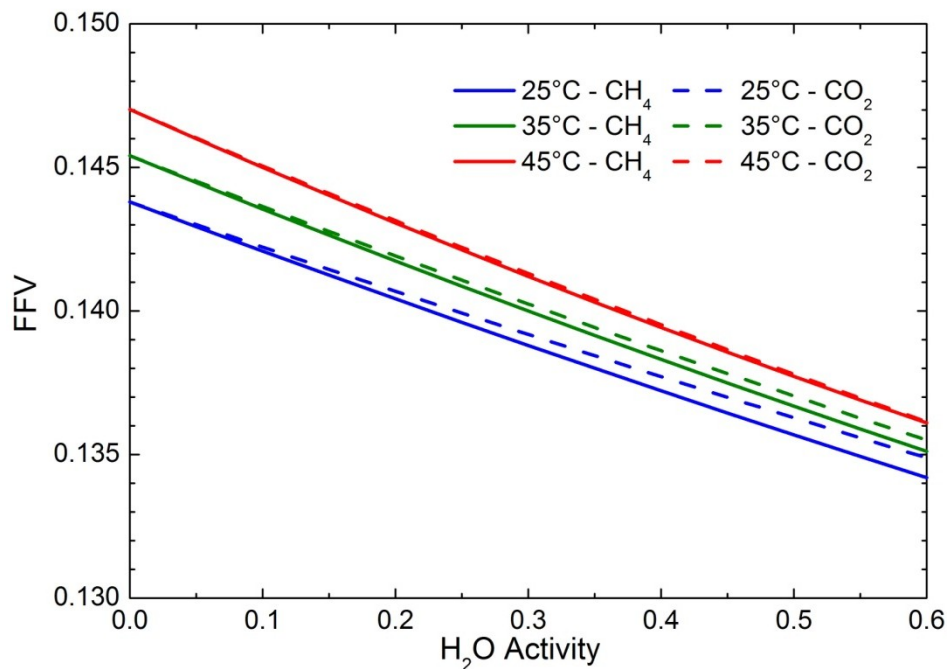


Figure 5.13 - FFV_{humid} available for CH₄ and CO₂ diffusion at different H₂O activity

However, the differences displayed in terms of FFV reduction between the two incondensable species (CO_2 and CH_4) are rather limited, for all the investigated conditions.

The diffusion coefficient has been modeled by means of the Free Volume Theory, starting from the results obtained for FFV variation along with the water concentration in the membrane, using the following equation:

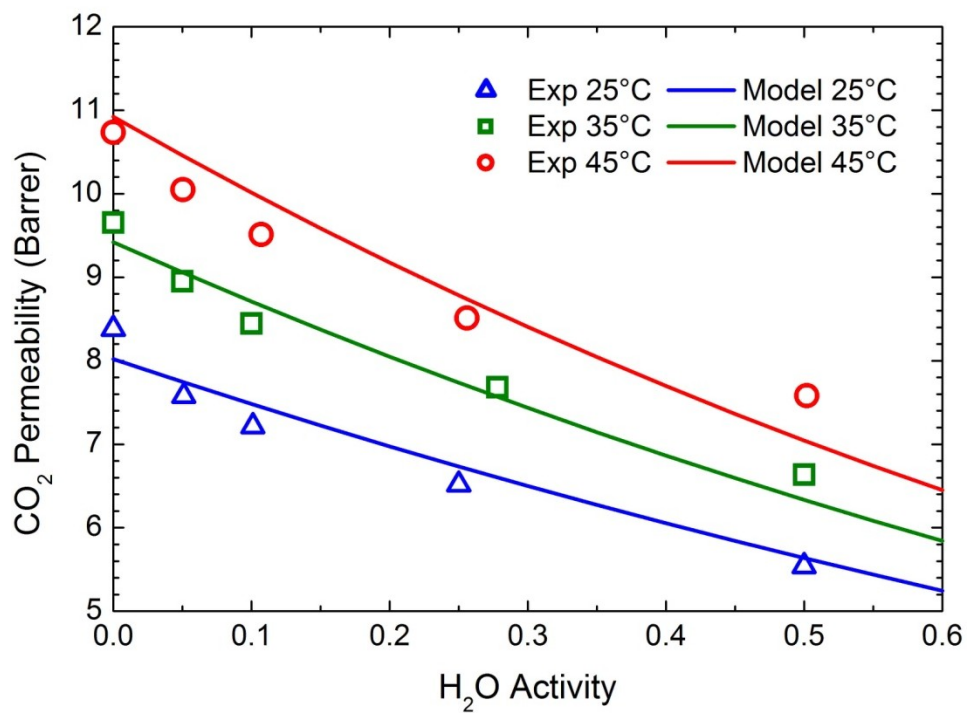
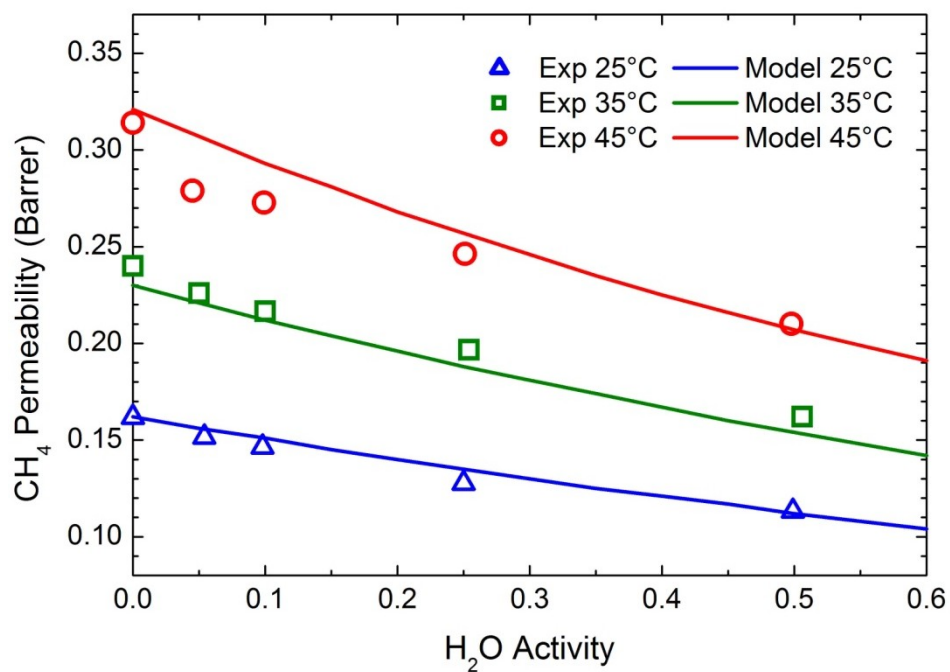
$$D_i = D_{i,0}(T) \cdot \exp\left(-\frac{\beta_i}{FFV}\right) = \left(D_{i,0} \cdot \exp\left(-\frac{E_{D,i}}{RT}\right)\right) \cdot \exp\left(-\frac{\beta_i}{FFV}\right) \quad (5.13)$$

in which $E_{D,i}$ is the activation energy of the kinetic part of the transport process (readily calculated from the experimental diffusivity data obtained in dry conditions, see Appendix, Table A.3), whereas $D_{i,0}$ and β_i are the pre-exponential coefficient and the penetrant-free volume interaction parameters characteristic of the diffusion. The values of these last two variables have been retrieved from the best fit of the permeability isotherms obtained experimentally for the two considered incondensable penetrants (Fig. 5.14 and 5.15) at different water activities. The permeability coefficient is thus obtained according to the solution diffusion mechanism (Eq. 1.4) for a given R.H. (fitting parameters are listed in Table 5.5) as the product of solubility and diffusivity coefficients.

In case of methane, the model is able to describe accurately the permeability data in the considered activity range. The model provides a good description of the experimental behavior also for CO_2 permeability, even though a slight overestimation is observed at activity values larger than 50%, likely related to the inaccuracy of the LF equation of state in describing the CO_2 - H_2O interactions, and in more general terms to the H_2O behavior in the high activity region.

CH_4			CO_2		
$D_{i,0}$ (cm^2/s)	β -	$E_{D,i}$ (kJ/mol)	$D_{i,0}$ (cm^2/s)	β -	$E_{D,i}$ (kJ/mol)
0.062	0.04	44.2	0.0685	0.4	33.6

Table 5.5 - Free Volume Theory parameters used to describe the diffusivity for the model

Figure 5.14 - NELF + Free Volume Theory Model results for CO₂ permeabilityFigure 5.15 - NELF + Free Volume Theory Model results for CH₄ permeability

Furthermore, the parameters listed in Table 5.5 allow also the estimation of the diffusion coefficient of the gaseous penetrants at different water activities, and the attained results for CO₂ and CH₄ are showed in Figure 5.17 and 5.18, respectively. In case of CO₂, the permeability depression at increasing water activity can be attributed equally to solubility and diffusivity coefficients, as the D_{CO_2} decreases up to a factor 20%, with respect to the dry value, and it is more pronounced for higher operative temperature. Conversely, the analysis of CH₄ diffusivity reveals a negligible effect on the D coefficient in the presence of water vapor, with a maximum reduction up to 4% of the dry value. Hence, the marked decrease of CH₄ solubility coefficient reported in Figure 5.12 seems to be the main reason for the permeability reduction, likely due to the lower critical temperature of methane, which determines a weak competition against water vapor for occupying the sorption sites available within the polymer matrix.

The proposed model is able to represent the experimental data very accurately, suggesting that the mathematical description is highly meaningful of the physical mechanisms involved in the transport process. Furthermore, the use of a more rigorous approach allows for a detailed description of phenomena, with the chance to analyze the effect of water vapor on the parameters characterizing the permeation process, i.e. diffusivity and solubility, separately. In particular, conversely to the assumption of the empirical model previously presented, the decrease in permeability in presence of water cannot be completely attributed to a variation of the kinetic factor, but it is caused by a dual effect on diffusion and solubility coefficient, whose extents are function of penetrant characteristics. Indeed, whereas for CO₂ a similar decrease is observed for both D and S , in case of CH₄ the solubility reduction dominates over the effect on the diffusion coefficient.

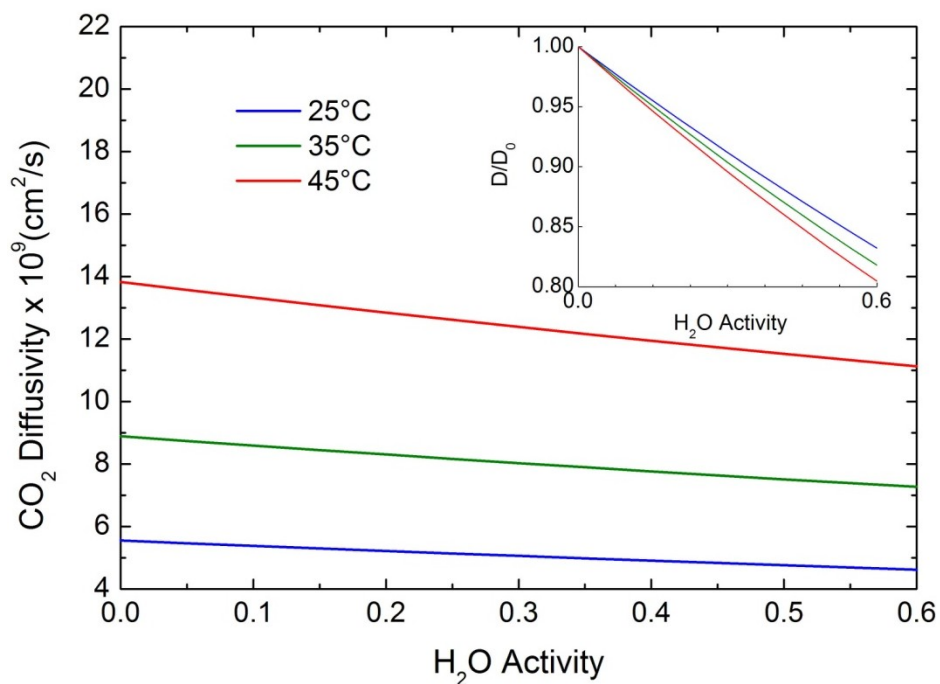


Figure 5.16 - CO₂ diffusion coefficient as estimated by the proposed model as a function of H₂O activity

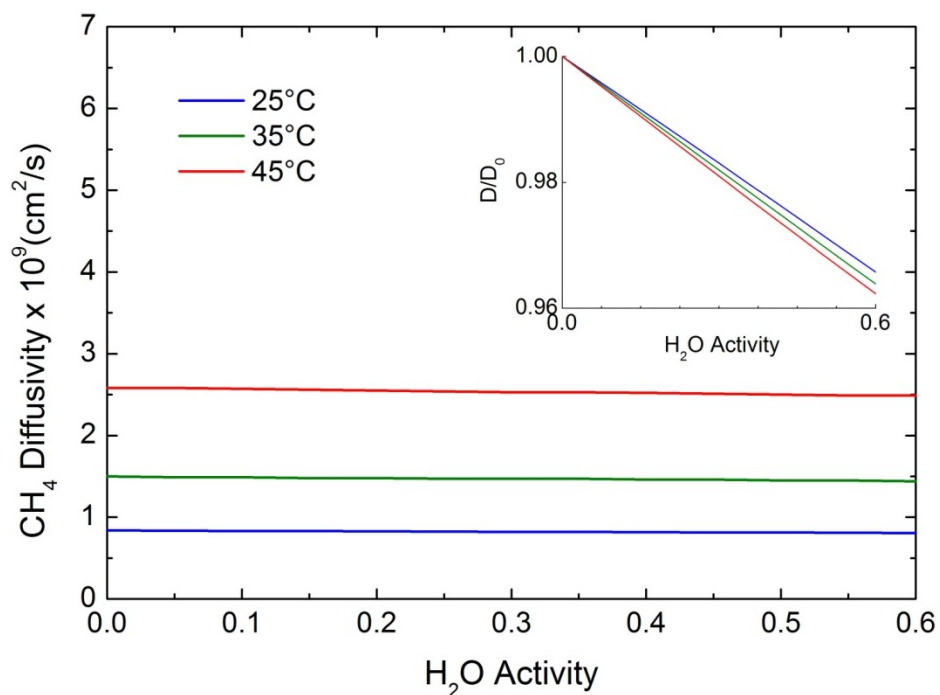


Figure 5.17 - CH₄ diffusion coefficient as estimated by the proposed model as a function of H₂O activity

5.5 Analysis of the facilitated transport: thickness influence

As reported in the paragraph 2.2, a general solution for the facilitated diffusion across a selective layer cannot be obtained, but specific boundary conditions must be fixed in order to solve the transport problem. An accurate mathematical model was proposed by Noble et al. [166] to describe the facilitated transport mechanism for the simplified reaction $A + B \leftrightarrow AB$, in which A represents the CO_2 , B is the carrier and AB is the activated complex. The basic differential equations were solved for the determination of the transport rate in steady-state conditions of both the solute and the carrier complexes, in the hypothesis that the carrier concentration can be considered constant across the selective layer. Assuming then no external mass-transfer resistance on both side of the membrane ($\text{Sh} \rightarrow \infty$) is present, the facilitation factor F , defined as the ratio between the solute total flux (J_{TOT}) and the part related to the solution-diffusion transport (J_{SD}), can be described by means of the following equation:

$$F = \frac{J_{TOT}}{J_{SD}} = \frac{1 + \frac{\alpha K}{1+K}}{1 + \frac{\alpha K}{1+K} \frac{\tanh(\lambda)}{\lambda}} \quad (5.14)$$

where α is the mobility ratio, K is the dimensionless equilibrium constant and λ is defined as:

$$\lambda = \frac{1}{2} \cdot \left(\frac{1 + (\alpha + 1)K}{\varepsilon(1 + K)} \right)^{0.5} \quad (5.15)$$

The thickness dependence of F is expressed by ε , the inverse of the Damköhler number, described as the ratio of the diffusive mass transport rate and the reaction rate:

$$\varepsilon = \frac{D_{AB}}{k_r \cdot \delta^2} \quad (5.16)$$

where D_{AB} is the diffusion coefficient of the CO_2 -carrier complex, k_r is the constant for the reverse reaction and δ is the selective layer thickness.

Once that the facilitation factor is evaluated, the total CO_2 permeability can be calculated as:

$$P_{CO_2}^{TOT} = \frac{J_{TOT} \cdot \delta}{\Delta p_{CO_2}} = \frac{F \cdot J_{SD} \cdot \delta}{\Delta p_{CO_2}} = F \cdot P_{CO_2}^{SD} \quad (5.17)$$

The facilitation factor represents the influence of reaction on the overall transport, and therefore it is clearly thickness dependent, suggesting that also gas permeability is thickness dependent in facilitated transport membranes, in agreement with the obtained results. Indeed, the considered experimental data can be well described by the recalled model assuming that a single overall model reaction is sufficient to describe the CO₂ transport in our membranes as it can be seen in Figure 5.19, in which the continuous and dashed lines have been obtained using Eq. 5.17 for the permeability evaluation. These results are obtained utilizing 5 different parameters, namely α , K , D_{AB} , k_r and P_{SD} , which have been set to conveniently selected values from the technical literature. The parameters are evaluated according to the assumption that, in view of the highly hydrophilic character of the system, the transport is considered to take place mainly in the water-filled domains present in the membrane, especially at the high water concentrations. Therefore parameters α and K were fixed to 15 and 5, respectively, as suggested by Kemena et al. [167], while D_{AB} was chosen equal to 3×10^{-5} cm²/s, in the same order of magnitude of ions diffusivity in water [65]. The reverse reaction constant k_r was then considered equal to 110 s⁻¹, in good agreement with data from the reaction of CO₂ and amines [168,169]. Finally, the P_{SD} , which is the CO₂ permeability related to the solution-diffusion mechanism, was set equal to 150 Barrer, reasonably in line with values reported for permeability in pure PVA membranes in saturation conditions [170], also accounting for the crosslink of the polymer macromolecules in the membranes investigated, and not far from the values estimated for permeability of CO₂ in pure liquid water [32]. The complete set of parameters used in this modeling effort are reported in Table 5.6, for the sake of completeness.

α	K	D_{AB}	k_r	P_{SD}
-	-	(cm ² /s)	(1/s)	(Barrer)
15	5	3×10^{-5}	110	150

Table 5.6 - Proposed parameters for facilitated transport model from Nobel et al. [166]

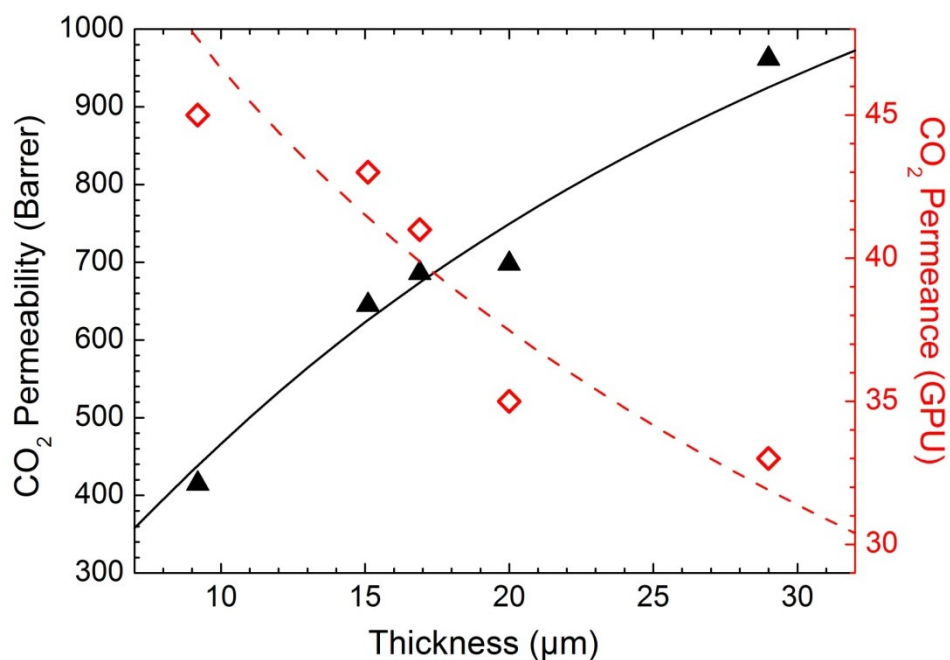


Figure 5.18 - Modeling the thickness influence on the CO₂ permeability and permance

Hence, the model is capable to represent the experimental trends, suggesting that the permeability behavior thickness dependent can be considered an intrinsic property of the mechanism of facilitate transport, mainly related to the diffusivity of the CO₂-carrier complex and to the reaction rate. In this concern, it is interesting to notice that the Damköhler numbers of the experimental data, calculated with the given set of model parameters, resulted always higher than 1, pointing out that the observed behavior takes place when the reaction rate is higher that the activated complex diffusion kinetics, which therefore controls the overall transport across the membrane.

Finally, Figure 5.20 reports as the continuous and dashed lines the gas pair selectivity CO₂/CH₄ and CO₂/H₂ obtained by the present model for the facilitated transport CO₂, and considering an H₂ and CH₄ average permeability equal to 15.3 Barrer and 2.9 Barrer (average values calculated from the permeability data obtained for the samples with different thicknesses) respectively. As one can see, the modeling results well compare with the experimental data.

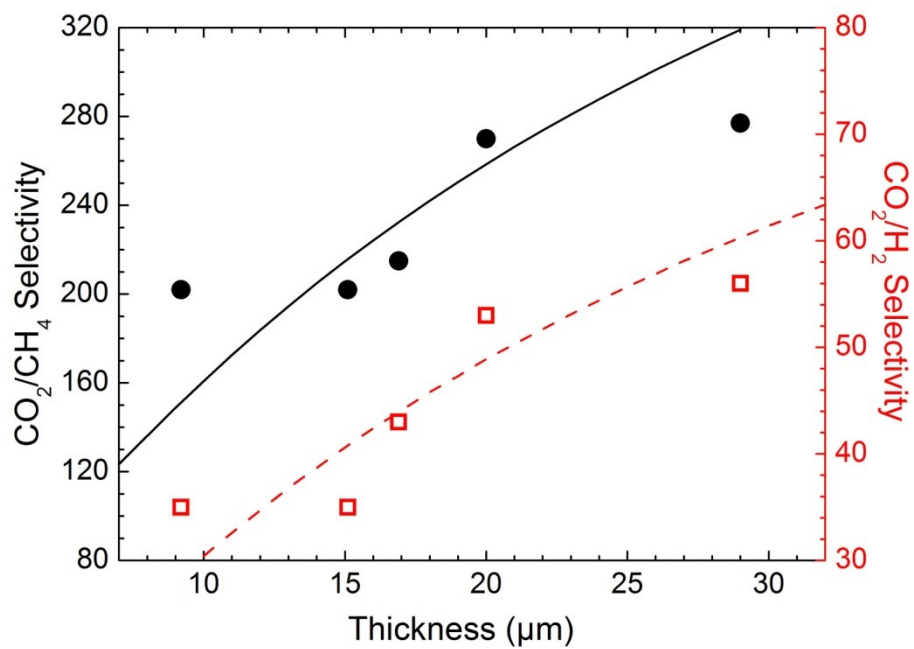


Figure 5.19 - Modeling the thickness influence on the CO₂/CH₄ and CO₂/H₂ selectivity

Conclusions

A thorough experimental analysis of the performances of different membranes for CO₂ separation were carried out, aiming at the evaluation of their potentialities in a wide range of experimental conditions, in order to have an insight of the physical and chemical phenomena involved in the transport mechanism. In this concern, different modeling approaches were proposed to represent the experimental data, with a deep analysis of all the parameters considered for the description of the mechanism of gas transport, and moreover their relative weight in the determination of the overall membrane performances. The proposed modeling study produced simple tools for the description, and possibly the prediction, of materials behavior under different experimental conditions.

In the first part, an exhaustive study of Matrimid, a commercial polyimide interesting for CO₂ separation applications (mainly CO₂/CH₄, and also CO₂/N₂), was carried out, analyzing the transport properties from different perspectives, useful both for a thorough theoretical characterization and for a possible scale up of the separation system.

The effect of different thermal treatments and of physical aging on the gas transport properties in Matrimid has been investigated by monitoring the variation of permeability and diffusivity of two different penetrants, CO₂ and CH₄ (paragraph 4.1). The gas permeability and diffusivity were observed to be significantly affected by the thermal treatment, although the temperature values explored were always well below the polymer T_g. Indeed, an increase of the pretreatment temperature corresponded to a pronounced permeability decreases: an overall variation close to 50% was obtained by changing the thermal pretreatment temperature from 50 to 200°C. The observed behavior was explained by the proposed theoretical interpretation based on the free volume theory, according to which the permeability decreased as the free volume available for the molecules to diffuse in the system was reduced by the thermal treatment. The energy supplied to the system by the lowest T

treatment was indeed not sufficient to overcome the energy barriers encountered by relaxation phenomena, generating a larger free volume within the matrix, hence a higher permeability and diffusivity. Conversely, at increasing the pretreatment temperature more energy is available for relaxation processes: a complex molecular chains rearrangement takes place, producing a free volume reduction, which directly affects the membrane performances.

Furthermore, the transport properties were also monitored over a period of 3000 hours, in order to investigate the occurrence of aging phenomena for specimens cured with different thermal protocols. Interestingly, the sample treated at 50°C exhibited a pronounced transport rate reduction over time, but the extent of this phenomenon decreased for higher pretreatment temperatures, insomuch as the samples treated at 150 and 200°C showed stable performance for the entire period of study. Once again, the results were congruous with a free volume based interpretation: the more permeable configuration of the samples treated at 50°C was characterized by a larger departure from the thermodynamic equilibrium, leading to a higher driving force of relaxation phenomena, and consequent a faster aging rate. Similar behaviors were observed for the transport properties of two different gases in Matrimid, as the permeation process was slowed down by the increasing pretreatment temperature and aging progress to approximately the same extent. The qualitative analysis of the experimental data by means of the free volume theory confirmed also the validity of the assumed theoretical interpretation (paragraph 5.3). Subsequently, the influence of the presence of water vapor on the polymer transport properties has been investigated for several gaseous penetrants (CH₄, N₂, CO₂ and He), chosen depending upon their different thermodynamic and kinetic features (paragraph 4.2). In general, water vapor affected negatively the incondensable species transport, and the gas permeability decreases down to 50% of dry permeability value at 75% R.H.. Surprisingly, the extent of decrease was found to be alike for all the investigated penetrants, in spite of their different kinetic and thermodynamic characteristics. In addition, the similar P/P_0 trend observed for the considered thermal conditions was in accordance with the negligible temperature dependence of water sorption isotherms. Hence, at a given R.H., the water effect on

the gas permeation has been directly related solely to the H₂O concentration inside the membrane matrix, which seemed to act independently from the thermal conditions.

On the basis of the above considerations, a simple modeling approach based on the free volume theory has been implemented to describe theoretically the humid permeation process in Matrimid, with the aim of extending it thereafter to polyimides in general (paragraph 5.4.1). The sorbed water has been assumed to merely fill a portion of the polymer free volume, thus reducing the amount available for other penetrants to diffuse across the membrane. According to the low water uptake observed in the sorption experiments, a negligible water-induced swelling effect has been assumed, thus considering the polymer density unchanged at increasing the water concentration in the membrane.

The fractional free volume available for the permeability in humid conditions, FFV_{humid} , was calculated by considering two limiting cases, a) non interacting water molecules, in which the volume occupied by the unit mass of water was constant and independent of R.H.; and b) the ideal clustering case, in which the clustered water molecules did not contribute to the available fractional free volume. The model has been able to accurately represent the experimental trends with the use of two polymer-penetrant specific parameters only, when information about pure water solubility behavior were available. Noteworthy, the values of the fitting parameters used for the different penetrants were in line with those already reported in the literature for the description of permeability under dry conditions. The satisfactory agreement with experimental data indicated that, despite the empirical nature, the model provides an accurate description of the basic physical mechanism governing the process of humid permeation in Matrimid.

In order to investigate more in detail the water influence on the transport mechanism in polyimides and to be able to use the proposed approach in lack of experimental solubility data, a more rigorous approach has then been also adopted. In particular the NELF model, able to predict the solubility of gaseous mixture in glassy polymers, was combined with the Free Volume Theory, in order to give a more complete description of

the permeation process, in the framework of solution diffusion mechanism (paragraph 5.4.2).

The results obtained from this approach revealed that the presence of an incondensable species on the sorption process of humid gases had a rather limited effect on H₂O solubility. Thanks to its higher condensability, water vapor can compete stronger for absorption in the empty voids present in the matrix, causing a consequent solubility decrease of the other compounds. Methane was affected more severely by the competitive sorption effect, so that the permeability reduction has been mainly attributed to the solubility variation rather than the diffusive one. On the other side, CO₂, according to its higher critical temperature, may compete strongly with water for sorption sites and the overall permeability decrease has been related to the reduction of both solubility and diffusivity to an equal extent.

Despite the inability of the considered equation of state to represent the water behavior when self-associating phenomena (e.g. clustering) of H₂O molecule occur, the proposed model was able to accurately represent the permeability behavior under humid conditions by means of only two adjustable parameters ($D_{i,0}$ and β_i) for the transport process. NELF model required two binary interaction parameters (k_{ij} for H₂O and the incondensable penetrant), for the description of pure gas and vapor solubility, allowing then the detailed representation of the mixed gas solubility data in a predictive fashion. The use of a different EoS specifically accounting for the self-association of water molecules would represent a significant improvement of the present work, together with the extension of the presented theory to other materials suitable for CO₂ separation under humid conditions.

In the second part, the synthesis of facilitated transport membranes containing amino-functionalized MWNTs has been carried out and their transport properties have been deeply investigated for different high pressure gas separation applications, aiming at the identification of the optimal operative conditions (paragraph 4.3).

Despite the outstanding results achieved in low pressure conditions using Lupamin[®] as fixed carrier, at 107°C, instability issues arose for a feed pressure of 15 atm, causing a significant decrease of membrane performance soon after the steady state was reached. In order to overcome the problem, different fixed carriers have been used for the fabrication

of the selective layer, and the results in terms of transport properties revealed the importance of a certain amount of high M_w species (HM_wS), which was able to provide good and stable separation performances. When the feed pressure has been increased to 28 atm, an increment of the HM_wS amount was required to achieve stable performance, further supporting the validity of this idea. Moreover, it has been observed that under such severe pressure conditions better performance could be achieved by using only KOH as mobile carrier.

According to the promising results obtained at 15 atm pressure conditions, the influence of several operative parameters, such as inorganic loading, water content, operative temperature and selective layer thickness, on the membrane transport properties has been examined in order to optimize the membrane efficiency and to improve the theoretical knowledge of the involved mechanisms.

The affinity between the hydrophilic polymeric chains and the hydrophobic graphene structure of MWNTs has been importantly enhanced carrying out an amino-functionalization of the fillers. The use of AF-MWNTs instead of raw MWNTs avoided the nanogaps formation at the polymer-filler interface, so that the separation performances remained constant at increasing the inorganic loading. Furthermore, the water concentration within the polymeric matrix has been observed to play a key role in controlling the CO_2 transport rate and the membrane selective feature, mainly because it is involved in the reaction mechanism and determines the ions mobility across the selective layer. Accordingly, also the operative temperature had to be carefully controlled to maximize the separation efficiency, since it can affect simultaneously the relative humidity of the system (at constant water amount in the feed), as well as the reaction kinetics and the gas molecules diffusion. However, the membrane performance reached their maximum in a very narrow range of these two parameters (T and R.H.) and this high sensitivity to the operative conditions could represent an issue for a further scale up of these membranes in a real separation process.

Finally, the measured CO_2 permeability was demonstrated to be thickness dependent, in the considered range of selective layer thicknesses. This feature has been analyzed by means of a specific mathematical representation of the transport mechanism in this peculiar system (paragraph 5.5). The experimental data have been indeed carefully

represented by the modeling approach proposed by Noble et al. [1], in which the diffusion reacting system is characterized through a single reaction, considered at equilibrium, whereas a constant carrier concentration is assumed throughout the membrane. By using fitting parameters with acceptable values from the practical point of view, the model was able to describe the permeability increase along with the thickness, suggesting that the phenomenon is an intrinsic feature of the reactive diffusion systems, mainly associated to the activated complex diffusivity and the reaction kinetics.

Thanks to the outstanding transport properties obtained in the present work and considering also the data available in literature, facilitated transport membrane represent promising materials for CO₂ membrane-based separation applications. However, in order to scale up this technology, the theoretical knowledge of permeation in these particular materials has to be improved, aiming at the understanding of physical and chemical mechanisms controlling the membrane performances as well as their sensitive dependency from the operative parameters.

Appendix

In the present appendix the data obtained for different permeation experiments are reported.

A.1. Thermal treatment and Aging in Matrimid

Aging (h)	Permeability (Barrer)						Diffusivity (cm^2/s) $\cdot 10^9$					
	CO_2			CH_4			CO_2			CH_4		
	Test temperatures			Test temperatures			Test temperatures			Test temperatures		
	35°C	45°C	55°C	35°C	45°C	55°C	35°C	45°C	55°C	35°C	45°C	55°C
<i>Thermal Pretreatment at 50°C</i>												
un-aged	17.9	19.7	21.6	0.46	0.63	0.85	10.3	14.8	20.2	1.91	2.82	4.51
360	17.1	-	-	0.45	-	-	10.0	-	-	1.56	-	-
1008	15.6	17.1	18.9	0.39	0.54	0.70	9.05	11.2	16.7	1.29	2.26	3.15
2232	14.9	16.3	17.9	0.34	0.47	0.62	7.57	11.5	15.7	1.12	1.82	3.44
2904	13.2	14.5	15.7	0.30	0.40	0.53	4.99	7.13	8.88	0.61	0.89	1.58
<i>Thermal Pretreatment at 100°C</i>												
un-aged	11.8	13.2	14.3	0.30	0.40	0.50	5.99	8.00	10.8	0.88	1.26	1.90
1032	11.0	12.3	13.6	0.27	0.36	0.46	5.61	7.71	10.9	0.74	1.14	2.11
2208	11.0	12.1	13.1	0.27	0.36	0.46	4.95	6.61	9.17	0.68	1.01	1.68
<i>Thermal Pretreatment at 150°C</i>												
un-aged	9.76	10.8	11.8	0.24	0.31	0.40	4.68	6.62	8.86	0.67	1.00	1.61
1008	9.88	10.6	12.0	0.23	0.31	0.41	5.02	7.40	9.72	0.70	1.10	1.75
2232	9.51	10.5	11.6	0.24	0.29	0.37	4.44	6.00	8.46	0.86	1.13	2.03
3456	9.53	10.5	11.7	0.23	0.29	0.39	5.08	7.28	10.0	0.68	1.16	1.83
<i>Thermal Pretreatment at 200°C</i>												
un-aged	9.50	10.5	11.5	0.24	0.31	0.40	5.66	7.93	10.6	0.85	1.30	1.84
1032	9.71	10.8	11.9	0.23	0.30	0.40	5.81	7.98	11.2	0.82	1.27	2.01
2232	9.92	11.0	12.2	0.23	0.29	0.40	5.47	7.74	10.6	0.94	1.34	2.18
3120	9.48	10.6	11.5	0.24	0.30	0.40	5.96	6.99	9.88	0.94	1.86	1.74

Table A.1 - Permeability and Diffusivity coefficients of CO_2 and CH_4 for Matrimid samples pretreated at different T at different aging times (un-aged correspond to 48 hours after casting)

A.2. Humid permeation in Matrimid

<i>R.H.</i>	<i>P</i>	<i>Err</i>	<i>R.H.</i>	<i>P</i>	<i>Err</i>	<i>R.H.</i>	<i>P</i>	<i>Err</i>
-	(Barrer)	%	-	(Barrer)	%	-	(Barrer)	%
25°C			35°C			45°C		
<i>CH₄</i>								
0.00	0.16	11.3	0.00	0.24	1.5	0.00	0.31	2.5
0.05	0.15	12.4	0.05	0.23	1.0	0.05	0.28	6.3
0.10	0.15	7.3	0.10	0.22	3.8	0.10	0.27	6.2
0.25	0.13	6.8	0.25	0.20	5.7	0.25	0.25	13.6
0.50	0.11	19.6	0.51	0.16	5.8	0.50	0.21	7.9
0.75	0.08	10.2	0.75	0.12	14.9	0.75	0.15	15.6
<i>N₂</i>								
0.00	0.20	2.4	0.00	0.26	3.9	0.00	0.35	1.3
0.05	0.19	2.9	0.05	0.25	7.0	0.05	0.33	2.0
0.10	0.19	3.9	0.10	0.24	4.1	0.10	0.32	3.3
0.25	0.17	10.8	0.25	0.22	9.3	0.25	0.27	7.1
0.50	0.15	12.6	0.50	0.18	9.2	0.50	0.22	13.1
0.75	0.11	6.4	0.75	0.14	14.6	0.74	0.16	13.5
<i>CO₂</i>								
0.00	8.4	0.18	0.00	9.7	0.31	0.00	10.8	0.27
0.05	7.6	0.11	0.05	9.0	0.72	0.05	10.1	0.18
0.10	7.2	0.08	0.10	8.5	0.75	0.11	9.5	0.50
0.25	6.5	0.37	0.28	7.7	0.29	0.26	8.5	0.39
0.50	5.5	0.53	0.50	6.6	1.31	0.50	7.6	0.19
0.75	4.1	1.55	0.74	5.1	3.42	0.75	6.3	1.35
<i>He</i>								
0.00	21.5	0.49	0.00	25.4	0.06	0.00	30.3	0.24
0.05	20.0	0.12	0.05	23.8	0.23	0.05	27.9	0.41
0.10	19.0	0.11	0.10	22.4	0.37	0.10	26.2	0.71
0.25	16.5	0.19	0.25	19.8	0.30	0.25	22.1	0.52
0.50	12.5	0.37	0.50	15.3	0.37	0.49	18.6	0.09
0.75	9.5	0.82	0.75	12.4	0.95	0.75	14.9	0.20

Table A.2 - CH₄, N₂, CO₂ and He permeability measured at different relative humidity and operative temperature for Matrimid (T pretreatment = 200°C)

$D_{CH_4} \cdot 10^{-9} (cm^2/s)$			$D_{CO_2} \cdot 10^{-9} (cm^2/s)$		
25°C	35°C	45°C	25°C	35°C	45°C
0.84	1.56	2.53	5.80	9.01	13.6

Table A.3 - Diffusion coefficient values measured under different thermal conditions in dry gas experiments of CO₂ and CH₄ for Matrimid (T pretreatment = 200°C)

A.3. Facilitated transport membranes

Sample	ℓ (μm)	Feed p (atm)	CO ₂ Perm (Barrer)	CO ₂ /H ₂ -	CO ₂ /N ₂ -	CO ₂ /CH ₄ -
S-01 ^{a,b}	16	2	3157	198	380	650
S-02 ^a	27	15	1036	31	-	171
S-03 ^a	19	15	999	35	-	182
S-04 ^b	22	15	729	27	181	-
S-05 ^b	24	15	760	23	155	-
S-06 ^b	31	15	1027	58	368	-
S-07 ^b	31	15	1002	62	379	-
S-08 ^{a,b}	29	15	962	56	360	277
S-09 ^a	30	15	986	53	-	266
S-10 ^a	33	15	880	54	-	250
S-11 ^b	21	15	886	54	428	-
S-12 ^a	32	15	986	54	-	283
S-13 ^a	33	15	1014	54	-	265
S-14 ^b	25	28	224	16	139	-
S-15 ^b	33	28	326	15	147	-
S-16 ^b	33	28	445	13	128	-

Table A.4 - Gas transport properties results for the different samples. Operative conditions: dry gas flow rate = 60/30 cm³/min (feed/sweep); for 2 atm R.H.=59.2%/47.4% (feed/sweep); for 15 and 28 atm R.H.=100%/72.5% (feed/sweep); T = 107°C; feed composition (a) 20%CO₂, 59.8%CH₄, 20.2% H₂, (b) 20%CO₂, 40%N₂, 40% H₂

Bibliography

- [1] B. Dalal-Clayton, S. Bass, *Sustainable Development Strategies: A Resource Book*. Organisation for Economic Co-operation and Development, Paris and United Nations Development Programme, New York, 2002.
- [2] European Commission, *Mainstreaming sustainable development into EU policies: 2009 Review of the European Union Strategy for Sustainable Development*, COM(2009) 400 final, 2009.
- [3] A. Stankiewicz, *Reactive separations for process intensification: an industrial perspective*, *Chem. Eng. Process.* 42 (2003) 137–144.
- [4] P. Bernardo, E. Drioli, G. Golemme, *Membrane Gas Separation: A Review/State of the Art*, *Ind. Eng. Chem. Res.* 48 (2009) 4638–4663.
- [5] W.J. Koros, G.K. Fleming, *Membrane-based gas separation*, *J. Memb. Sci.* 83 (1993) 1–80.
- [6] E. Drioli, A.I. Stankiewicz, F. Macedonio, *Membrane engineering in process intensification - An overview*, *J. Memb. Sci.* 380 (2011) 1–8.
- [7] T.C. Merkel, H. Lin, X. Wei, R. Baker, *Power plant post-combustion carbon dioxide capture: An opportunity for membranes*, *J. Memb. Sci.* 359 (2010) 126–139.
- [8] E. Favre, *Carbon dioxide recovery from post-combustion processes: Can gas permeation membranes compete with absorption?*, *J. Memb. Sci.* 294 (2007) 50–59.
- [9] R.W. Baker, K. Lokhandwala, *Natural Gas Processing with Membranes: An Overview*, *Ind. Eng. Chem. Res.* 47 (2008) 2109–2121.
- [10] R.W. Baker, *Future Directions of Membrane Gas Separation Technology*, *Ind. Eng. Chem. Res.* 41 (2002) 1393–1411.
- [11] S. Basu, A.L. Khan, A. Cano-Odena, C. Liu, I.F.J. Vankelecom, *Membrane-based technologies for biogas separations.*, *Chem. Soc. Rev.* 39 (2010) 750–68.
- [12] K. Ramasubramanian, Y. Zhao, W.S.W. Ho, *CO₂ Capture and H₂ Purification: Prospects for CO₂ -Selective Membrane Processes*, *AIChE J.* 59 (2013) 1033–1045.
- [13] B.S. Ghanem, N.B. McKeown, P.M. Budd, J.D. Selbie, D. Fritsch, *High-Performance Membranes from Polyimides with Intrinsic Microporosity*, *Adv. Mater.* 20 (2008) 2766–2771.

- [14] C. A. Scholes, C.P. Ribeiro, S.E. Kentish, B.D. Freeman, Thermal rearranged poly(benzoxazole-co-imide) membranes for CO₂ separation, *J. Memb. Sci.* 450 (2014) 72–80.
- [15] H.B. Tanh Jeazet, C. Staudt, C. Janiak, Metal-organic frameworks in mixed-matrix membranes for gas separation., *Dalton Trans.* 41 (2012) 14003–27.
- [16] J. Ahmad, M.-B. Hägg, Preparation and characterization of polyvinyl acetate/zeolite 4A mixed matrix membrane for gas separation, *J. Memb. Sci.* 427 (2013) 73–84.
- [17] M. Askari, Y. Xiao, P. Li, T.-S. Chung, Natural gas purification and olefin/paraffin separation using cross-linkable 6FDA-Durene/DABA co-polyimides grafted with α , β , and γ -cyclodextrin, *J. Memb. Sci.* 390-391 (2012) 141–151.
- [18] Y. Zhao, W.S.W. Ho, CO₂-Selective Membranes Containing Sterically Hindered Amines for CO₂/H₂ Separation, *Ind. Eng. Chem. Res.* 3 (2012).
- [19] Y. Zhao, B.T. Jung, L. Ansaloni, W.S. Winston Ho, Multiwalled carbon nanotube mixed matrix membranes containing amines for high pressure CO₂/H₂ separation, *J. Memb. Sci.* 459 (2014) 233–243.
- [20] T. Visser, N. Masetto, M. Wessling, Materials dependence of mixed gas plasticization behavior in asymmetric membranes, *J. Memb. Sci.* 306 (2007) 16–28.
- [21] A. Bos, I.G.M. Punt, M. Wessling, H. Strathmann, CO₂-induced plasticization phenomena in glassy polymers, *J. Memb. Sci.* 155 (1999) 67–78.
- [22] L. Deng, M.-B. Hägg, Techno-economic evaluation of biogas upgrading process using CO₂ facilitated transport membrane, *Int. J. Greenh. Gas Control.* 4 (2010) 638–646.
- [23] D.Q. Vu, W.J. Koros, S.J. Miller, Effect of Condensable Impurities in CO₂/CH₄ Gas Feeds on Carbon Molecular Sieve Hollow-Fiber Membranes, *Ind. Eng. Chem. Res.* 42 (2003) 1064–1075.
- [24] A.Y. Ku, P. Kulkarni, R. Shisler, W. Wei, Membrane performance requirements for carbon dioxide capture using hydrogen-selective membranes in integrated gasification combined cycle (IGCC) power plants, *J. Memb. Sci.* 367 (2011) 233–239.
- [25] B. Metz, O. Davidson, H. de Coninck, M. Loos, L. Meyer, IPCC Special Report on Carbon Dioxide Capture and Storage, Cambridge University Press, United Kingdom & New York, NY, USA, 2005.
- [26] S. Wiederhorn, R. Fields, S. Low, B. Gun-Woong, A. Wehrstedt, J. Hahn, et al., Mechanical Properties (Part C/7), in: Springer Handb. Mater. Meas. Methods, 2006: pp. 283–397.
- [27] J.S. Vrentas, C.M. Vrentas, Solvent Self-Diffusion in Glassy Polymer-Solvent Systems, *Macromolecules.* 27 (1994) 5570–5576.

- [28] L.M. Robeson, Polymer membranes for gas separation, *Curr. Opin. Solid State Mater. Sci.* 4 (1999) 549–552.
- [29] D. Paul, Y. Yampolskii, *Polymeric gas separation membranes*, CRC Press, Boca Raton, FL, 1994.
- [30] L.M. Robeson, Correlation of separation factor versus permeability for polymeric membranes, *J. Memb. Sci.* 62 (1991) 165–185.
- [31] L.M. Robeson, The upper bound revisited, *J. Memb. Sci.* 320 (2008) 390–400.
- [32] M. Giacinti Baschetti, M. Minelli, J. Catalano, G.C. Sarti, Gas permeation in perfluorosulfonated membranes: Influence of temperature and relative humidity, *Int. J. Hydrogen Energy.* 38 (2013) 11973–11982.
- [33] A. Tena, L. Fernandez, M. Sanchez, L. Palacio, A.E. Lozano, A. Herna, Mixed matrix membranes of 6FDA-6FpDA with surface functionalized γ -alumina particles. An analysis of the improvement of permselectivity for several gas pairs, *Chem. Eng. Sci.* 65 (2010) 2227–2235.
- [34] C.E. Sroog, Polyimides, *Prog. Polym. Sci.* 16 (1991) 561–694.
- [35] L. Struik, Physical aging in plastics and other glassy materials, *Polym. Eng. Sci.* 17 (1977).
- [36] J.M. Hutchinson, Physical Aging of Polymers, *Prog. Polym. Sci.* 20 (1995) 703–760.
- [37] L.C.E. Struik, Volume relaxation and secondary transitions in amorphous polymers, *Polymer (Guildf)*. 28 (1987) 1869–1875.
- [38] L. Struik, *Physical aging in amorphous polymers and other materials*, Elsevier, Amsterdam, 1977.
- [39] B.W. Rowe, B.D. Freeman, D.R. Paul, Physical aging of ultrathin glassy polymer films tracked by gas permeability, *Polymer.* 50 (2009) 5565–5575.
- [40] C. Consolati, I. Genco, M. Pecoraro, L. Zanderighi, Positron Annihilation lifetime (PAL) in Poly [1-(trimethyl- silyl) propine] (PTMSP): Free Volume Determination and Time Dependence of Permeability, *J. Polym. Sci. Part B Polym. Phys.* 34 (1996) 357–367.
- [41] X. Duthie, S. Kentish, S. Pas, A.J. Hill, C. Powell, K. Nagai, G. Stevens, G. Qiao, Thermal treatment of dense polyimide membranes, *J. Polym. Sci. Part B Polym. Phys.* 46 (2008) 1879–1890.
- [42] T.M. Murphy, B.D. Freeman, D.R. Paul, Physical aging of polystyrene films tracked by gas permeability, *Polymer.* 54 (2013) 873–880.

- [43] H. Wang, T.-S. Chung, D.R. Paul, Physical aging and plasticization of thick and thin films of the thermally rearranged ortho-functional polyimide 6FDA–HAB, *J. Memb. Sci.* 458 (2014) 27–35.
- [44] J.H. Kim, W.J. Koros, D.R. Paul, Physical aging of thin 6FDA-based polyimide membranes containing carboxyl acid groups. Part I. Transport properties, *Polymer*. 47 (2006) 3094–3103.
- [45] Y. Huang, D.R. Paul, Physical aging of thin glassy polymer films monitored by gas permeability, *Polymer*. 45 (2004) 8377–8393.
- [46] Y. Huang, X. Wang, D.R. Paul, Physical aging of thin glassy polymer films: Free volume interpretation, *J. Memb. Sci.* 277 (2006) 219–229.
- [47] J.T. Vaughn, W.J. Koros, J.R. Johnson, O. Karvan, Effect of thermal annealing on a novel polyamide–imide polymer membrane for aggressive acid gas separations, *J. Memb. Sci.* 401–402 (2012) 163–174.
- [48] S.L. Simon, D.J. Plazek, J.W. Sobieski, E.T.M.C. Gregor, Physical Aging of a Polyetherimide: Volume Recovery and Its Comparison to Creep and Enthalpy Measurements, *J. Polym. Sci. Part B Polym. Phys.* 35 (1996) 929–936.
- [49] Y.-J. Fu, S.-W. Hsiao, C.-C. Hu, K.-R. Lee, J.-Y. Lai, Prediction of long-term physical aging of poly(methyl methacrylate) membranes for gas separation, *Desalination*. 234 (2008) 51–57.
- [50] C.M. Laot, E. Marand, B. Schmittmann, R.K.P. Zia, Effects of Cooling Rate and Physical Aging on the Gas Transport Properties in Polycarbonate, *Macromolecules*. 36 (2003) 8673–8684.
- [51] C.A. Scholes, G.Q. Chen, W.X. Tao, J. Bacus, C. Anderson, G.W. Stevens, S.E. Kentish, The effects of minor components on the gas separation performance of membranes for carbon capture, *Energy Procedia*. 4 (2011) 681–687.
- [52] D. Rivin, C.E. Kendrick, P.W. Gibson, N.S. Schneider, Solubility and transport behavior of water and alcohols in Nafion, *Polymer*. 42 (2001) 623–635.
- [53] J. Catalano, T. Myezwa, M.G. De Angelis, M.G. Baschetti, G.C. Sarti, The effect of relative humidity on the gas permeability and swelling in PFSI membranes, *Int. J. Hydrogen Energy*. 37 (2012) 6308–6316.
- [54] S. Motupally, A.J. Becker, J.W. Weidner, Diffusion of Water in Nafion 115 Membranes, *J. Electrochem. Soc.* 147 (2000) 3171.
- [55] K. Schmidt-Rohr, Q. Chen, Parallel cylindrical water nanochannels in Nafion fuel-cell membranes, *Nat. Mater.* 7 (2008) 75–83.

- [56] M. Minelli, M.G. Baschetti, F. Doghieri, M. Ankerförs, T. Lindström, I. Siró, et al., Investigation of mass transport properties of microfibrillated cellulose (MFC) films, *J. Memb. Sci.* 358 (2010) 67–75.
- [57] K. Okamoto, N. Tanihara, H. Watanabe, K. Tanaka, H. Kita, A. Nakamura, et al., Sorption and diffusion of water vapor in polyimide films, *J. Polym. Sci. Part B Polym. Phys.* 30 (1992) 1223–1231.
- [58] T. Watari, H. Wang, K. Kuwahara, K. Tanaka, H. Kita, K. Okamoto, Water vapor sorption and diffusion properties of sulfonated polyimide membranes, *J. Memb. Sci.* 219 (2003) 137–147.
- [59] V. Detallante, D. Langevin, C. Chappey, M. Métayer, R. Mercier, M. Pinéri, Water vapor sorption in naphthalenic sulfonated polyimide membranes, *J. Memb. Sci.* 190 (2001) 227–241.
- [60] G.Q. Chen, C. a. Scholes, G.G. Qiao, S.E. Kentish, Water vapor permeation in polyimide membranes, *J. Memb. Sci.* 379 (2011) 479–487.
- [61] K. Tanaka, M.N. Islam, M. Kido, H. Kita, K. Okamoto, Gas permeation and separation properties of sulfonated polyimide membranes, *Polymer (Guildf)*. 47 (2006) 4370–4377.
- [62] M. Pourafshari Chenar, M. Soltanieh, T. Matsuura, A. Tabe-Mohammadi, K.C. Khulbe, The effect of water vapor on the performance of commercial polyphenylene oxide and Cardo-type polyimide hollow fiber membranes in CO₂/CH₄ separation applications, *J. Memb. Sci.* 285 (2006) 265–271.
- [63] S.R. Reijerkerk, R. Jordana, K. Nijmeijer, M. Wessling, Highly hydrophilic, rubbery membranes for CO₂ capture and dehydration of flue gas, *Int. J. Greenh. Gas Control*. 5 (2011) 26–36.
- [64] B. Bae, K. Miyatake, M. Watanabe, Effect of the hydrophobic component on the properties of sulfonated poly (arylene ether sulfone) s, *Macromolecules*. 42 (2009) 1873–1880.
- [65] E.L. Cussler, *Diffusion: Mass Transfer in Fluid Systems*, Third Edit, Cambridge University Press, New York, 2009.
- [66] W.S.W. Ho, K.K. Sirkar, *Membrane Handbook*, Reprint, Kluwer Academic, 2001.
- [67] S. Kentish, C. Scholes, G. Stevens, Carbon Dioxide Separation through Polymeric Membrane Systems for Flue Gas Applications, *Recent Patents Chem. Eng.* 1 (2008) 52–66.
- [68] G. Sartori, D.W. Savage, Sterically Hindered Amines for CO₂, Removal from Gases, *Ind. Eng. Chem. Fundam.* 22 (1987) 239–249.
- [69] Y. Zhao, W.S.W. Ho, Steric hindrance effect on amine demonstrated in solid polymer membranes for CO₂ transport, *J. Memb. Sci.* 415-416 (2012) 132–138.

- [70] L.J. Shulik, G. Sartori, W.S. Ho, W. a. Thaler, G.E. Milliman, J.C. Wilbur, A Novel, V 5+-Stable K_2CO_3 Promoter for CO_2 Absorption, *Sep. Sci. Technol.* 31 (1996) 1663–1673.
- [71] Y. Tee, J. Zou, W.S.W. Ho, CO_2 -Selective Membranes Containing Dimethylglycine Mobile Carriers and Polyethylenimine Fixed Carrier, *J. Chinese Inst. Chem. Eng.* 37 (2006) 37–47.
- [72] H. Bai, W.S.W. Ho, New Carbon Dioxide-Selective Membranes Based on Sulfonated Polybenzimidazole (SPBI) Copolymer Matrix for Fuel Cell Applications, *Ind. Eng. Chem. Res.* 48 (2009) 2344–2354.
- [73] J. Zou, J. Huang, W. Ho, CO_2 -selective water gas shift membrane reactor for fuel cell hydrogen processing, *Ind. Eng. Chem. Res.* 46 (2007) 2272–2279.
- [74] L. Deng, T.-J. Kim, M.-B. Hägg, Facilitated transport of CO_2 in novel PVAm/PVA blend membrane, *J. Memb. Sci.* 340 (2009) 154–163.
- [75] H. Bai, High temperature proton exchange an fuel processing membranes for fuel cell and other applications, The Ohio State University, 2008.
- [76] P. Luangrujiwong, a Sungpet, R. Jiratananon, J. Way, Investigation of the carrier saturation in facilitated transport of unsaturated hydrocarbons, *J. Memb. Sci.* 250 (2005) 277–282.
- [77] H. Bai, W.S.W. Ho, Carbon dioxide-selective membranes for high-pressure synthesis gas purification, *Ind. Eng. Chem. Res.* 50 (2011) 12152–12161.
- [78] R. Xing, W.S.W. Ho, Crosslinked polyvinylalcohol–polysiloxane/fumed silica mixed matrix membranes containing amines for CO_2/H_2 separation, *J. Memb. Sci.* 367 (2011) 91–102.
- [79] J. Crank, *The Mathematics of Diffusion*, 2nd ed., Clarendon Press, Oxford, 1975.
- [80] G.C. Kapantaidakis, G.H. Koops, High flux polyethersulfone–polyimide blend hollow fiber membranes for gas separation, *J. Memb. Sci.* 204 (2002) 153–171.
- [81] M. Kiyono, Carbon molecular sieve membranes for natural gas separations, Georgia Institute of Technology, 2010.
- [82] C. Scholes, W. Tao, G. Stevens, S. Kentish, Sorption of methane, nitrogen, carbon dioxide, and water in Matrimid 5218, *J. Appl. Polym. Sci.* 117 (2010) 2284–2289.
- [83] R. Whitehouse, Process for latex production by melt emulsification, US Pat. App. 13/767,522. (2013).
- [84] M. Morgan, L. a. Fielding, S.P. Armes, Synthesis and characterisation of sterically stabilised polypyrrole particles using a chemically reactive poly(vinyl amine)-based stabiliser, *Colloid Polym. Sci.* 291 (2012) 77–86.

- [85] BASF, Lupamin® 9095, BASF Tech. Data. (2009).
- [86] E. Poptoshev, M. Rutland, P. Claesson, Surface forces in aqueous polyvinylamine solutions. I. Glass surfaces, *Langmuir*. 15 (1999) 7789–7794.
- [87] G.-W. Lee, J. Kim, J. Yoon, J.-S. Bae, B.C. Shin, I.S. Kim, et al., Structural characterization of carboxylated multi-walled carbon nanotubes, *Thin Solid Films*. 516 (2008) 5781–5784.
- [88] J. Zhang, H. Zou, Q. Qing, Y. Yang, Q. Li, Z. Liu, et al., Effect of Chemical Oxidation on the Structure of Single-Walled Carbon Nanotubes, *J. Phys. Chem. B*. 107 (2003) 3712–3718.
- [89] A. Shanmugaraj, J. Bae, K. Lee, W. Noh, S. Lee, S. Ryu, Physical and chemical characteristics of multiwalled carbon nanotubes functionalized with aminosilane and its influence on the properties of natural rubber composites, *Compos. Sci. Technol*. 67 (2007) 1813–1822.
- [90] J. Kathi, K.Y. Rhee, Surface modification of multi-walled carbon nanotubes using 3-aminopropyltriethoxysilane, *J. Mater. Sci*. 43 (2007) 33–37.
- [91] R. Peña-Alonso, F. Rubio, J. Rubio, J.L. Oteo, Study of the hydrolysis and condensation of γ -Aminopropyltriethoxysilane by FT-IR spectroscopy, *J. Mater. Sci*. 42 (2006) 595–603.
- [92] B. Bolto, T. Tran, M. Hoang, Z. Xie, Progress in Polymer Science Crosslinked poly(vinyl alcohol) membranes, *Prog. Polym. Sci*. 34 (2009) 969–981.
- [93] K. Ramasubramanian, CO₂ (H₂S)-selective Membranes for Fuel Cell Hydrogen Purification and Flue Gas Carbon Capture: An Experimental and Process Modeling Study, The Ohio State University, 2013.
- [94] M. Minelli, M. Deangelis, F. Doghieri, M. Marini, M. Toselli, F. Pilati, Oxygen permeability of novel organic–inorganic coatings: I. Effects of organic–inorganic ratio and molecular weight of the organic component, *Eur. Polym. J*. 44 (2008) 2581–2588.
- [95] L. Ansaloni, M. Minelli, M.G. Baschetti, G.C. Sarti, Effects of thermal treatment and physical aging on the gas transport properties in Matrimid®, *Oil Gas Sci. Technol.* (2014).
- [96] J. Zou, W.S.W. Ho, CO₂-selective polymeric membranes containing amines in crosslinked poly(vinyl alcohol), *J. Memb. Sci*. 286 (2006) 310–321.
- [97] L. Shao, Y. Bai, X. Huang, L. Meng, J. Ma, Fabrication and Characterization of Solution Cast MWNTs/PEI Nanocomposites, *J. of Applied Polymer Sci*. 113 (2009) 1879–1886.
- [98] C. Troiano, Studio dell' assorbimento di liquidi in membrane polimeriche per separazioni, Alma Mater Studiorum - University of Bologna, 2012.
- [99] Sartorius Lab Holding GmbH, Manual of Weighing Applications - Part 1 - Density, 1999.

- [100] H. Kawakami, M. Mikawa, S. Nagaoka, Gas transport properties in thermally cured aromatic polyimide membranes, *J. Memb. Sci.* 118 (1996) 223–230.
- [101] F. Galvani, A. Ruvolo-Filho, L.A. Pessan, Influence of Molecular Structure and Packing on Sorption and Transport Properties of Dichloromethane in Polyetherimides, *J. Macromol. Sci. Part B.* 46 (2007) 931–948.
- [102] K. Tanaka, H. Kita, K. Okamoto, A. Nakamura, Y. Kusuki, The effect of morphology on gas permeability and permselectivity in polyimide based on 3, 3', 4, 4'-biphenyltetracarboxylic dianhydride and 4, 4'-oxydianiline., *Polym. J.* 21 (1989) 127 – 135.
- [103] T.W. Cheng, H. Keskkula, D.R. Paul, Thermal aging of impact-modified polycarbonate, *J. Appl. Polym. Sci.* 45 (1992) 531–551.
- [104] J. Cowie, S. Harris, I. McEwen, Physical aging in poly (vinyl acetate). 2. Relative rates of volume and enthalpy relaxation, *Macromolecules.* 9297 (1998) 2611–2615.
- [105] A. Bos, I.G.M. Pünt, M. Wessling, H. Strathmann, Plasticization-resistant glassy polyimide membranes for CO₂/CO₄ separations, *Sep. Purif. Technol.* 14 (1998) 27–39.
- [106] S. Shishatskiy, C. Nistor, M. Popa, S.P. Nunes, K.V. Peinemann, Polyimide Asymmetric Membranes for Hydrogen Separation: Influence of Formation Conditions on Gas Transport Properties, *Adv. Eng. Mater.* 8 (2006) 390–397.
- [107] D. Vu, W. Koros, S. Miller, Mixed matrix membranes using carbon molecular sieves: I. Preparation and experimental results, *J. Memb. Sci.* 211 (2003) 311–334.
- [108] Y. Zhang, I.H. Musselman, J.P. Ferraris, K.J. Balkus, Gas Permeability Properties of Mixed-Matrix Matrimid Membranes Containing a Carbon Aerogel: A Material with Both Micropores and Mesopores, *Ind. Eng. Chem. Res.* 47 (2008) 2794–2802.
- [109] R. Recio, L. Palacio, P. Pradanos, A. Hernandez, A. Lozano, A. Marcos, J.G. de la Campa, J. de Abajo, Gas separation of 6FDA–6FpDA membranes Effect of the solvent on polymer surfaces and permselectivity, *J. Memb. Sci.* 293 (2007) 22–28.
- [110] A.C. Comer, D.S. Kalika, B.W. Rowe, B.D. Freeman, D.R. Paul, Dynamic relaxation characteristics of Matrimid[®] polyimide, *Polymer (Guildf).* 50 (2009) 891–897.
- [111] C. Joly, D. Le Cerf, C. Chappey, D. Langevin, G. Muller, Residual solvent effect on the permeation properties of fluorinated polyimide films, *Sep. Purif. Technol.* 16 (1999) 47–54.
- [112] Y.-J. Fu, S.-W. Hsiao, C.-C. Hu, H. Qui, K.-R. Lee, J.-Y. Lai, Effect of physical aging on sorption and permeation of small molecules in polyimide membranes, *Desalination.* 234 (2008) 58–65.
- [113] B. Freeman, Basis of permeability/selectivity tradeoff relations in polymeric gas separation membranes, *Macromolecules.* 32 (1999) 375–380.

- [114] A.Y. Alentiev, Y. Yampolskii, Free volume model and tradeoff relations of gas permeability and selectivity in glassy polymers, *J. Memb. Sci.* 165 (2000) 201–216.
- [115] W.-H. Lin, T.-S. Chung, Gas permeability, diffusivity, solubility, and aging characteristics of 6FDA-durene polyimide membranes, *J. Memb. Sci.* 186 (2001) 183–193.
- [116] K. Lokhandwala, S. Nadakatti, S. Stern, Solubility and transport of water vapor in some 6FDA-based polyimides, *J. Polym. Sci. Part B Polym. Phys.* 33 (1995) 965–975.
- [117] D. Yang, W. Koros, H. Hopfenberg, V. Stannett, The effects of morphology and hygrothermal aging on water sorption and transport in Kapton[®] polyimide, *J. Appl. Polym. Sci.* 31 (1986) 1619–1629.
- [118] J. Seo, K. Cho, H. Han, Dependence of water sorption in polyimides on the internal linkage in the diamine component, *Polym. Degrad. Stab.* 74 (2001) 133–137.
- [119] E. Sacher, J. Susko, Water permeation of polymer films. I. Polyimide, *J. Appl. Polym. Sci.* 23 (1979) 2355–2364.
- [120] G.Q. Chen, C.A. Scholes, C.M. Doherty, A.J. Hill, G.G. Qiao, S.E. Kentish, Modeling of the sorption and transport properties of water vapor in polyimide membranes, *J. Memb. Sci.* 409–410 (2012) 96–104.
- [121] J. Huang, E.J. Cranford, T. Matsuura, C. Roy, Water vapor permeation properties of aromatic polyimides, *J. Memb. Sci.* 215 (2003) 129–140.
- [122] P. Tin, T. Chung, Y. Liu, R. Wang, S. Liu, K. Pramoda, Effects of cross-linking modification on gas separation performance of Matrimid membranes, *J. Memb. Sci.* 225 (2003) 77–90.
- [123] J.S. Lee, W. Madden, W.J. Koros, Antiplasticization and plasticization of Matrimid[®] asymmetric hollow fiber membranes. Part B. Modeling, *J. Memb. Sci.* 350 (2010) 242–251.
- [124] R. Chern, W. Koros, E. Sanders, R. Yui, “Second component” effects in sorption and permeation of gases in glassy polymers, *J. Memb. Sci.* 15 (1983) 157–169.
- [125] F. Piroux, E. Espuche, R. Mercier, The effects of humidity on gas transport properties of sulfonated copolyimides, *J. Memb. Sci.* 232 (2004) 115–122.
- [126] M. Minelli, G. Cocchi, L. Ansaloni, M. Baschetti Giacinti, M.G. De Angelis, F. Doghieri, Vapor and liquid sorption in Matrimid polyimide: experimental characterization and modeling, *Ind. Eng. Chem. Res.* 52 (2013) 8936–8945.
- [127] O.C. David, D. Gorri, A. Urtiaga, I. Ortiz, Mixed gas separation study for the hydrogen recovery from H₂/CO/N₂/CO₂ post combustion mixtures using a Matrimid membrane, *J. Memb. Sci.* 378 (2011) 359–368.

- [128] H. Zhao, Y. Cao, X. Ding, M. Zhou, Q. Yuan, Effects of cross-linkers with different molecular weights in cross-linked Matrimid 5218 and test temperature on gas transport properties, *J. Memb. Sci.* 323 (2008) 176–184.
- [129] H.H. So, J.W. Cho, N.G. Sahoo, Effect of carbon nanotubes on mechanical and electrical properties of polyimide/carbon nanotubes nanocomposites, *Eur. Polym. J.* 43 (2007) 3750–3756.
- [130] M.C. Paiva, B. Zhou, K. a. S. Fernando, Y. Lin, J.M. Kennedy, Y.-P. Sun, Mechanical and morphological characterization of polymer–carbon nanocomposites from functionalized carbon nanotubes, *Carbon N. Y.* 42 (2004) 2849–2854.
- [131] M. Shaffer, X. Fan, A. Windle, Dispersion and packing of carbon nanotubes, *Carbon N. Y.* 36 (1998) 1603–1612.
- [132] H. Cong, J. Zhang, M. Radosz, Y. Shen, Carbon nanotube composite membranes of brominated poly (2, 6-diphenyl-1, 4-phenylene oxide) for gas separation, *J. Memb. Sci.* 294 (2007) 178–185.
- [133] T.-J. Kim, B. Li, M.-B. Hägg, Novel fixed-site-carrier polyvinylamine membrane for carbon dioxide capture, *J. Polym. Sci. Part B Polym. Phys.* 42 (2004) 4326–4336.
- [134] S. Kim, L. Chen, J.K. Johnson, E. Marand, Polysulfone and functionalized carbon nanotube mixed matrix membranes for gas separation: Theory and experiment, *J. Memb. Sci.* 294 (2007) 147–158.
- [135] S. Kim, T.W. Pechar, E. Marand, Poly(imide siloxane) and carbon nanotube mixed matrix membranes for gas separation, *Desalination.* 192 (2006) 330–339.
- [136] J. Choi, J. Jegal, W. Kim, Modification of performances of various membranes using MWNTs as a modifier, *Macromol. Symp.* 249-250 (2007) 610–617.
- [137] L. Ge, Z. Zhu, F. Li, S. Liu, L. Wang, Investigation of Gas Permeability in Carbon Nanotube (CNT) - Polymer Matrix Membranes via Modifying CNTs with Functional Groups/Metals and Controlling Modification Location, *J. Phys. Chem. C.* (2011) 6661–6670.
- [138] Y. Zhao, Carbon Dioxide-Selective Membranes Containing Sterically Hindered Amines, The Ohio State University, 2013.
- [139] L.A. El-Azzami, E.A. Grulke, Carbon dioxide separation from hydrogen and nitrogen Facilitated transport in arginine salt–chitosan membranes, *J. Memb. Sci.* 328 (2009) 15–22.
- [140] H. Matsuyama, K. Matsui, Y. Kitamura, T. Maki, M. Teramoto, Effects of membrane thickness and membrane preparation condition on facilitated transport of CO₂ through ionomer membrane, *Sep. Purif. Technol.* 17 (1999) 235–241.

- [141] S.S. Jordan, W.J. Koros, A Free Volume Distribution Model of Gas Sorption and Dilatation in Glassy Polymers, *Macromolecules*. 28 (1995) 2228–2235.
- [142] M.H. Cohen, D. Turnbull, Molecular Transport in Liquids and Glasses, *J. Chem. Phys.* 31 (1959) 1164.
- [143] J.S. Vrentas, J.L. Duda, Diffusion in Polymer-Solvent Systems. I. Reexamination of the Free-Volume Theory, *J. Polym. Sci. Polym. Phys. Ed.* 15 (1977) 403–416.
- [144] J.S. Vrentas, C.M. Vrentas, Solvent Self-Diffusion in Rubbery Polymer-Solvent Systems, *Macromolecules*. 27 (1994) 4684–4690.
- [145] P. Noegi, *Diffusion in Polymers*, First, Marcel Dekker Inc., New York, 1996.
- [146] A. Bondi, *Physical properties of molecular crystals, liquids and glasses*, John Wiley & Sons, Inc., New York, 1969.
- [147] W.M. Lee, Selection of barrier materials from molecular structure, *Polym. Eng. Sci.* Vol. 20 (1980) 65 – 69.
- [148] R.N. Haward, Occupied Volume of Liquids and Polymers, *J. Macromol. Sci. Part C Polym. Rev.* 4 (1970) 191–242.
- [149] A. Bondi, Van der Waals Volumes and Radii, *J. Phys. Chem.* 68 (1964) 441–451.
- [150] J.Y. Park, D.R. Paul, Correlation and prediction of gas permeability in glassy polymer membrane materials via a modified free volume based group contribution method, *J. Memb. Sci.* 125 (1997) 23–39.
- [151] A. Thran, G. Kroll, F. Faupel, Correlation Between Fractional Free Volume and Diffusivity of Gas Molecules in Glassy Polymers, *J. Polym. Sci. Part B Polym. Phys.* 37 (1999) 3344–3358.
- [152] R. Recio, A.E. Lozano, P. Pradanos, A. Marcos, F. Tejerina, A. Hernandez, Effect of Fractional Free Volume and T_g on Gas Separation Through Membranes Made with Different Glassy Polymers, *J. Appl. Polym. Sci.* 107 (2008) 1039 – 1046.
- [153] K. Ganesh, R. Nagarajan, J.L. Duda, Rate of gas transport in glassy polymers: a free volume based predictive model, *Ind. Eng. Chem. Res.* 31 (1992) 746–755.
- [154] W.J. Koros, Model for sorption of mixed gases in glassy polymers, *J. Polym. Sci. Part B Polym. Phys. Polym. Phys. Ed.* 18 (2003) 981 – 992.
- [155] R. Wissinger, M. Paulaitis, Molecular thermodynamic model for sorption and swelling in glassy polymer-carbon dioxide systems at elevated pressures, *Ind. Eng. Chem. Res.* (1991) 842–851.

- [156] R. Conforti, T. Barbari, P. Vimalchand, M.D. Donohue, A lattice-based activity coefficient model for gas sorption in glassy polymers, *Macromolecules*. 24 (1991) 3388–3394.
- [157] F. Doghieri, G.C. Sarti, Nonequilibrium Lattice Fluids: A Predictive Model for the Solubility in Glassy Polymers, *Macromolecules*. 29 (1996) 7885–7896.
- [158] R.H. Lacombe, I.C. Sanchez, Statistical Thermodynamics of Fluid Mixtures, *J. Phys. Chem.* 80 (1976) 2568–2580.
- [159] M. Minelli, S. Campagnoli, M.G. De Angelis, F. Doghieri, G.C. Sarti, Predictive Model for the Solubility of Fluid Mixtures in Glassy Polymers, *Macromolecules*. 44 (2011) 4852–4862.
- [160] M. Minelli, F. Doghieri, A predictive model for vapor solubility and volume dilation in glassy polymers, *Ind. Eng. Chem. Res.* 51 (2012) 16505–16516.
- [161] W. Koros, R. Chern, A model for permeation of mixed gases and vapors in glassy polymers, *J. Polym. Sci. Polym. Phys. Ed.* 19 (1981) 1513–1530.
- [162] M.C. Ferrari, J. Catalano, M. Giacinti Baschetti, M.G. De Angelis, G.C. Sarti, FTIR-ATR Study of Water Distribution in a Short-Side-Chain PFSI Membrane, *Macromolecules*. 45 (2012) 1901 – 1912.
- [163] E.M. Davis, M. Minelli, M. Giacinti Baschetti, G.C. Sarti, Y.A. Elabd, Nonequilibrium Sorption of Water in Polylactide, *Macromolecules*. 45 (2012) 7486–7494.
- [164] B. Zimm, J. Lundberg, Sorption of vapors by high polymers, *J. Phys. Chem.* 425 (1956) 6–9.
- [165] J.R. Scherer, The partial molar volume of water in biological membranes, *Proc. Natl. Acad. Sci. USA*. 84 (1987) 7938–7942.
- [166] R.D. Noble, D.J. Way, L.A. Powers, Effect of External Mass-Transfer Resistance on Facilitated Transport, *Ind. Eng. Chem. Fundam.* 25 (1986) 450–452.
- [167] L.L. Kemena, R.D. Noble, N.J. Kemp, Optimal Regime for Facilitated Transport, *J. Memb. Sci.* 15 (1983) 259 – 274.
- [168] X. Wang, W. Conway, D. Fernandes, R. Burns, G. Puxty, M. Maeder, Kinetics of the Reversible Reaction of CO₂ (aq) with Ammonia in Aqueous Solution, *J. Phys. Chem. A*. 115 (2011) 6405 – 6412.
- [169] G. Versteeg, W. Van Swaaij, On the kinetics between CO₂ and alkanolamines both in aqueous and non-aqueous solutions - I. Primary and secondary amines, *Chem. Eng. Sci.* 43 (1988) 573–585.

- [170] H. Matsuyama, A. Terada, T. Nakagawara, Y. Kitamura, M. Teramoto, Facilitated transport of CO₂ through polyethylenimine/poly(vinyl alcohol) blend membrane, *J. Memb. Sci.* 163 (1999) 221–227.

List of Publications

Journal Papers

- Minelli M., Cocchi G., Ansaloni L., Baschetti Giacinti M., De Angelis M.G., Doghieri F., *Vapor and liquid sorption in Matrimid polyimide: experimental characterization and modeling*, Industrial & Engineering Chemistry Research, 2013, **52**, 8936–8945.
- Ansaloni L., Minelli M., Giacinti Baschetti M., Sarti G.C., *Effects of thermal treatment and physical aging on the gas transport properties in Matrimid[®]*, Oil & Gas Science and Technology, Revue d'IFP Energies Nouvelles, Dossier - Interactions Fluids Polymers: Permeability, Durability, DOI: 10.2516/ogst/2013188 (2014).
- Zhao Y., Jung B.T., Ansaloni L., Ho W.S.W., *Multiwalled carbon nanotube mixed matrix membranes containing amines for high pressure CO₂/H₂ separation*, Journal of Membrane Science, **459**, 2014, 233–243.

Oral Presentation

- Ansaloni L., Minelli M., Giacinti Baschetti M., Sarti G.C., *Studio delle proprietà di trasporto in Matrimid[®]: effetto della storia termica e dell'invecchiamento fisico*, Convegno Nazionale GRICU 2012, 16 - 19 September 2012, Montesilvano (PE).
- Ansaloni L., Zhao Y., Ramasubramanian K., Giacinti Baschetti M., Ho W.S.W., *Multiwalled Carbon Nanotube Mixed-Matrix Membranes Containing Amines for Acid Gas Removal From Natural Gas*, 2013 AIChE Annual Meeting, 3 - 8 November 2013, San Francisco (CA).

Conference Proceeding

- Ansaloni L., Minelli M., Giacinti Baschetti M., Sarti G.C., *Investigation of Mass transport properties under humid conditions of Matrimid dense films*, EMS Summerschool, 10 - 13 July 2012, Nancy, France.
- Ansaloni L., Giacinti Baschetti M., Minelli M., G.C. Sarti, *Study of Transport Properties of Matrimid Polyimide: Effect of Thermal History and of Physical Aging*, Procedia Engineering, **44** (2012) 840–842.
- Ansaloni L., Minelli M., Giacinti Baschetti M., Sarti G.C., *Mass transport properties of gases and vapors in Matrimid Polyimide*, 2012 AIChE Annual Meeting, 28 October - 2 November 2012, Pittsburgh (PA).
- Ansaloni L., Minelli M., Giacinti Baschetti M., Sarti G.C., *Influence of relative humidity on the gas transport properties of polyimides*, NAMS 23rd Annual Meeting, 8 - 12 June 2013, Boise, ID.
- Ansaloni L., Tsvigu C., Minelli M., Giacinti Baschetti M., Sarti G.C., *Analysis of the Humid Gas Permeation in Glassy Polyimides: A Modeling Approach*, 2013 AIChE Annual Meeting, 3 - 8 November 2013, San Francisco (CA).
- Ansaloni L., Zhao Y., Ramasubramanian K., Giacinti Baschetti M., Ho W.S.W., *Facilitated Transport Membranes for Natural Gas Separation*, 2013 AIChE Annual Meeting, 3 - 8 November 2013, San Francisco (CA).

Acknowledgments

Bearing in mind that it is impossible to frame in a single page all the people who shared with me parts of this 3 years long adventure, here below I just would like to write an incomplete list of thanks. I apologize in advance for all the people I forgot.

First of all, I would like to express my gratitude to my advisor, Dr. Marco Giacinti Baschetti, whose help and guidance have been of fundamental importance to achieve this result. I am very grateful also to Dr. Matteo Minelli for the practical tips and the essential advices. Moreover, I would like to thank also Prof. Giulio Cesare Sarti and Dr. Maria Grazia De Angelis for all the precious encouragements and Dr. Giovanni Cocchi for the productive discussions on polymer and thermodynamics.

I would like to express also my gratitude to Dr. W.S. Winston Ho for the possibility he gave me to be part of his research group at the Ohio State University and for all the valuable advices. I am endless grateful also to Dr. Yanan Zhao, Dr. Kartik Ramasubramanian, Varun Vakaria, and all the people from Dr. Ho's research group, whose help has been essential to achieve the results presented in this thesis. I want to thank also my American family (Mark, Nancy and Star), all my friends from IFI and from OSU.

Moreover, I need to thank all my labmates in Bologna, Claudia, Jucii, Jocelia, Antonio, Micaela, Andrea, Roberta, Giacomo, Ada, Daniele and also my modenese friends Andre, Fiore, Aba, Richi, Marco, Cave, Lance and Alle.

Finally I want to thank my family, my mom, Ughetta, my two brothers, Matteo and Fabio, and my grandparents, Franca and Giorgio, for the support and the patience during the hard times I went through during this part of my life.

Last, but first in my heart, I want to say thanks to my Mari Superdandy: without your love and your support this wouldn't have been possible.